

For Reference

NOT TO BE TAKEN FROM THIS ROOM

For Reference

NOT TO BE TAKEN FROM THIS ROOM

Ex LIBRIS
UNIVERSITATIS
ALBERTAENSIS



Regulations Regarding Theses and Dissertations

[illegible]

THE UNIVERSITY OF ALBERTA

A STUDY OF SOME $1f_{7/2}$ SHELL NUCLEI WITH THE (d,n) REACTION

by



Thomas Boyde Grandy

A THESIS

SUBMITTED TO THE FACULTY OF GRADUATE STUDIES

IN PARTIAL FULFILLMENT OF THE REQUIREMENTS FOR THE DEGREE

OF DOCTOR OF PHILOSOPHY

DEPARTMENT OF PHYSICS

EDMONTON, ALBERTA

September, 1967



Digitized by the Internet Archive
in 2019 with funding from
University of Alberta Libraries

<https://archive.org/details/Grandy1967>

UNIVERSITY OF ALBERTA
FACULTY OF GRADUATE STUDIES

The undersigned certify that they have read, and recommend to the Faculty of Graduate Studies for acceptance, a thesis entitled A STUDY OF SOME $1f_{7/2}$ SHELL NUCLEI WITH THE (d,n) REACTION, submitted by Thomas Boyde Grandy in partial fulfillment of the requirements for the degree of Doctor of Philosophy.

ABSTRACT

Angular distributions of neutrons from the reaction $^{40}\text{Ca}(\text{d},\text{n})^{41}\text{Sc}$ ($E_d = 5.0, 6.0$ and 6.5 MeV), $^{42}\text{Ca}(\text{d},\text{n})^{43}\text{Sc}$ ($E_d = 5.15$ MeV), $^{48}\text{Ca}(\text{d},\text{n})^{49}\text{Sc}$ ($E_d = 5.5$ and 6.0 MeV) have been measured. A large number of levels have been observed and studied. In particular, strongly populated states at 6.155 MeV in ^{43}Sc and 11.571 MeV in ^{49}Sc have been tentatively identified as the isobaric analogs of the $2P_{\frac{3}{2}}$ level at 2.048 MeV in ^{43}Ca and the ^{49}Ca ground state, respectively. A distorted wave analysis of these reactions has been carried out and spectroscopic information for the more intense transitions is reported.

An attempt was made to evaluate the distorted wave method of data analysis in the study of the $^{40}\text{Ca}(\text{d},\text{n})^{41}\text{Sc}$ and $^{48}\text{Ca}(\text{d},\text{n})^{49}\text{Sc}$ reactions. This work was a part of a continuing project, by several groups, to study the application of DWBA theory to (d,d) (d,p) and (d,n) reactions on $1f_7$ shell nuclei.

ACKNOWLEDGEMENTS

I would like to thank my supervisor, Dr. W. K. Dawson and also Dr. G. C. Neilson for suggesting a project that has turned out to be both interesting and rewarding. Thanks are extended to Dr. W. J. McDonald for his interest in my work and his patience in reading this exposition.

Particular thanks are due to Dr. W. G. Davies for the experience gained in working with him. In addition, the author wishes to thank Mr. D. A. Gedcke, Mr. H. G. Leighton, Mr. D. Gurd and Mr. S. T. Lam for many illuminating discussions on the more subtle aspects of this work without which I might have been finished six months earlier.

The co-operating effort, in data taking, of the various individuals in the time of flight group is gratefully acknowledged. In particular, my thanks are extended to Mr. N. E. Davison who gave freely of his time on all three experiments and to Mr. D. A. Hutcheon who helped in the initial stages of this project. Credit is given to Dr. G. C. Neilson, Dr. W. J. McDonald, Dr. W. K. Dawson and Mr. D. A. Gedcke whose efforts to improve the time resolution of the spectrometer made these experiments feasible.

I am very grateful to Mr. J. B. Elliott, first for obtaining excellent beam conditions while my experiments were running and second, for the extra effort that was extended in getting my drawings finished

on time. The help of the rest of the staff of the Nuclear Research Center has been appreciated throughout the past years.

Thanks are also due to Miss E. Hawirko for her meticulous efforts in typing this thesis.

Finally, I would like to thank the University of Alberta for financial support during the course of this work.

TABLE OF CONTENTS

	Page
CHAPTER 1 INTRODUCTION	1
1.1 Objectives	1
1.2 General Background	2
1.3 General Experimental Details	6
CHAPTER 2 THE $^{40}\text{Ca}(\text{d},\text{n})^{41}\text{Sc}$ REACTION	10
2.1 Introduction	10
2.2 Experimental Method	12
2.3 Results	17
2.4 DWBA Analysis of the Ground State Angular Distributions	31
2.5 Plane Wave Analysis	41
2.6 DWBA Fitting of Unbound States	44
2.7 The $^{16}\text{O}(\text{d},\text{n})^{17}\text{F}$ Reaction	48
2.8 Discussion	53
CHAPTER 3 THE $^{42}\text{Ca}(\text{d},\text{n})^{43}\text{Sc}$ REACTION	56
3.1 Introduction	56
3.2 Experimental Method	57
3.3 Experimental Results	60
3.4 Analysis of the Angular Distributions	70
3.5 Isobaric Analog States in ^{43}Sc	80
3.6 Summary	81

CHAPTER 4	THE $^{48}\text{Ca}(\text{d},\text{n})^{49}\text{Sc}$ REACTION	83
4.1	Introduction	83
4.2	Experimental Method	84
4.3	Experimental Results	88
4.4	Analysis of the Angular Distributions	96
4.5	Observation of the ^{49}Ca Ground State Analog in ^{49}Sc	103
4.6	Summary	108
CHAPTER 5	CONCLUSIONS	109
APPENDIX I	A FORTRAN IV PROGRAM FOR THE CALCULATION OF NEUTRON DETECTION EFFICIENCY	112
A1.1	Introduction	112
A1.2	Formalism for the Calculated Efficiency	112
A1.3	Experimental Aspects and Comparison to Calculations	117
APPENDIX II	NUMERICAL VALUES FOR THE MEASURED CROSS SECTIONS	
REFERENCES		

FIGURES

	Page
1- 1 Essential features of the beam pulsing system	9
2- 1 Block diagram of the time of flight electronics	13
2- 2 Excitation functions for the ground and first excited states of ^{41}Sc taken at 90° to the incident beam	18
2- 3 A time of flight spectrum for the reaction $^{40}\text{Ca}(\text{d},\text{n})^{41}\text{Sc}$	20
2- 4 $^{40}\text{Ca}(\text{d},\text{n})^{41}\text{Sc}$ ground state angular distributions at deuteron bombarding energies of 5.0, 6.0 and 6.5 MeV	23
2- 5 Centre of mass angular distributions for neutrons leading to the 1.718 MeV state of ^{41}Sc from the reaction $^{40}\text{Ca}(\text{d},\text{n})^{41}\text{Sc}$	24
2- 6 Centre of mass angular distributions for neutrons leading to the 2.096 MeV state of ^{41}Sc from the reaction $^{40}\text{Ca}(\text{d},\text{n})^{41}\text{Sc}$	25
2- 7 Centre of mass angular distributions for neutrons leading to the 2.415 MeV state of ^{41}Sc from the reaction $^{40}\text{Ca}(\text{d},\text{n})^{41}\text{Sc}$	26
2- 8 Centre of mass angular distributions for neutrons leading to the 2.719 MeV state of ^{41}Sc from the reaction $^{40}\text{Ca}(\text{d},\text{n})^{41}\text{Sc}$ at 6.0 MeV bombarding energy	27
2- 9 Centre of mass angular distributions for neutrons leading to the 3.463 MeV state of ^{41}Sc from the reaction $^{40}\text{Ca}(\text{d},\text{n})^{41}\text{Sc}$ at 6.0 and 6.5 MeV bombarding energies	28
2-10 Centre of mass angular distributions for the ground state and 2.365 MeV state of ^{13}N from the reaction $^{12}\text{C}(\text{d},\text{n})^{13}\text{N}$ at a deuteron bombarding energy of 6.5 MeV	30
2-11 Neutron compound elastic cross section on calcium (Wi 64)	37
2-12 Ground state angular distribution of neutrons from the reaction $^{40}\text{Ca}(\text{d},\text{n})^{41}\text{Sc}$ at a deuteron bombarding energy of 3.981 MeV	40

Figures continued

2-13	DWBA fits to the $^{40}\text{Ca}(\text{d},\text{n})^{41}\text{Sc}$ transitions leading to the unbound levels at 1.718 and 2.415 MeV in ^{41}Sc	47
2-14	Centre of mass angular distributions for neutrons leading to the ground state of ^{17}F from the reaction $^{16}\text{O}(\text{d},\text{n})^{17}\text{F}$ at bombarding energies of 6.0 and 6.5 MeV	49
2-15	Centre of mass angular distributions of neutrons leading to the 0.500 MeV state of ^{17}F from the reaction $^{16}\text{O}(\text{d},\text{n})^{17}\text{F}$ at bombarding energies of 6.0 and 6.5 MeV	50
3- 1	Block diagram of the time of flight electronics used in data gathering for the $^{42}\text{Ca}(\text{d},\text{n})^{43}\text{Sc}$ reaction	58
3- 2	$^{42}\text{Ca}(\text{d},\text{n})^{43}\text{Sc}$ excitation functions for several low-lying states in ^{43}Sc taken at 30° to the incident beam	61
3- 3	Excitation function for the $^{42}\text{Ca}(\text{d},\text{n})^{43}\text{Sc}$ reaction leading to the ^{43}Ca 2.048 MeV isobaric analog state at 6.155 MeV excitation energy in ^{43}Sc	62
3- 4	A semi-log plot of a time of flight spectrum for the reaction $^{42}\text{Ca}(\text{d},\text{n})^{43}\text{Sc}$	64
3- 5	Centre of mass angular distribution for neutrons leading to the ground state of ^{43}Sc from the reaction $^{42}\text{Ca}(\text{d},\text{n})^{43}\text{Sc}$ at a deuteron bombarding energy of 5.15 MeV	71
3- 6	Centre of mass angular distributions for neutron from the reaction $^{42}\text{Ca}(\text{d},\text{n})^{43}\text{Sc}$ leading to states in ^{43}Sc at excitation energies of 0.475, 1.177 and 1.817 MeV	72
3- 7	Centre of mass angular distributions for neutrons from the reaction $^{42}\text{Ca}(\text{d},\text{n})^{43}\text{Sc}$ leading to states in ^{43}Sc at excitation energies of 0.860 and 1.947 MeV	73
3- 8	Centre of mass angular distributions for neutrons from the reaction $^{42}\text{Ca}(\text{d},\text{n})^{43}\text{Sc}$ leading to two unbound states in ^{43}Sc at excitation energies of 5.026 and 5.647 MeV	74
3- 9	Centre of mass angular distribution for neutrons from the reaction $^{42}\text{Ca}(\text{d},\text{n})^{43}\text{Sc}$ leading to a state in ^{43}Sc at an excitation energy of 6.155 MeV	75
4- 1	A semi-log plot of a time of flight spectrum from the reaction $^{48}\text{Ca}(\text{d},\text{n})^{49}\text{Sc}$	86

Figures continued

4- 2	Centre of mass angular distribution of neutrons from the reaction $^{48}\text{Ca}(\text{d},\text{n})^{49}\text{Sc}$ leading to the ground state of ^{49}Sc	89
4- 3	Centre of mass angular distributions of neutrons from the reaction $^{48}\text{Ca}(\text{d},\text{n})^{49}\text{Sc}$ leading to levels in ^{49}Sc at excitation energies of 3.071 and 4.472 MeV	90
4- 4	Centre of mass angular distributions of neutrons from the reaction $^{48}\text{Ca}(\text{d},\text{n})^{49}\text{Sc}$ leading to levels in ^{49}Sc at excitation energies of 5.008, 5.655 and 7.050 MeV	91
4- 5	Centre of mass angular distribution of neutrons from the reaction $^{48}\text{Ca}(\text{d},\text{n})^{49}\text{Sc}$ leading to the 5.080 MeV level in ^{49}Sc	92
4- 6	Centre of mass angular distribution of neutrons from the reaction $^{48}\text{Ca}(\text{d},\text{n})^{49}\text{Sc}$ leading to a state in ^{49}Sc at an excitation energy of 6.873 MeV	93
4- 7	A time of flight spectrum for the reaction $^{48}\text{Ca}(\text{d},\text{n})^{49}\text{Sc}$ taken at a deuteron bombarding energy of 6.0 MeV	105
4- 8	Relative angular distribution, in the laboratory system, for neutrons from the reaction $^{48}\text{Ca}(\text{d},\text{n})^{49}\text{Sc}$ leading to the 11.571 MeV state in ^{49}Sc	106
A1-1	Scintillator cross section	113
A1-2	Absolute efficiency calculated with the present program compared with the relative efficiency for the XP 1040 detector and an NE 213 scintillator	120

TABLES

	Page
2-1 Excitation Energies of Levels in ^{41}Sc in MeV	21
2-2 Optical Model Parameters from Deuteron Elastic Scattering on ^{40}Ca	33
2-3 Average Neutron Optical Model Parameters used in the Analysis of the $^{40}\text{Ca}(\text{d},\text{n})^{41}\text{Sc}$ Reaction	33
2-4 Relative reduced widths from a plane wave analysis of the $^{40}\text{Ca}(\text{d},\text{n})^{41}\text{Sc}$ data at 6.0 MeV bombarding energy	44
3-1 Q values for the reaction $^{42}\text{Ca}(\text{d},\text{n})^{43}\text{Sc}$ and Excitation Energies of Levels in ^{43}Sc	65
3-2 Q values for the $^{32}\text{S}(\text{d},\text{n})^{33}\text{Cl}$ reaction and Excitation Energies of Levels in ^{33}Cl	69
3-3 Optical Model Parameters	76
4-1 Q values for the $^{48}\text{Ca}(\text{d},\text{n})^{49}\text{Sc}$ reaction and Excitation Energies of Levels in ^{49}Sc	94
4-2 Optical Model Parameters	96
4-3 Spectroscopic factors from the present study of the $^{48}\text{Ca}(\text{d},\text{n})^{49}\text{Sc}$ reaction compared to recent $^{48}\text{Ca}({}^3\text{He},\text{d})^{49}\text{Sc}$ measurements and to the calculated values	99
A1-1 Program Input parameters	122
A1-2 Sample Output	124

CHAPTER 1

INTRODUCTION

1.1 Objectives

The objectives which form a basis for the work presented here may be classified into four categories

- (1) the study of the single nucleon transfer reaction in the vicinity of doubly magic nuclei; in the first case with the nucleus ^{40}Ca as a target and in the second, ^{48}Ca .
- (2) the study of the single nucleon transfer reaction away from a closed shell; in this work the nucleus ^{42}Ca was used as a target
- (3) a test of the applicability of the Distorted Wave Born Approximation method to describe deuteron stripping reactions.
- (4) an investigation into the feasibility of accurately calculating neutron detector efficiencies.

1.2 General Background

A great deal of experimental and theoretical interest has been expressed recently in nuclei of the $1f_{7/2}$ shell. For example, excitation energies arising from the $(f_{7/2})^3$ configuration have been calculated by McCullen (Mc 64) and attempts to reproduce the main features of the ^{43}Sc nucleus in terms of the shell model have been presented by Flowers (Fl 67). Recent attempts to understand the ^{41}Sc structure in terms of $3p - 2h$ states has been presented by Gerace (Ge 67e).

Experimentally, $1f_{7/2}$ shell nuclei have been explored, most thoroughly, through a number of charged particle reactions. Some of these are discussed, specifically, in the main text. The present work reports experimental information gained through a study of the (d,n) stripping reaction on some nuclei in the $1f_{7/2}$ shell. The (d,n) reaction should preferentially proceed through the capture of protons into single particle orbits. If this transfer results in the formation of a nucleus which can be described in terms of closed shells plus one nucleon, then the analysis of the reaction is expected to be straight forward. From a simple shell model picture, the ground state of these nuclei are expected to be characterized by a single nucleon in the $1f_{7/2}$ shell. Excited states should be formed by promoting the captured proton to $2p_{3/2}$, $1f_{5/2}$ and $2p_{1/2}$ shell model orbits. When a nucleus is formed several nucleons away from a closed shell, the structure is expected to be more complicated because the nucleons in the unfilled shell can interact with the captured proton and with each other (configura-

tion mixing).

The usefulness of a stripping reaction in obtaining the spins and parities of nuclear levels has been pointed out by Butler (Bu 51). In deuteron stripping reactions, the angular distribution of neutrons or protons is characterized by a high differential cross section in the forward direction. The reaction yield tends to have a prominent maximum in the forward direction and secondary maxima at larger angles. The angular momentum, $l\hbar$, carried into the target nucleus by the captured nucleon is the major factor in determining the shape of the angular distribution. From the position of the primary maximum in the angular distribution of reaction products, it has been possible to find the relative parities of the target and residual nuclei and to determine possible values for the orbital angular momentum transferred by the captured particle. When the absolute reaction cross section is measured, it is possible to extract spectroscopic information, namely, the extent to which the final state can be described by the simple shell model picture.

Two main theories exist for the calculation of the angular distribution formed in the transfer of a single nucleon. The theories are commonly referred to as the Plane Wave Born Approximation (PWBA) and the Distorted Wave Born Approximation (DWBA). Both of these theories have been used in the present work. In some cases, it has been possible to test the ability of these theories to extract information on nuclear structure.

The Butler Plane Wave Approximation considers that the initial and

final states can be treated as incoming and outgoing plane waves. The transferred nucleon is assumed to have no interaction with the final nucleus except that it is bound in a harmonic oscillator well to the target with the correct binding energy. Usually, the plane wave calculations describe only the main features of the angular distribution. In general, only the forward maximum of the distribution is reproduced with secondary maxima falling far below that observed. In addition, it calculates a cross section which is usually considerably larger than the experimental value, and thus, cannot be used reliably to extract spectroscopic information.

The inadequacies of the PWBA stimulated the development of a theory in which the distortions of the incident deuteron and emergent proton or neutron waves by the coulomb and nuclear fields are taken into account (To 61). The distortions are assumed to be the same as those occurring in elastic scattering so that they may be calculated from the appropriate elastic scattering data.

The distorted wave theory gives improved agreement with the experimental data in several respects. It gives the Coulomb distortion correctly and usually fits the backward cross section better than the PWBA. The absolute magnitudes of the cross section are much more accurate so that reliable spectroscopic information can be extracted.

The differential cross section for a direct reaction of the form $A(a,b)B$, in the distorted wave Born Approximation can be written as (Au 63, Au 64)

$$\frac{d\sigma}{d\Omega} = \frac{\mu_a \mu_b}{(2\pi\hbar^2)^2} \frac{(2J_B + 1)}{(2J_A + 1)} \frac{k_b}{k_a} \sum_{\ell s j} \frac{|A_{\ell s j}|^2}{2s_a + 1} \sum_m |\beta_{s j}^{\ell m}|^2$$

where

μ_a and μ_b are the reduced masses of the pairs (a,A) and (b,B);

k_a and k_b are the wave vectors for particles a and b;

J_A , J_B , S_a and S_b are the spins of particles A, B, a and b, respectively with corresponding z components M_A , M_B , m_a and m_b ;

$A_{\ell s j}$ is related to the spectroscopic factor $S_{\ell j}$,

$$\beta_{s j}^{\ell m} = \frac{1}{(2\ell+1)^{1/2}} i^{-\ell} \int dr_a \int dr_b \chi_b^{(-)*}(k_b, r_b) f_{\ell s j m}(r_b, r_a) \chi_a^{(+)}(k_a, r_a)$$

$\chi_b^{(-)}$ is the outgoing elastic scattering waves,

$\chi_a^{(+)}$ is the incoming elastic scattering wave,

$f_{\ell s j m}$ is proportional to the radial wave function of the bound nucleon in deuteron stripping reactions.

The elastic scattering waves and the bound nucleon wave function are solutions of the radial Schrödinger equation

$$\Phi_\ell''(r) - \frac{2m}{\hbar^2} [E_{c.m.} + V(r) - \frac{\hbar^2}{2m} \frac{\ell(\ell+1)}{r^2}] \Phi_\ell = 0$$

where the potential $V(r)$ is the optical model potential.

For deuteron stripping in the so called zero range approximation, the factor $A_{\ell s j}$ is related to the spectroscopic factor $S_{\ell j}$ by the

relation (Sa 64)

$$|A_{\ell sj}|^2 = 1.48 * 10^4 (2S_a + 1) S_{\ell j}$$

Under these conditions, the spectroscopic factor is defined as

$$S = \frac{\sigma(\text{experimental})}{\sigma \text{ DWBA}}$$

These properties of direct interactions make the (d,p) and (d,n) reactions very powerful tools for the study of the structure of the nucleus.

1.3 General Experimental Details

In fast neutron spectroscopy, the most accurate measurement of neutron energy is by means of a time of flight spectrometer which determines the energies of neutrons by individually timing their flight over an accurately measured path. A neutron time of flight spectrometer must accurately fix two time points:

- (1) a zero or start time related to the production of the neutron at the target.
- (2) a stop time determined by the arrival of the neutron at a detector.

From the measurement of time and distance, the neutron velocity and hence energy can be calculated. For the University of Alberta, spectrometer neutron flight paths of 1 to 6 meters can be used, this typically

results in flight times ranging from 50 to 500 nanoseconds. For a precise energy measurement, the nuclear reaction producing the neutron must be localized in a time interval that is small compared to the flight time. This can be achieved by pulsing the beam. The beam repetition rate is arranged so that the slowest neutrons reach the detector before the next beam burst.

Several methods for beam pulsing have been developed in the past:

- (1) chopping the continuous beam from a Van de Graaff by means of a beam deflector and slits (Ne 59).
- (2) pulsing before acceleration (Fo 60, Be 62).
- (3) compression of the pulsed beam from (2) after acceleration (Cr 61, Ts 66).

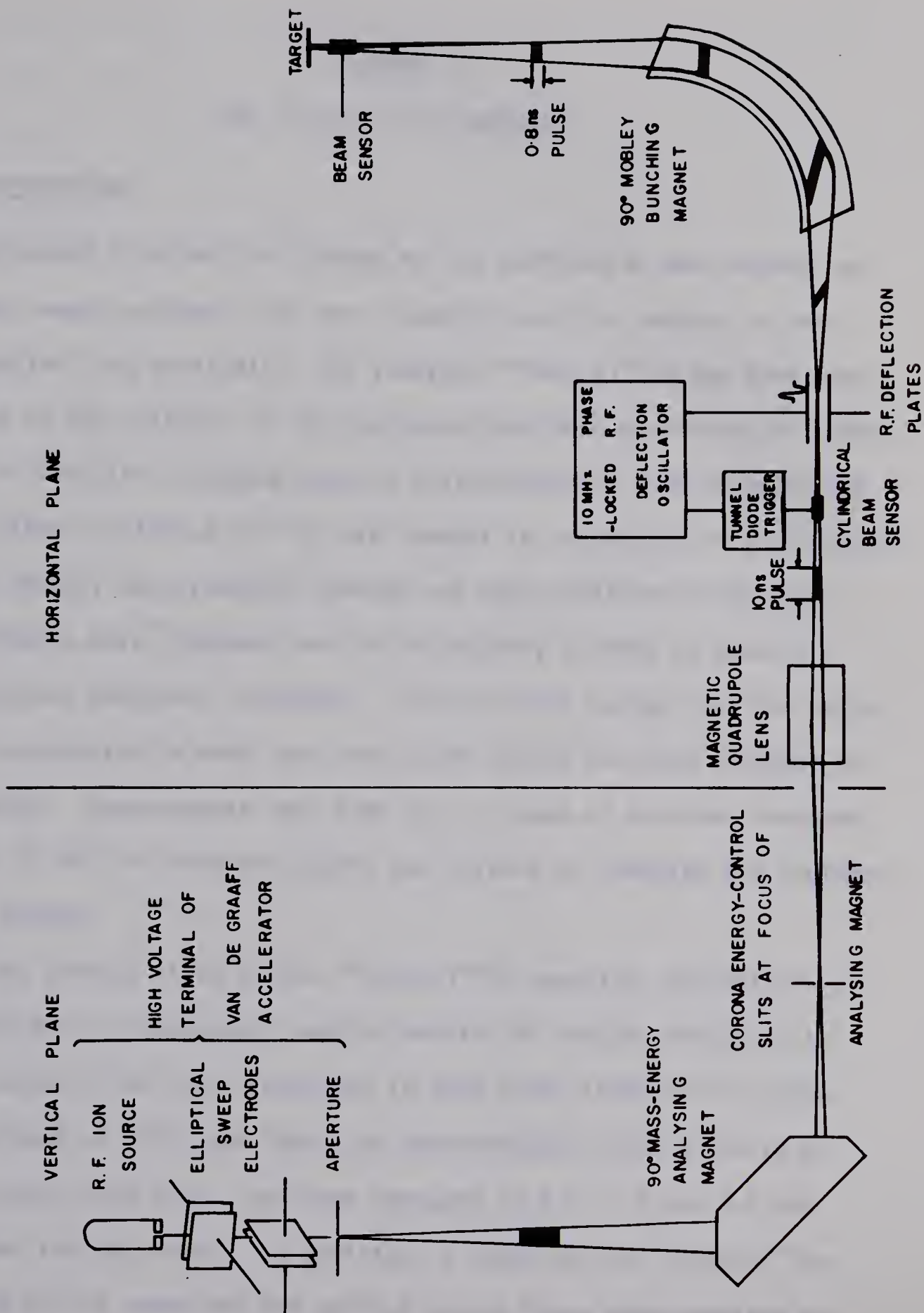
Method (1) suffers from severe loss of beam on the chopping slits and unwanted neutron and gamma ray background from inevitable contaminants on these slits. Method (2) is undesirable since one is limited to a time resolution of approximately 4 ns even with beam repetition rate of 5 MHz. The background problems of (1) are eliminated since slits in the target area are not required. In addition, beam loss is not severe since ion sources are available which deliver a pre-acceleration current of approximately 1 - 2 milli-amp. After chopping, 10 micro-amp of beam is typically delivered on target. Method (3) which combines pre-acceleration pulsing and post-acceleration compression of this pulsed beam with a Mobley bunching magnet has been the most successful. Beam bursts less than 1 ns (FWHM) with an average current of 3.0 μ A are easily obtained. Such a system was used for the experimental work to be presented here. A simpli-

fied diagram of the beam handling and pulsing system together with the Mobley magnet is shown in figure 1-1. A more complete description of the system is given in the Ph.D thesis of W.G. Davies (Da 66).

An R.F. ion source located at the high voltage terminal of the Van de Graaff accelerator delivers approximately 2 milli-amps of d.c. beam. This beam is swept in an elliptical path over a $\frac{1}{16}$ inch aperture by two sets of R.F. deflection plates set at right angles to each other and driven 90° out of phase by a 1 MH oscillator. The resulting beam bursts have a time resolution of 10 - 15 ns (FWHM) and an average current of approximately 10 μ A. Energy (momentum) analysis of the beam is achieved by a 90° analyzing magnet located at the base of the accelerator.

The principle of operation of the Mobley magnet is shown schematically in figure 1-1. A beam burst entering the deflection plates of the phase locked deflection oscillator is swept in such a manner that the first particles leaving the deflector take the longest paths through the magnet while those leaving last take the shortest paths with intermediate particles being deflected to paths appropriate to their time of departure. If the phase and amplitude of the deflector are properly adjusted, all particles will arrive at the target at almost the same time. A 90° Mobley magnet with a radius of 75 inches is used in the present installation. Accurate measurements of the optimum pulse duration (Ge 67) indicates that 0.4 ± 0.05 ns is possible with the present bunching system in contrast to the value of 0.8 ns measured by Davies (Da 66).

Figure 1-1 Essential features of the beam pulsing system



CHAPTER 2

THE $^{40}\text{Ca}(\text{d},\text{n})^{41}\text{Sc}$ REACTION

2.1 Introduction

The nuclei ^{41}Ca and ^{41}Sc formed by the addition of one nucleon to the doubly magic nucleus ^{40}Ca , have recently been the subject of much investigation. In particular, the reaction $^{40}\text{Ca}(\text{d},\text{p})^{41}\text{Ca}$ has been used as a test of the validity of the Distorted Wave Born Approximation (DWBA) (Le 64) to describe stripping angular distributions. This reaction was chosen, since the levels of ^{41}Ca are thought to correspond to good single particle states; spectroscopic factors are then predicted to be unity. This allowed a more rigorous test of the ability of DWBA to predict absolute cross sections. Moreover, ^{40}Ca was heavy enough that the difficulties encountered in work with very light nuclei were not expected to be important. Measurements were made over a range of deuteron energies from 7 to 12 MeV in order to observe the effects of changing the incident deuteron energy.

In the present study of the $^{40}\text{Ca}(\text{d},\text{n})^{41}\text{Sc}$ reaction, the ability of the DWBA theory to adequately predict details of nuclear structure is further tested. The (d,n) reaction, in this case, leads to ^{41}Sc , the mirror nucleus of ^{41}Ca , and thus, the spectroscopic factors should be equal to unity here also. Deuteron energies of 5.0, 6.0 and 6.5 MeV were chosen for the study. In addition, a study of the $^{40}\text{Ca}(\text{d},\text{d})^{40}\text{Ca}$ and $^{40}\text{Ca}(\text{d},\text{p})^{41}\text{Ca}$ reactions was carried out at these same energies by

another group in this laboratory (Le 67). This provided the necessary optical model information for the incoming channel and also provided a complementary study of two possible outgoing channels. It is hoped that a unified experimental approach of this kind can shed some light on the inadequacies that now exist in our understanding of reaction theory.

In the case of ^{41}Sc , the test is limited to the ground state transition, since all the excited states are unbound to proton emission. Commonly available distorted wave programs require the captured particle to be bound in a Woods-Saxon well whose depth is adjusted to give the captured particle a binding energy equal to its separation energy. Unbound states can be studied in an approximate manner by artificially adjusting the value of the separation energy to just make the level look bound. The feasibility of this approach has been tested in the present study.

The plane wave stripping theory of Butler can handle stripping to unbound states. An analysis with the Butler theory has been carried out, and its ability to describe the experimental data is examined.

A number of levels in ^{41}Sc had not been seen before through the $^{40}\text{Ca}(d,n)^{41}\text{Sc}$ reaction. The spectroscopy of these levels is discussed in terms of the information available from plane wave fits.

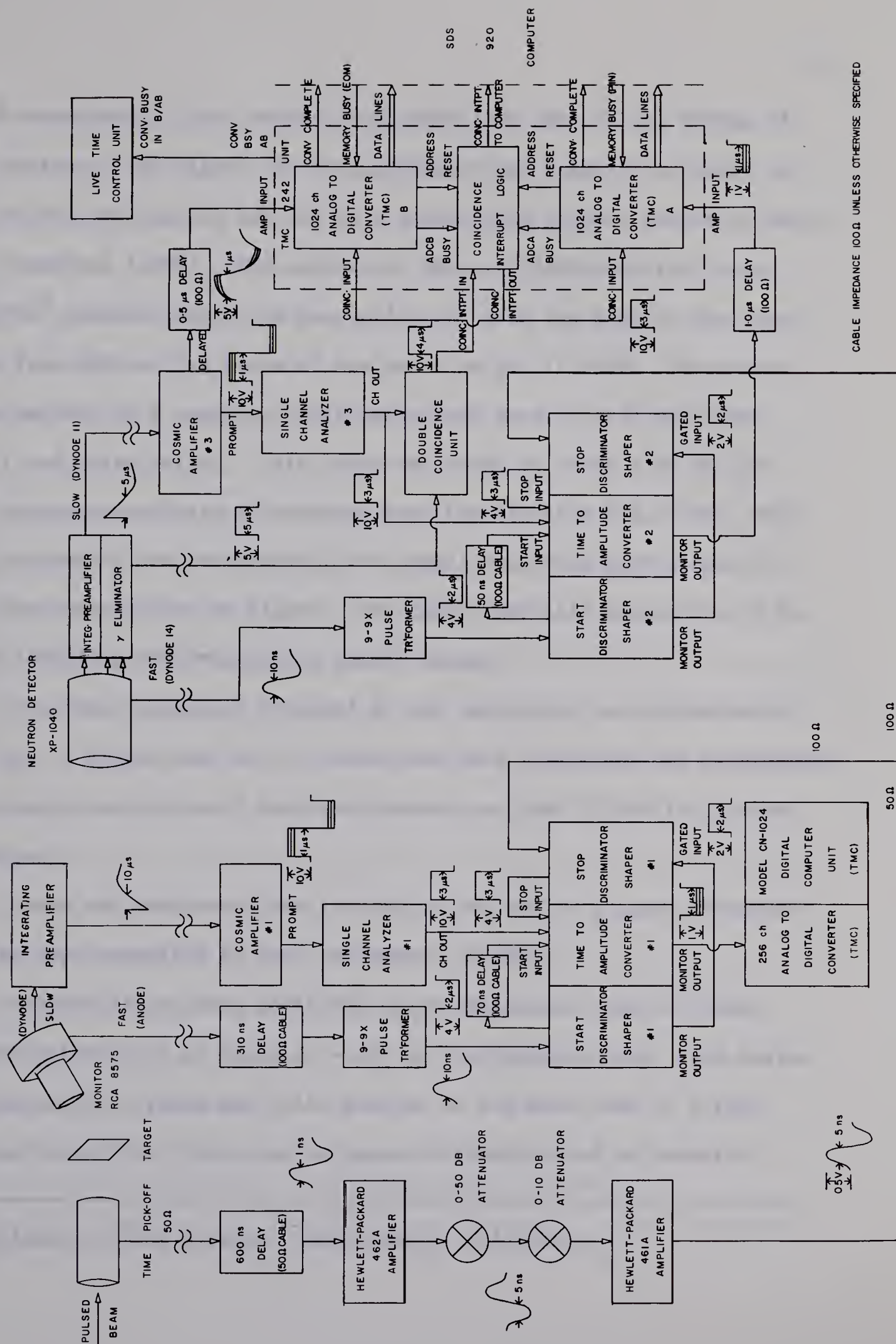
2.2 Experimental Method

The experiment was performed with the University of Alberta 5.5 MeV Van de Graaff accelerator and associated Mobley Magnet Compression System both of which have been described earlier.

A block diagram of the time of flight electronics is shown in figure 2-1. The start signal for the time of flight measurement was derived from dynode 14 of the neutron detector. The stop signal came from a 3 cm long cylindrical beam sensing capacitor located 30 cm before the target. It is advantageous to use the detector rather than the capacitor pulse for a start signal since the analysis of an event is initiated only when a neutron is detected. The stop signal does not, in actual fact, originate from the beam pulse that produced the neutron, but from the following pulse. The use of the following pulse introduces a time jitter less than 40 pico-sec. (Ge 67a) which is small compared to other factors influencing the time resolution.

The start and stop signals were fed into a time to amplitude converter (TAC) based on a design by D.L. Wieber (Wi 63). The output of the TAC was fed to a 1024 channel analog to digital converter (ADCA). In order to improve the time resolution of the spectrometer, a correction was made for timing signal walk in the start pulse. Walk is introduced into the system from this signal because of the large range of amplitudes associated with the proton recoil spectrum. The neutron detection process involves looking at the light output from recoiling protons whose energy

Figure 2-1 Block diagram of the time of flight electronics



(and consequently light output) can range from zero to the energy of the neutron. The signal for the correction was taken from dynode 11 of the photomultiplier and fed to a second 1024 channel analog to digital converter (ADCB). The outputs of ADCA and ADCB were fed to an SDS-920* computer where the correction for walk was made to the spectrum from ADCA on the basis of the pulse height in ADCB. The correction amounts to a spectrum shift determined from a table relating shift and pulse height. This table was found by using a 32 by 128 two parameter analysis of neutrons from the reaction $T(d,n)^4\text{He}$. The two parameters are respectively the signal amplitude from dynode 11 and the neutron time of flight. The shift typically ranged from 0 to 4 ns depending upon the proton recoil energy.

The time resolution obtained in the experiment was approximately 0.9 ns. A flight path of 4.0 meters was used throughout the experiment. The energy resolution of the spectrometer was then 70 KeV for 5.0 MeV neutrons.

Gamma ray background was reduced by the use of a gamma eliminator of the type described by Reid and Hummel (Re 66).

Neutron fluxes were monitored by an additional time of flight system situated at an angle of -30° to the incoming beam. The design of the monitor system was quite similar to the main time of flight system except that there was no gamma elimination and no computer

* Scientific Data Systems, Santa Monica, California.

correction for walk. Crossover timing was, however, used to minimize the walk. A flight path of 2.0 meters was used for the monitor detector. The use of a monitor of this kind eliminates the effects of target non-uniformities in the determination of relative angular distributions.

The main detector was a cylindrical (3.45" diameter x 0.75" length) NE 213* liquid scintillator coupled to a Philips XP 1040 photomultiplier. A Naton phosphor† coupled to an RCA 8575 photomultiplier served as the monitor detector.

The relative efficiency of the main neutron detector from cut-off energy (0.60 MeV) to 3.80 MeV was determined in a separate experiment with the reaction $T(p,n)^3\text{He}$ as a source of mono-energetic neutrons. The neutron yield of the $T(p,n)^3\text{He}$ reaction, as a function of bombarding energy, was monitored by a McKibben long counter. The relative efficiency for neutrons above 3.8 MeV was obtained by a normalization of the relative efficiency curve to the total n-p scattering cross section. Absolute efficiencies were obtained by normalization of the relative efficiency curve to two absolute efficiency measurements at 2.75 and 4.11 MeV. The absolute efficiency had been previously measured at these two points (Bu 67) by the associated particle method with the reaction $D(d,n)^3\text{He}$. The error in the measurement of absolute efficiency is estimated to be $\pm 5\%$.

* Nuclear Enterprises Ltd., Winnipeg, Manitoba, Canada.

† Nash and Thompson Ltd., Hookrise South, Tolworth, Surrey, England.

Calcium targets were prepared by evaporation of natural calcium unto 0.005" gold backings. In an attempt to minimize calcium oxidation, all target transfer operations were carried out in a helium atmosphere. Even with the care taken contaminant peaks from the reactions $^{16}\text{O}(\text{d},\text{n})^{17}\text{F}$ and $^{12}\text{C}(\text{d},\text{n})^{13}\text{N}$ were present in all spectra. A target thickness of 130 $\mu\text{g}/\text{cm}^2$ was used for the studies at 5.0 and 6.0 MeV deuteron bombarding energy. The target thickness at 6.5 MeV bombarding energy was 50 $\mu\text{g}/\text{cm}^2$. Target thicknesses were measured by weighing at the completion of the experiments.

A check on the stability of the targets under bombardment was obtained by determining the ratio of yields to the ^{17}F ground state and the ^{41}Sc ground state in the monitor spectra. Throughout the experiment, no change in this ratio was detected. It was, thus, concluded that neither target evaporation, nor oxidation had taken place. The ratio of charge to the ^{13}N ground state yield in the monitor spectrum was also found for each run and showed no increase throughout the experiment.

A charge of 1800 uc was collected for each run with an Elcor Model A309A current integrator. Beam was stopped in the 0.005" target backing which was biased to + 300 volts to suppress secondary electron emission. The target backing was anchored to a 0.030" gold plate which was air cooled. This arrangement was found to be quite adequate in dissipating the 10 - 15 watts normally deposited in the target backing.

At the completion of the experiments, it was found that the ratio of charge to monitor counts was constant to within statistics. This

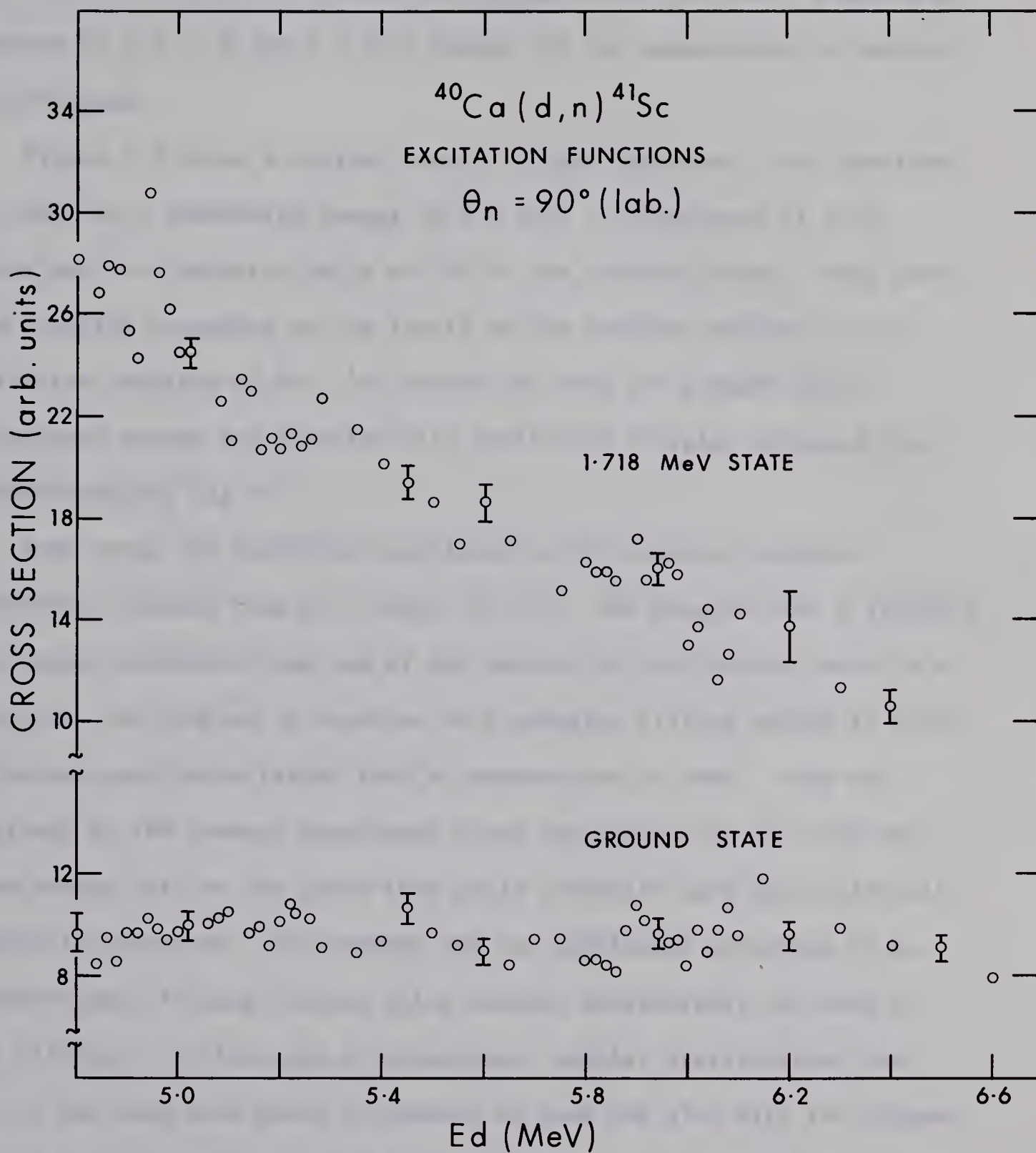
indicated that the target was probably quite uniform (making the determination of target thickness by weighing more feasible), and that alternate pulsing of the beam had not occurred. Alternate pulsing can occur when the top terminal RF system sweeps the beam over the chopping slits twice per RF cycle. This unwanted beam is 90° out of phase for modulation by the Mobley RF system and so appears as debunched beam on the target. The result is unwanted background and incorrect charge collection. Alternate pulsing is easily eliminated by carefully setting up the accelerator before data collection.

The bombarding energy was measured with a 90° analyzing magnet. The magnet was calibrated in terms of the ground state thresholds for the reactions ${}^7\text{Li}(p,n){}^7\text{Be}$, ${}^{13}\text{C}(p,n){}^{13}\text{N}$, ${}^{19}\text{F}(p,n){}^{19}\text{Ne}$ and ${}^{27}\text{Al}(p,n){}^{27}\text{Si}$ (Ma 66a). The bombarding energy is estimated to be accurate to within ± 3 KeV at 6.0 MeV.

2.3 Results

Figure 2-2 shows excitation curves for the ground and first excited state measured at 90° to the incident beam. These measurements were taken to ensure that the energies chosen for angular distribution studies were not near strong compound nucleus resonances. Little structure was observed for both of these excitation curves. A similar observation was also made for deuteron elastic scattering on ${}^{40}\text{Ca}$ at 90° (Le 67). It would seem then that the (d,n) reaction should satisfy well the

Figure 2-2 Excitation functions for the ground and first excited states of ^{41}Sc taken at 90° to the incident beam. Representative error bars are shown



optical model condition of smoothly varying cross sections. Bombarding energies of 5.0, 6.0 and 6.5 were chosen for the measurement of angular distributions.

Figure 2-3 shows a typical time of flight spectrum. This spectrum was taken at a bombarding energy of 6.5 MeV, a flight path of 4.00 meters and at a detector angle of 30° to the incident beam. Peaks have been labelled according to the levels in the residual nucleus. The excitation energies of the ^{41}Sc levels are from the present work. Contaminant groups are labelled with excitation energies obtained from AJZENBERG-SELOVE (Aj 59).

Peak areas and positions were found by the computer program "Anneliese" obtained from J.W. Tepel (Te 66). The program fits a standard peak shape determined from one of the spectra to the various peaks in a spectrum. The program is superior to a gaussian fitting method in that the actual peak shape rather than an assumed one is used. This was important in the present experiment since the correction for walk left a low energy tail on the peaks that would otherwise have been difficult to take into account. The program has the additional advantage of an automatic peak finding routine which reduces considerably the work of peak fitting. For the sake of comparison, angular distributions for the 5.0 MeV data were found by summing by hand and also with the program. Without exception, the angular distributions produced by the program were smoother than those produced by hand. This would tend to indicate that a more objective approach is taken by the program than by the individual.

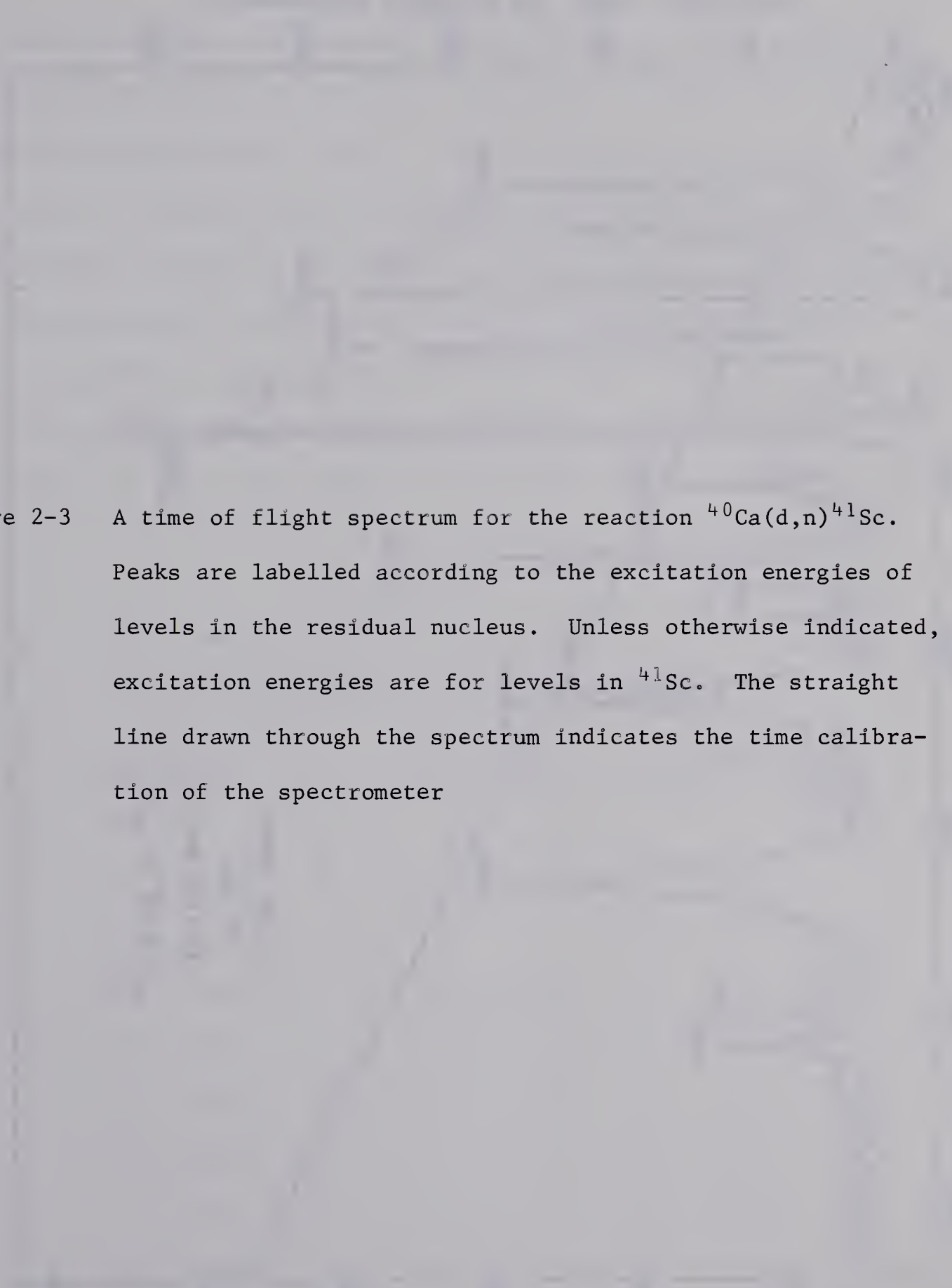


Figure 2-3 A time of flight spectrum for the reaction $^{40}\text{Ca}(\text{d},\text{n})^{41}\text{Sc}$. Peaks are labelled according to the excitation energies of levels in the residual nucleus. Unless otherwise indicated, excitation energies are for levels in ^{41}Sc . The straight line drawn through the spectrum indicates the time calibration of the spectrometer

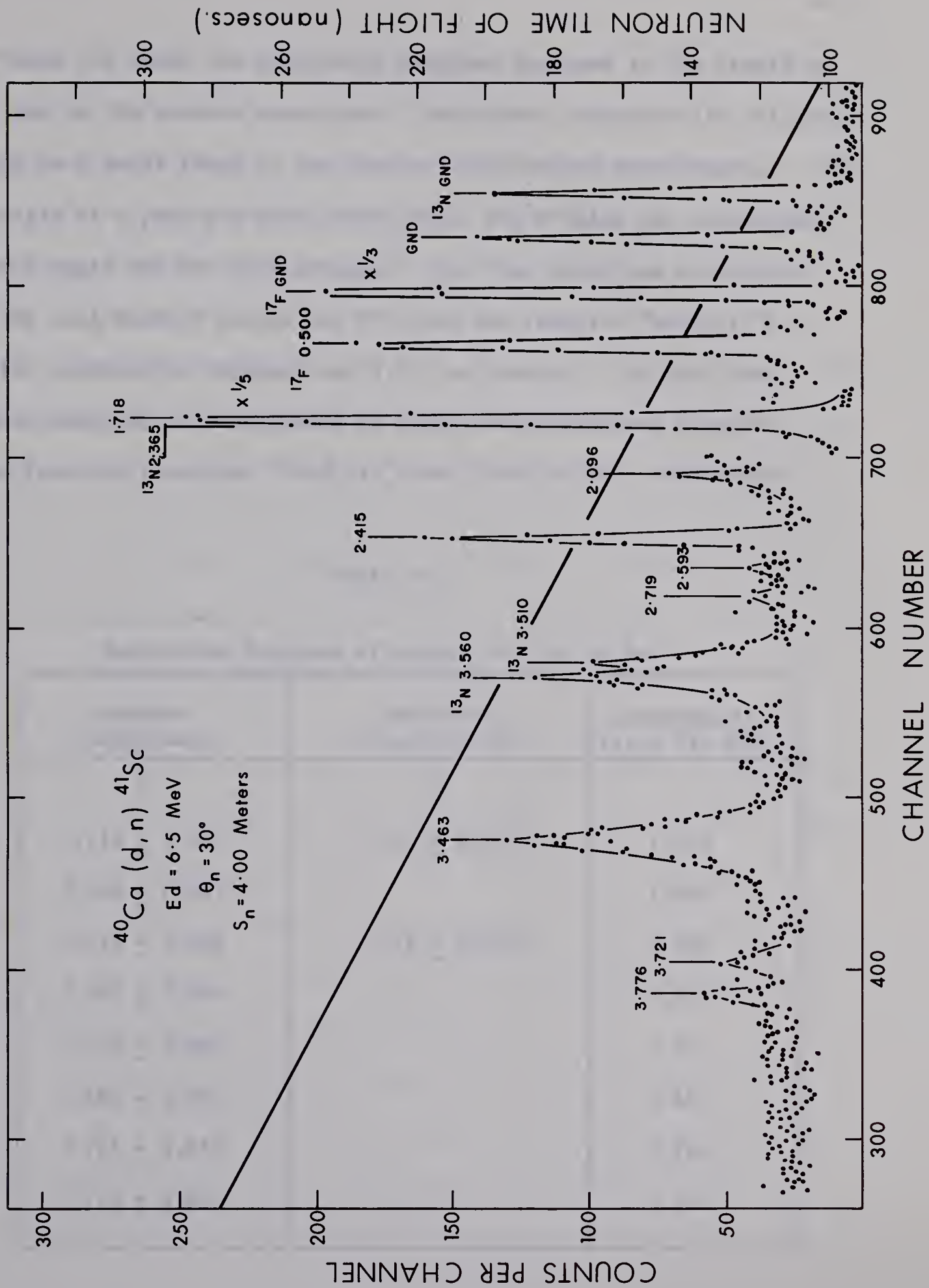


Table 2-1 shows the excitation energies assigned to the levels of ^{41}Sc seen in the present experiment. Peaks were kinematically followed through each angle taken in the angular distribution measurements. Once the origin of a peak had been established, the Q value was determined for each angle and the data averaged. The time scale was calibrated with the well known Q values (Aj 59) from the reaction $^9\text{Be}(d,n)^{10}\text{B}$. The time calibration obtained was 0.276 ns/channel. The zero time for each spectrum was determined by using the contaminant neutron groups from the reactions $^{16}\text{O}(d,n)^{17}\text{F}$ and $^{12}\text{C}(d,n)^{13}\text{N}$. Calibration

Table 2-1

Excitation Energies of Levels in ^{41}Sc in MeV

Present Experiment	Macefield (d,n) (Ma 61)	Youngblood (p, γ) (Yo 65)
0	0	
1.718 \pm 0.007	1.709 \pm 0.030	1.714
2.096 \pm 0.007		2.094
2.415 \pm 0.008	2.476 \pm 0.030	2.409
2.593 \pm 0.009		2.584
2.719 \pm 0.008		2.713
3.463 \pm 0.009		3.467
3.721 \pm 0.010		3.729
3.776 \pm 0.010		3.778

of the zero time in terms of these contaminant groups eliminated the effects of baseline shifts in the time analyzer. A Q value of -1.146 ± 0.006 was found for the transition to the ^{41}Sc ground state. The error quoted for this Q value arises from an error of ± 3 KeV in bombarding energy, a roughly estimated 3 KeV spread from target thickness, ± 3 KeV from errors in peak positions on the spectra and a ± 3 KeV spread from the transverse momentum imparted to the beam by the Mobley RF system. The present Q value for the ground state transition is in good agreement with the value of 1.147 ± 0.015 MeV previously found by Macefield (Ma 61). An excitation energy of 1.718 ± 0.007 found for the first excited state of ^{41}Sc is also in good agreement with the value of 1.709 ± 0.030 MeV found by Macefield (Ma 61). A weak level at an excitation energy of 2.096 ± 0.007 MeV, not observed by Macefield (Ma 61), was seen in the present experiment. A value of 2.476 ± 0.030 MeV found by Macefield for the excitation energy of the third excited state of ^{41}Sc is quite different from the present value of 2.415 ± 0.008 MeV. All excitation energies agree to within experimental errors with those recently obtained by Youngblood (Yo 65) in a $^{40}\text{Ca}(p,\gamma)^{41}\text{Sc}$ experiment. The excitation energies obtained by Youngblood, for the states seen in the present experiment, are presented in the third column of Table 2-1.

The results of the angular distribution measurements are shown in figures 2-4 to 2-9. The error bars shown with the experimental points indicate relative error only. They arise from statistical errors, background subtraction and the relative variation in detector efficiency.

Figure 2-4 $^{40}\text{Ca}(d,n)^{41}\text{Sc}$ ground state angular distributions at deuteron bombarding energies of 5.0, 6.0 and 6.5 MeV. Error bars are indicated except where they are smaller than the experimental points. The curves shown with each distribution are DWBA calculations

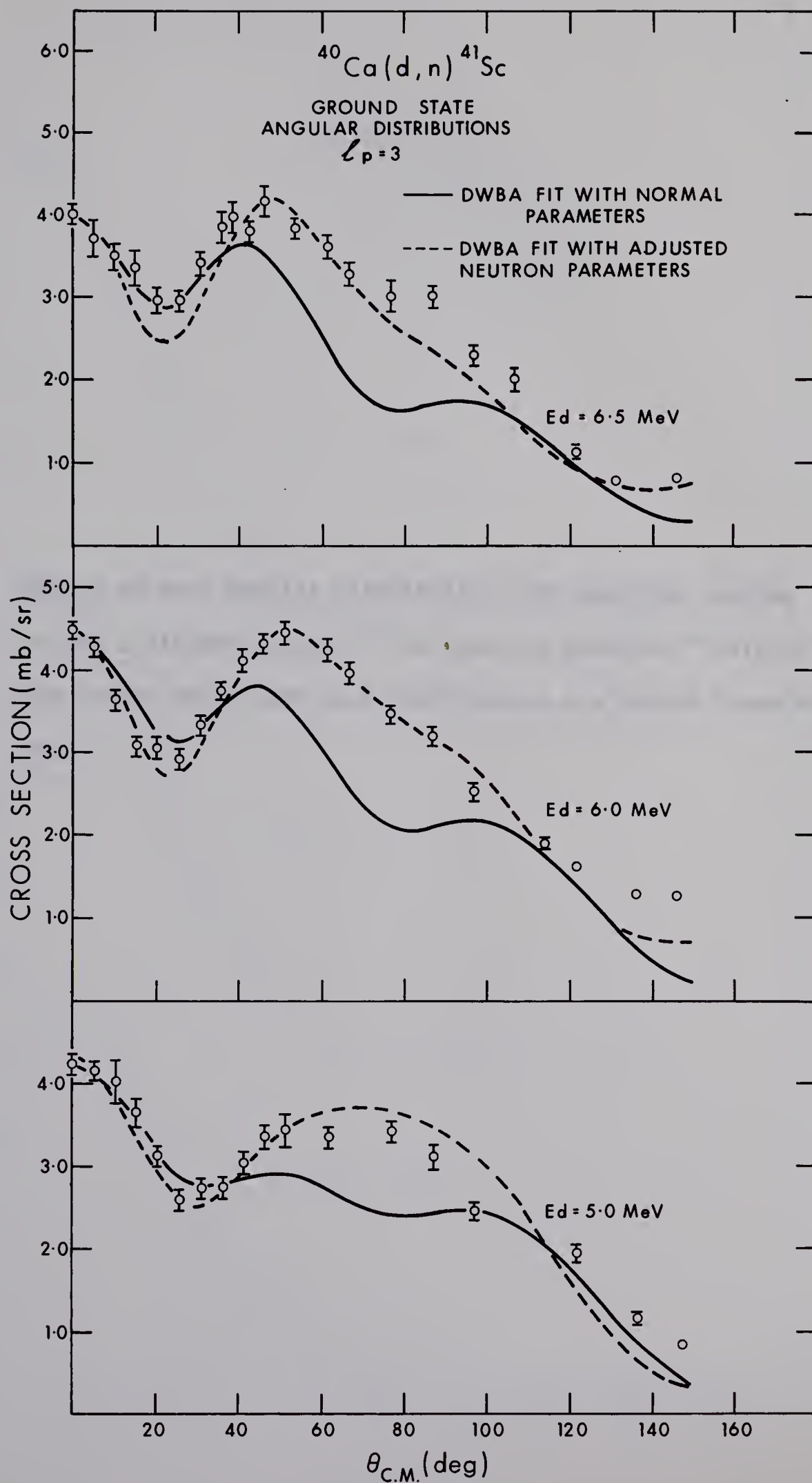


Figure 2-5 Centre of mass angular distributions for neutrons leading to the 1.718 MeV state of ^{41}Sc from the reaction $^{40}\text{Ca}(d,n)^{41}\text{Sc}$. The curves shown with each distribution are Butler Plane Wave fits

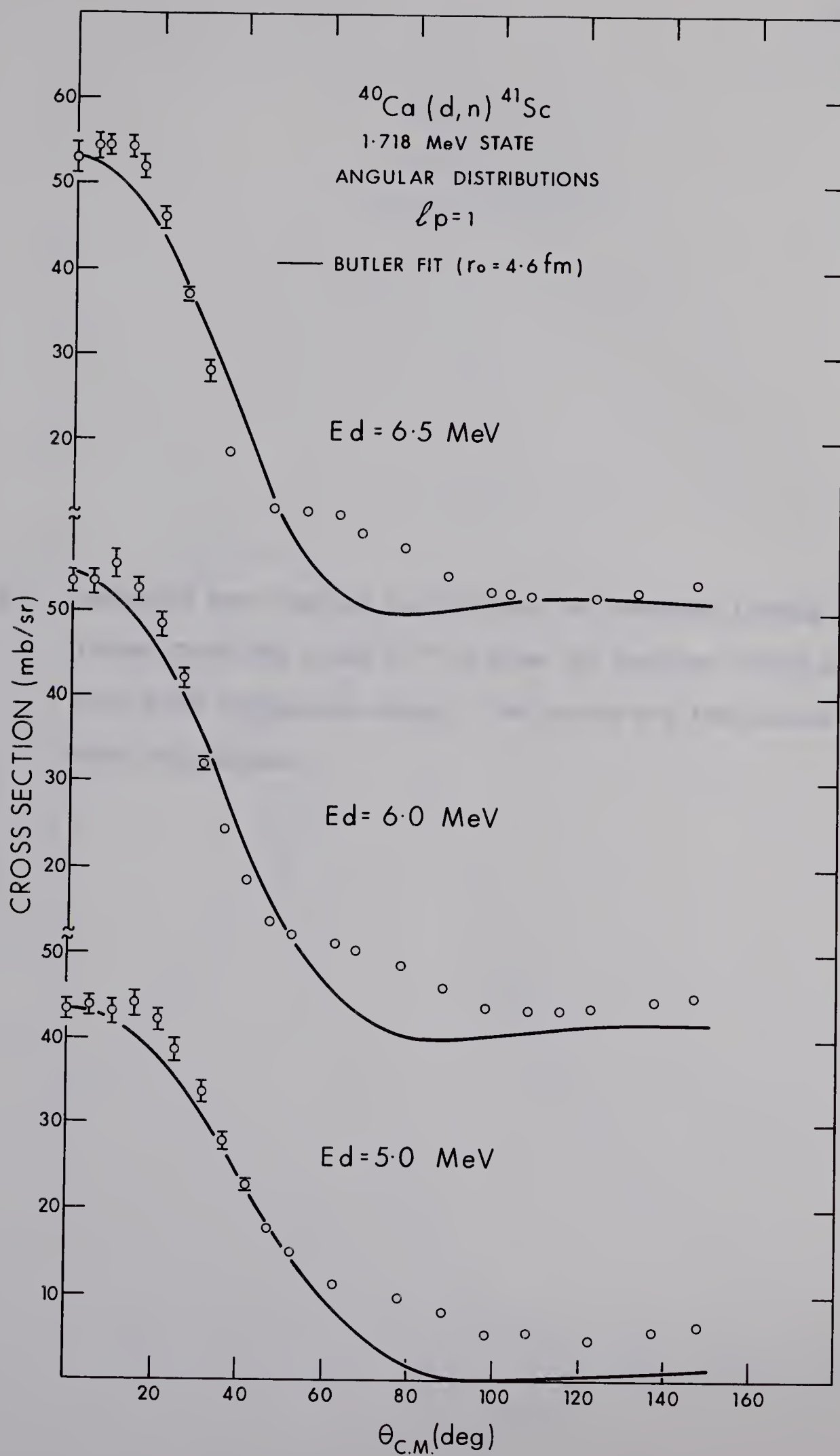


Figure 2-6 Centre of mass angular distribution for neutrons leading to the 2.096 MeV state of ^{41}Sc from the reaction $^{40}\text{Ca}(d,n)^{41}\text{Sc}$ at 5.0 MeV bombarding energy. The curves are from Butler Plane Wave calculations

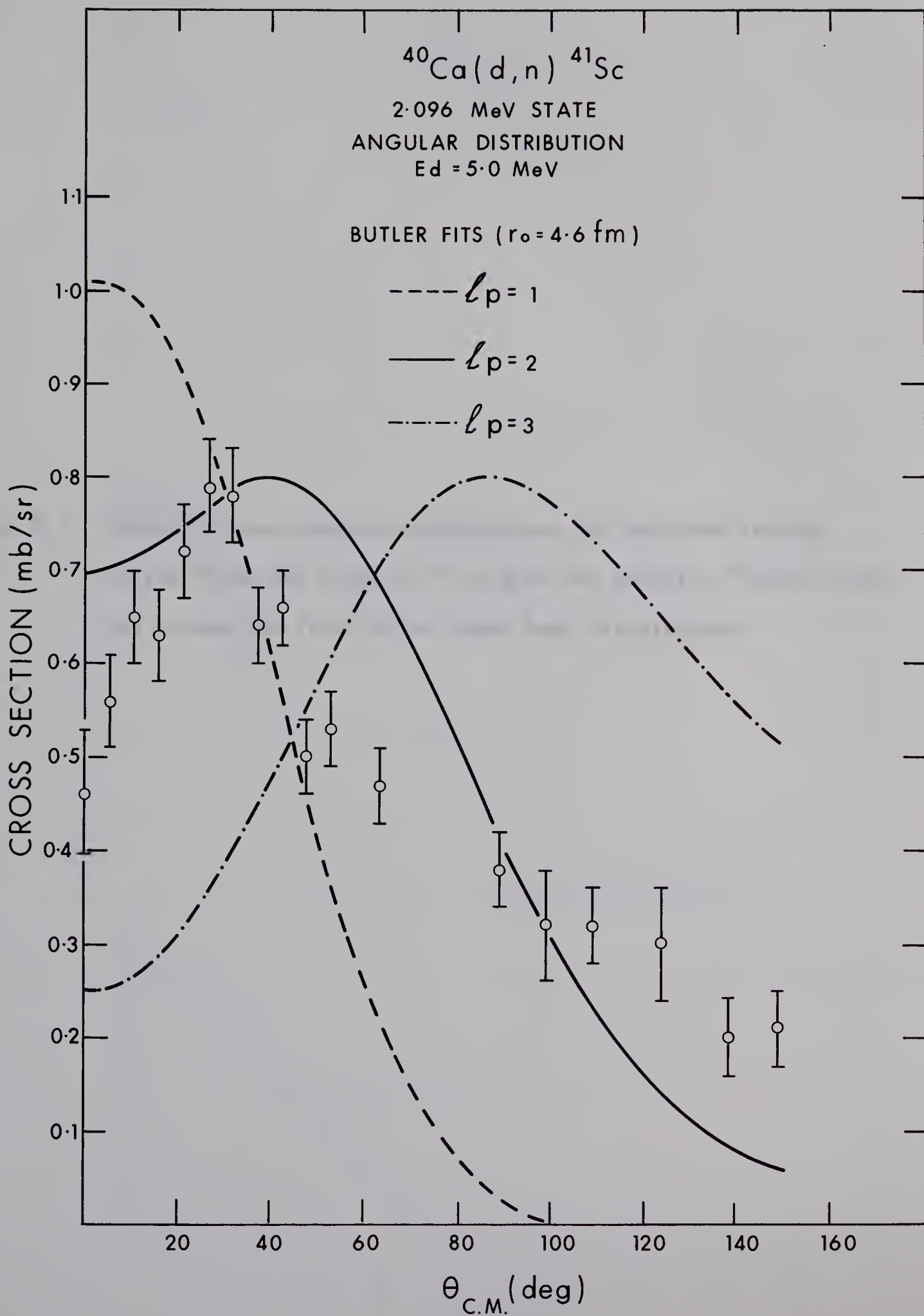




Figure 2-7 Centre of mass angular distributions for neutrons leading to the 2.415 MeV state of ^{41}Sc from the reaction $^{40}\text{Ca}(d,n)^{41}\text{Sc}$. The curves are from Butler Plane Wave calculations

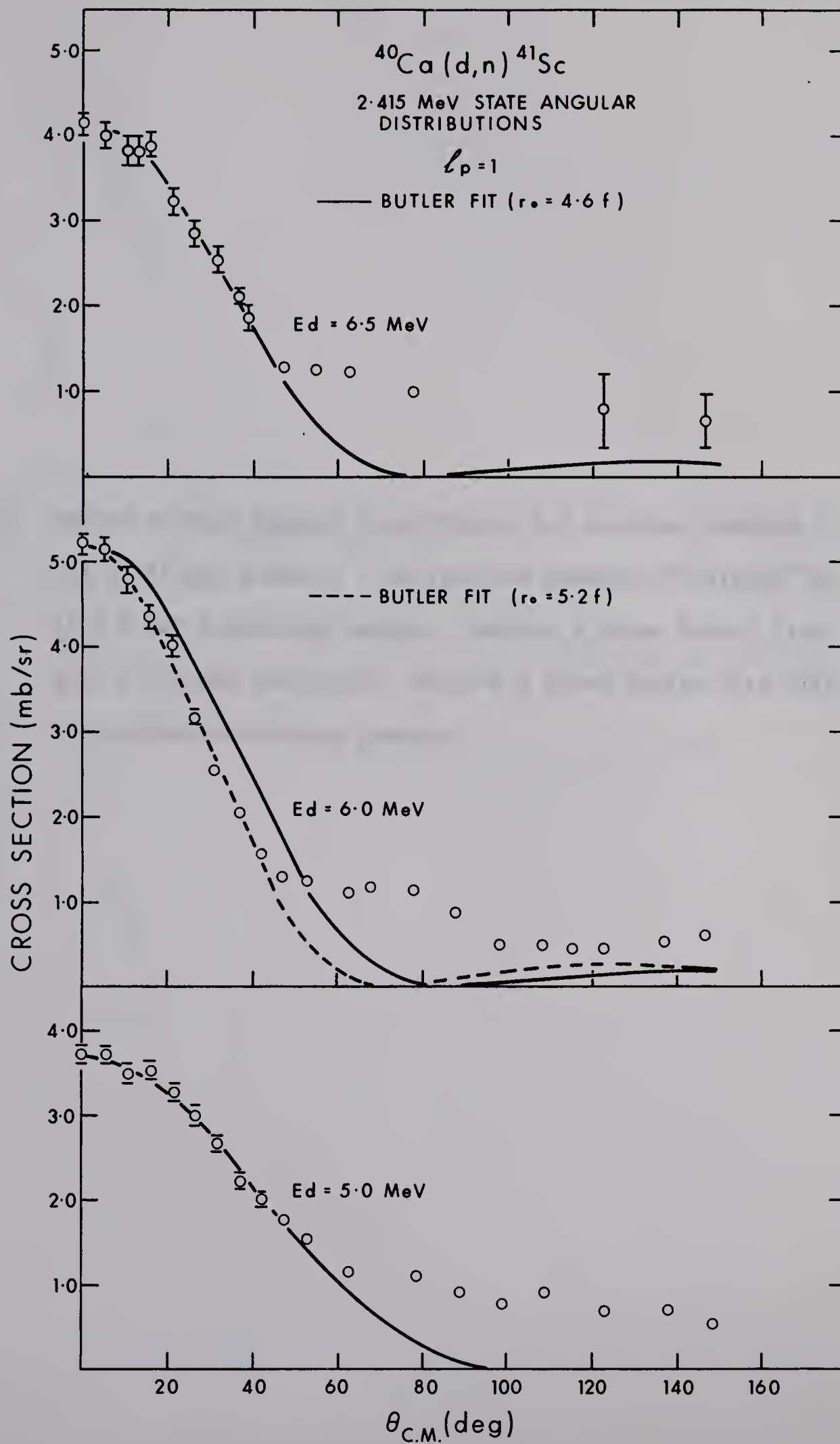
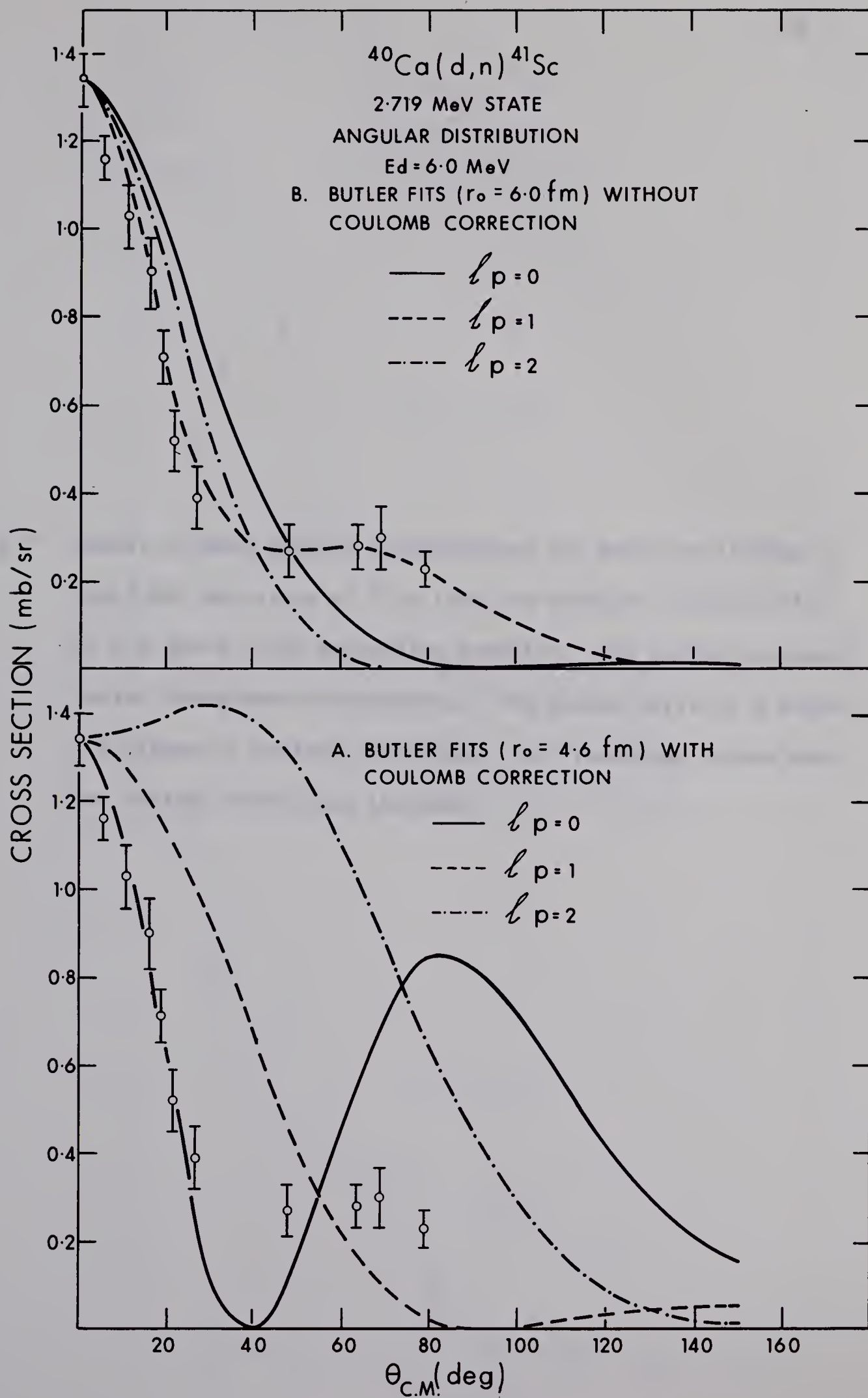


Figure 2-8 Centre of mass angular distribution for neutrons leading to the 2.719 MeV state of ^{41}Sc from the reaction $^{40}\text{Ca}(\text{d},\text{n})^{41}\text{Sc}$ at 6.0 MeV bombarding energy. Section A shows Butler fits with a coulomb correction, Section B shows Butler fits with the coulomb correction removed



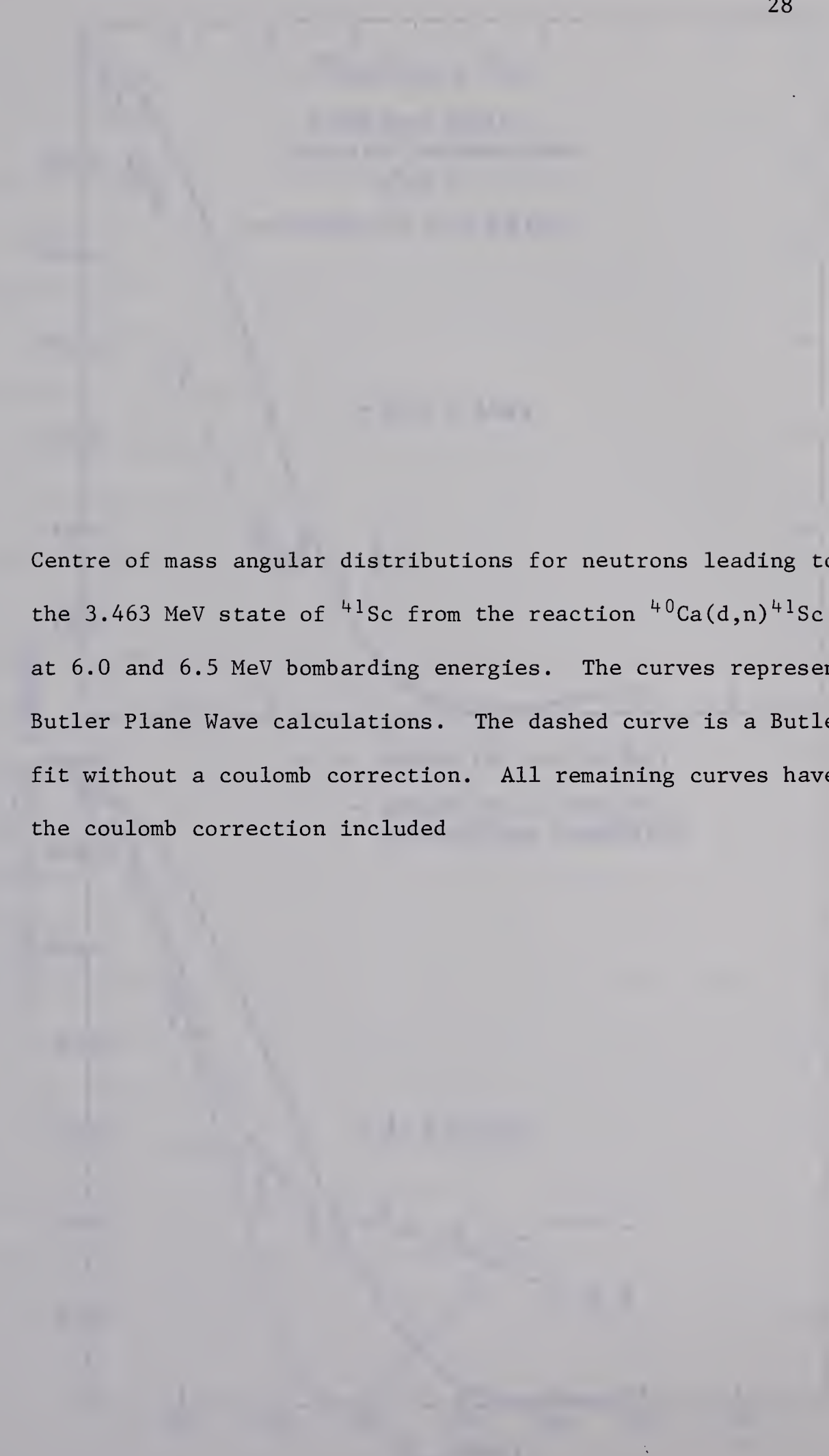
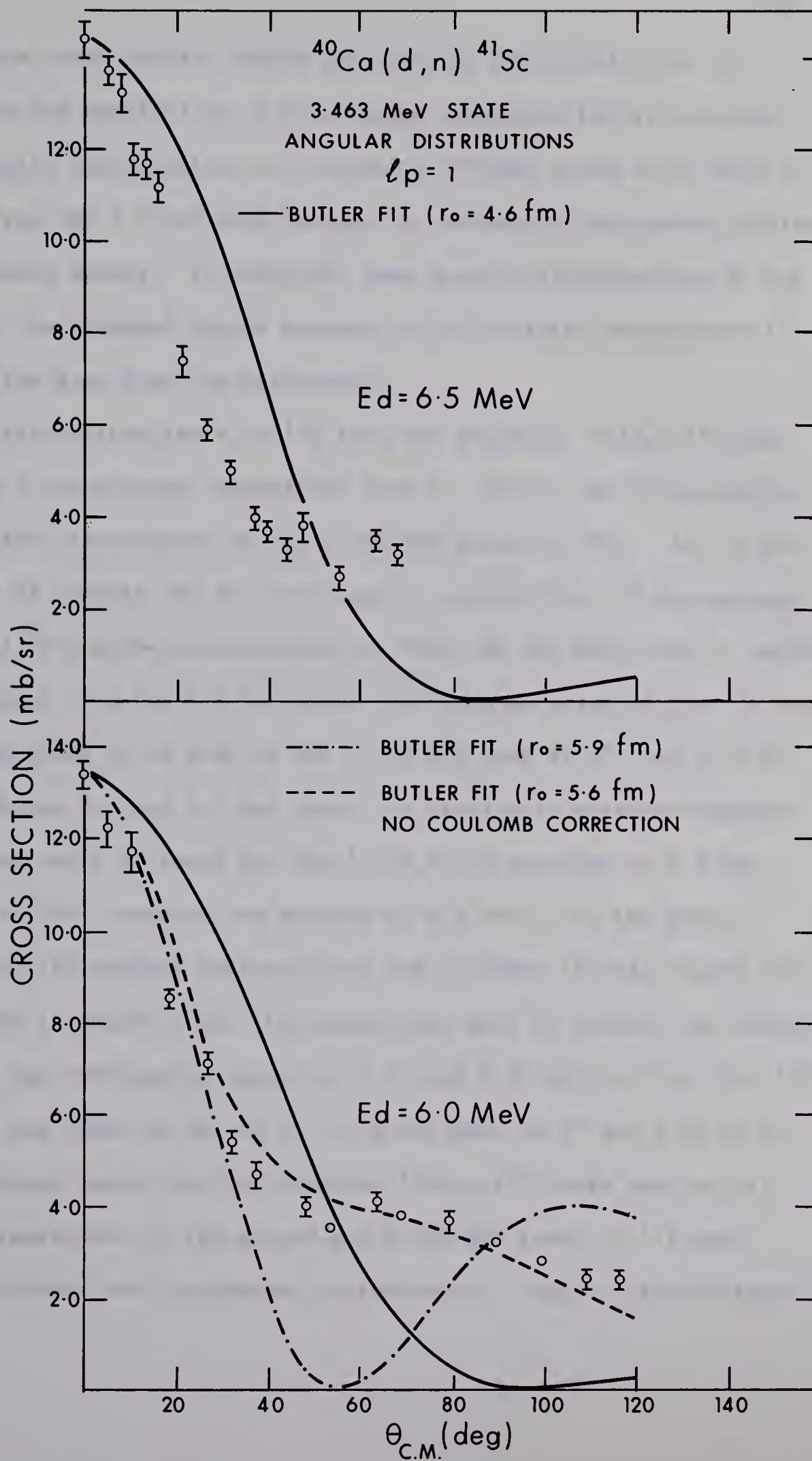


Figure 2-9 Centre of mass angular distributions for neutrons leading to the 3.463 MeV state of ^{41}Sc from the reaction $^{40}\text{Ca}(d,n)^{41}\text{Sc}$ at 6.0 and 6.5 MeV bombarding energies. The curves represent Butler Plane Wave calculations. The dashed curve is a Butler fit without a coulomb correction. All remaining curves have the coulomb correction included



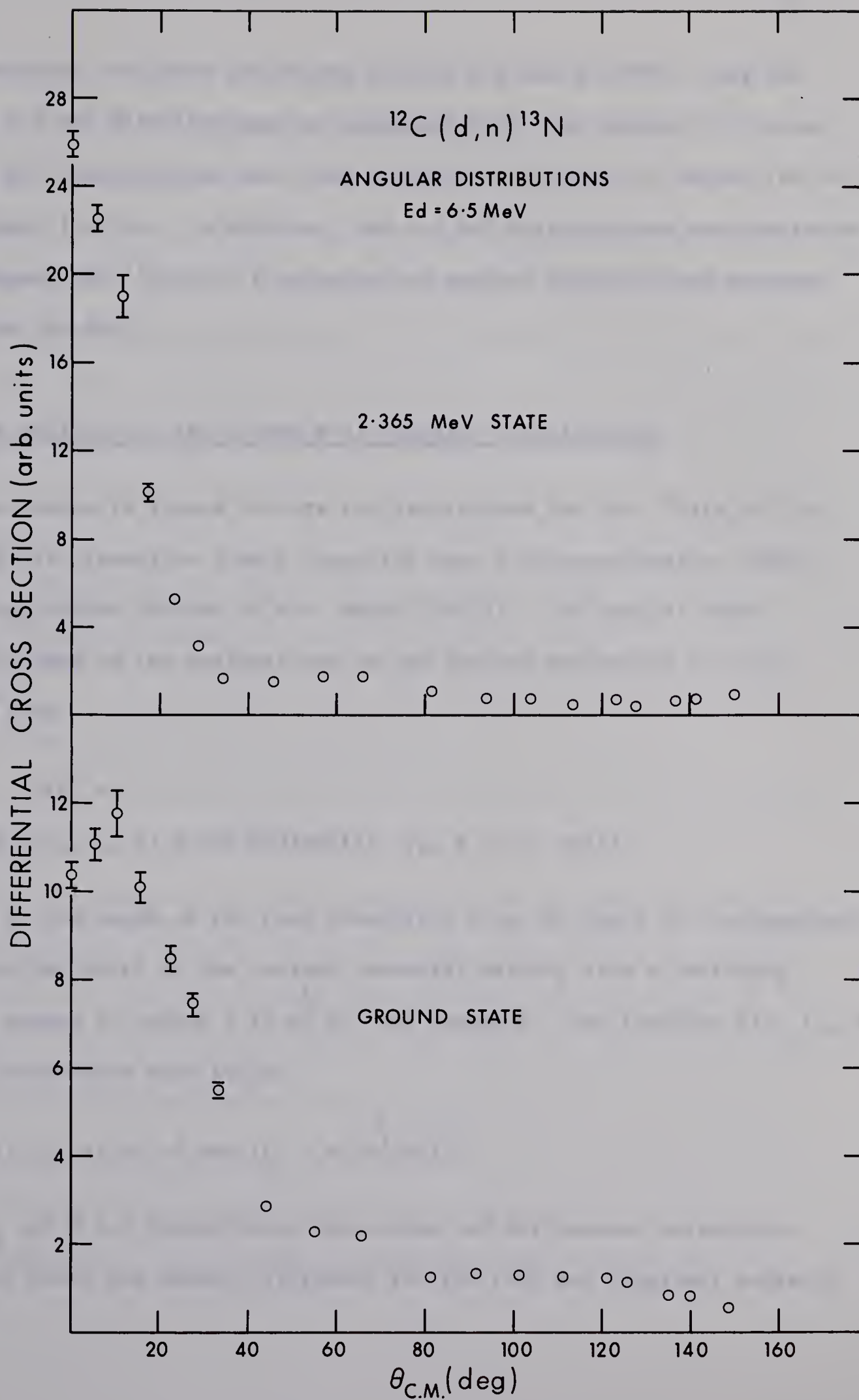
Absolute cross section values may have an additional error of $\pm 20\%$ due to the possibility of some target oxidation before weighing.

An angular distribution for the weak 2.096 MeV state could only be extracted from the 5.0 MeV data because of increasing background problems with increasing energy. In addition, some angular distributions do not extend into the backward angles because of difficulties encountered in extracting the data from the background.

The first excited state of ^{13}N from the reaction $^{12}\text{C}(\text{d},\text{n})^{13}\text{N}$ was found to be a troublesome contaminant from $0 - 45^\circ$ in the determination of the angular distribution of the 1.718 MeV state in ^{41}Sc . At 5.0 MeV, the results of Yaramis (Ya 61) were used to extract the ^{13}N contaminant. The $^{12}\text{C}(\text{d},\text{n})^{13}\text{N}$ angular distributions of Obst (Ob 66) were used to extract the contaminant from the 6.0 MeV data. The maximum value of the ^{13}N contaminant was found to be 4.5% of the 1.718 MeV peak at 0° , and 0.7% at 30° for both the 5.0 and 6.0 MeV data. No previously measured angular distributions could be found for the $^{12}\text{C}(\text{d},\text{n})^{13}\text{N}$ reaction at 6.5 MeV. Consequently, this reaction was studied at 6.5 MeV. For the sake of completeness, the angular distributions are included in this report and are presented in figure 2-10. No attempt was made to extract any information on the two overlapping states at 3.51 and 3.56 MeV in ^{13}N . The ^{13}N contaminant was found to be 14% of 1.718 MeV peak at 0° and 1.5% at 30° .

Contaminant peaks from the reaction $^{16}\text{O}(\text{d},\text{n})^{17}\text{F}$ were seen on all spectra. Transitions to the ground and 0.500 MeV level in ^{17}F were observed, but were not troublesome contaminants. Angular distributions

Figure 2-10 Centre of mass angular distributions for the ground state and 2.365 MeV state of ^{13}N from the reaction $^{12}\text{C}(\text{d},\text{n})^{13}\text{N}$ at a deuteron bombarding energy of 6.5 MeV. Error bars are shown where they exceed the size of the experimental points. Numerical values of these cross sections are presented in Appendix II



were extracted for these two states at 5.0, 6.0 and 6.5 MeV. Only the 6.0 and 6.5 MeV distributions are presented here (see section 2.7) since the 5.0 MeV distributions have been presented previously by Davies (Da 66) and Yaramis (Ya 61). In addition, the 6.0 MeV distributions were extracted to accompany the $^{16}\text{O}(\text{d},\text{n})^{17}\text{F}$ polarization angular distributions measured by Gedcke (Ge 67b).

2.4 DWBA Analysis of the Ground State Angular Distributions

The curves in figure 2-4 are the predictions for the $^{40}\text{Ca}(\text{d},\text{n})^{41}\text{Sc}$ ground state transition from a Distorted Wave Born Approximation (DWBA) stripping program written by W.R. Smith (Sm 65). The optical model potential used in the analysis was of the surface-absorption type and had the form

$$U(r) = -V f(r, r_0, a) + i4a'W(d/dr)f(r, r_0, a') + U_c(r)$$

where V is the depth of the real potential, W is the depth of the imaginary potential and $U_c(r)$ is the coulomb potential arising from a uniformly charged sphere of radius $1.25 A^{\frac{1}{3}}$ fm. and charge Z . The function $f(r, r_0, a)$ is the Woods-Saxon form factor

$$f(r, r_0, a) = \{1 + \exp [(r - r_0 A^{\frac{1}{3}})/a]\}^{-1}$$

where r_0 and a are respectively the radius and diffuseness parameters.

Note that these are usually different for the real and imaginary parts of

the potential. A finite range correction (Bu 64, Di 65) to the zero range approximation was included as an option in the program. This option was used throughout the present DWBA calculations.

The proton wave functions for the bound particle were calculated in a Woods-Saxon potential well with radius $r_0 = 1.25$ fm and diffuseness $a = 0.65$ fm. The proton potential had no imaginary part, but did include a derivative type of spin-orbit potential with a depth of 6.0 MeV. With these parameters, a well depth of 53.39 MeV was required for the $\ell = 3$ ground state transition to give the proton a binding equal to its separation energy.

Optical model parameters for the incoming channel were found from deuteron elastic scattering studies by Leighton (Le 67) on ^{40}Ca at the same energies as in the present experiment. These parameters are listed in Table 2-2 for the three energies studied.

Two sets of curves are presented in figure 2-4 for each bombarding energy studied. In each case, these represent two distinct sets of optical model parameters for the outgoing neutron channel. The solid curve represents calculations with the average set of neutron parameters due to Perey and Buck (Table 2-3) which were summarized by Rosen at the Karlsruhe Conference on Polarization, Sept., 1965 (Ro 66). The three solid curves are normalized to the experimental data at zero degrees and give spectroscopic factors 0.78, 0.83 and 0.81. The shape of the angular distribution is duplicated only at angles lower than 30° and greater than 110° . In all cases, the predicted second maximum at 45°

Table 2-2 Optical Model Parameters from deuteron elastic scattering on ^{40}Ca .

Deuteron Energy (MeV)	V (MeV)	W (MeV)	r_o (fm)	a (fm)	r_o' (fm)	a' (fm)	r_c (fm)
5.0	110.0	9.82	1.027	0.920	1.640	0.530	1.25
6.0	110.0	9.90	1.065	0.806	1.568	0.550	1.25
6.5	110.0	11.5	1.063	0.825	1.592	0.550	1.25

Table 2-3 Average neutron optical model parameters used in the analysis of the $^{40}\text{Ca}(d,n)^{41}\text{Sc}$ reaction.

Reference	V (MeV)	W (MeV)	r_o (fm)	a (fm)	r_o' (fm)	a' (fm)	r_c (fm)
Perey and Buck (Ro 66)	48 -0.29E	9.6	1.27	0.66	1.27	0.47	1.25
Rosen (Ro 66)	49.3 -0.33E	5.75	1.25	0.65	1.25	0.70	1.25
14 MeV Neutrons (Ro 66)	44	11	1.25	0.70	1.25	0.98	1.25

falls far below that observed experimentally and is approximately 5° out of phase. A more disturbing feature is a second minimum predicted at 80° which is not seen at all in the experimental distributions. A different set of neutron parameters developed by Rosen (Ro 66) and shown in Table 2-3 were tried in an attempt to produce more acceptable fits to the experimental data. These parameters gave angular distributions with essentially the same shape and magnitude as before. At this point, it was resolved to continue calculations with the neutron parameters of Perey.

The 6.0 MeV data was taken as representative and studied more exhaustively. The possibility was considered that the elastic scattering deuteron parameters were inadequate to describe the incoming channel. This possibility was tested by gridding the deuteron parameters over reasonable ranges. It was found that this procedure, in general, gave poor fits to the experimental data. Two features of this approach became obvious: (1) gridding gave spectroscopic factors which were highly unreasonable, in many cases considerably greater than unity (2) the unobserved minimum at 80° was present in all sets of calculations. To further check the incoming channel, ^{40}Ca deuteron elastic scattering parameters from studies at higher energies were tried. It has been pointed out by Perey (Pe 67) that one should expect the imaginary potential, W , to decrease in the application of high energy elastic scattering data to stripping at low energies. This can be understood as allowing fewer and fewer channels to be open for the breakup and absorption of the deuteron in elastic scattering

as fewer levels become available at lower and lower energies. Deuteron parameters sets from Bassel (Ba 64) (deuteron energies 7 - 12 MeV) and Perey (Pe 66) (deuteron energies 11.8 and 21.4 MeV) were tried with the reported values of W_d and with values stepped from 2 to 30 MeV. In no case was an acceptable fit obtained, even though in two cases the parameters above were successfully used to predict proper (d,p) stripping patterns on ^{40}Ca (Le 66), (Be 65). Some of the parameter sets published by Perey (Pe 66) contain a spin orbit term that was included in the present investigation. A zero range program written by B.E.F. Macefield* was used to do these calculations. No improvement in the fits was observed. It should be pointed out that the neutron parameter sets presented by Rosen and Perey contained a spin orbit term that was simply dropped in the calculations, since the program written by Smith had no provision for spin-orbit coupling. This approach was justified on the basis that calculations with the spin-orbit potential included in the Macefield program gave the same angular distribution as that obtained from the Smith program.

One might expect the deuteron parameters presented by Bassel (Ba 66) to work well in the energy range 5.0 to 6.5 MeV, since Strobel (St 66) has recently extended the 7.0 MeV parameters to $^{40}\text{Ca}(d,p)^{41}\text{Ca}$ stripping at 2.0 MeV and obtained acceptable fits. In this particular study, the same program written by Smith was used. At this energy, the angular distribution should be characterized strongly by Coulomb distortions. The acceptable

* B.E.F. Macefield, Program for calculating (d,p) and (d,n) polarization.

reproduction of the differential cross sections would suggest that Coulomb effects in the deuteron channel are being adequately calculated.

Two conclusions can be drawn from this study of the ingoing deuteron channel

- (1) the optical model parameters derived from elastic scattering at 5.0, 6.0 and 6.5 MeV give the best fits to the data.
- (2) It then seems probable that the average neutron parameters used in the outgoing channel are inadequate in the particular case of ^{41}Sc .

It is possible that compound nucleus effects are filling in the 80° minimum observed in the direct reaction calculations. In this case, one cannot expect to duplicate the cross sections observed experimentally, unless compound nucleus processes are accounted for. One might attempt such an analysis with the Hauser-Feshbach theory. These calculations are difficult since a large number of open channels are available in the present reaction, and these are mostly to nuclear states of unknown spin. There is some evidence that compound nucleus effects may be important at the neutron energies (3.8 - 5.3 MeV) produced in the present experiment. Figure 2-11 reproduces data from Wilmore (Wi 64) which shows neutron compound elastic cross sections on calcium. If one can extend this data to ^{41}Sc , it would indicate that compound elastic scattering can contribute up to a neutron energy of 7 MeV. Perey (Pe 62) in a study of neutron elastic scattering over an energy range of 0.38 to 24.0 MeV, and for elements higher than Cu found, as well, that 4.0 MeV is a transition region for the appearance of compound elastic effects. A program to

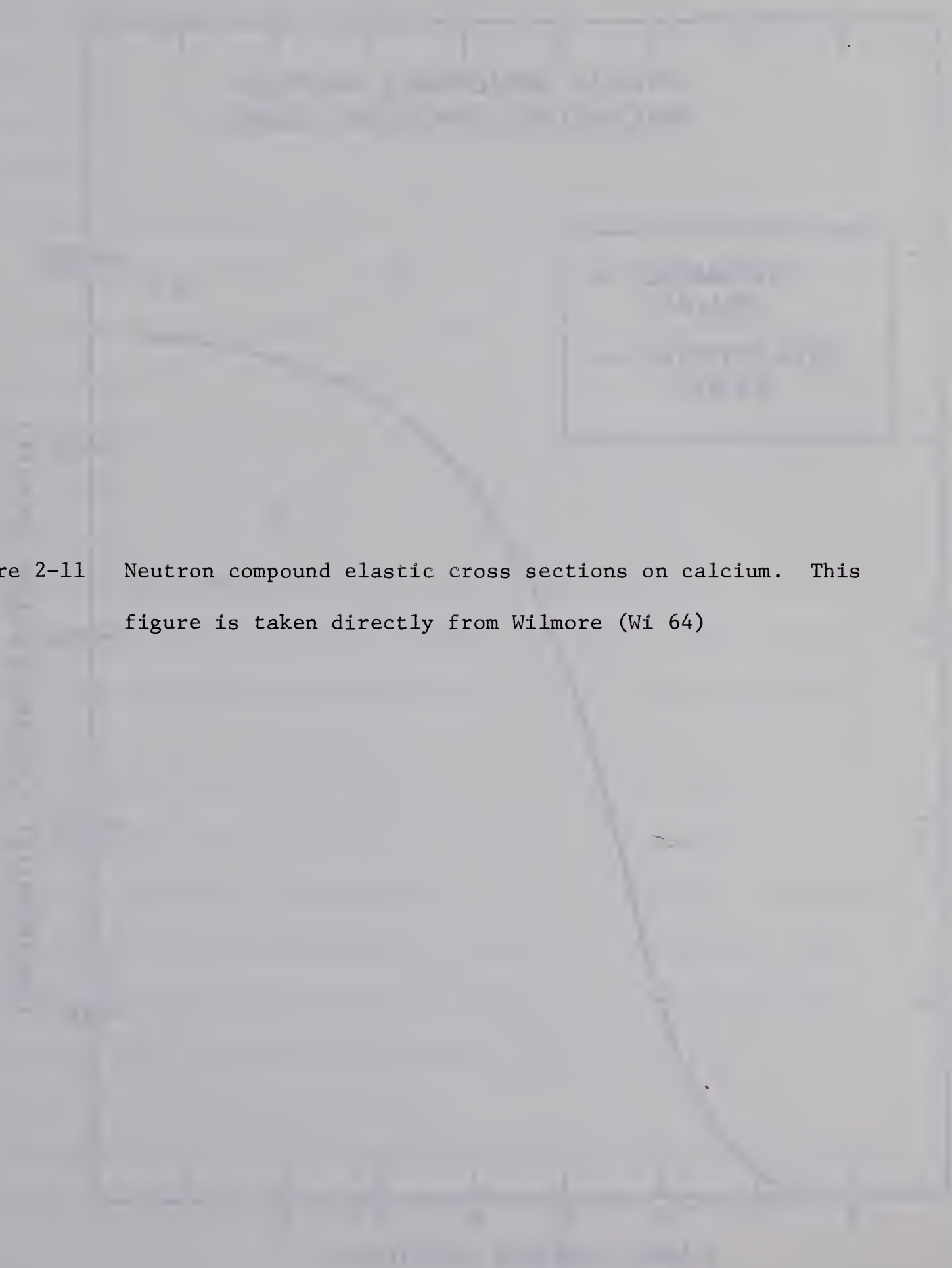
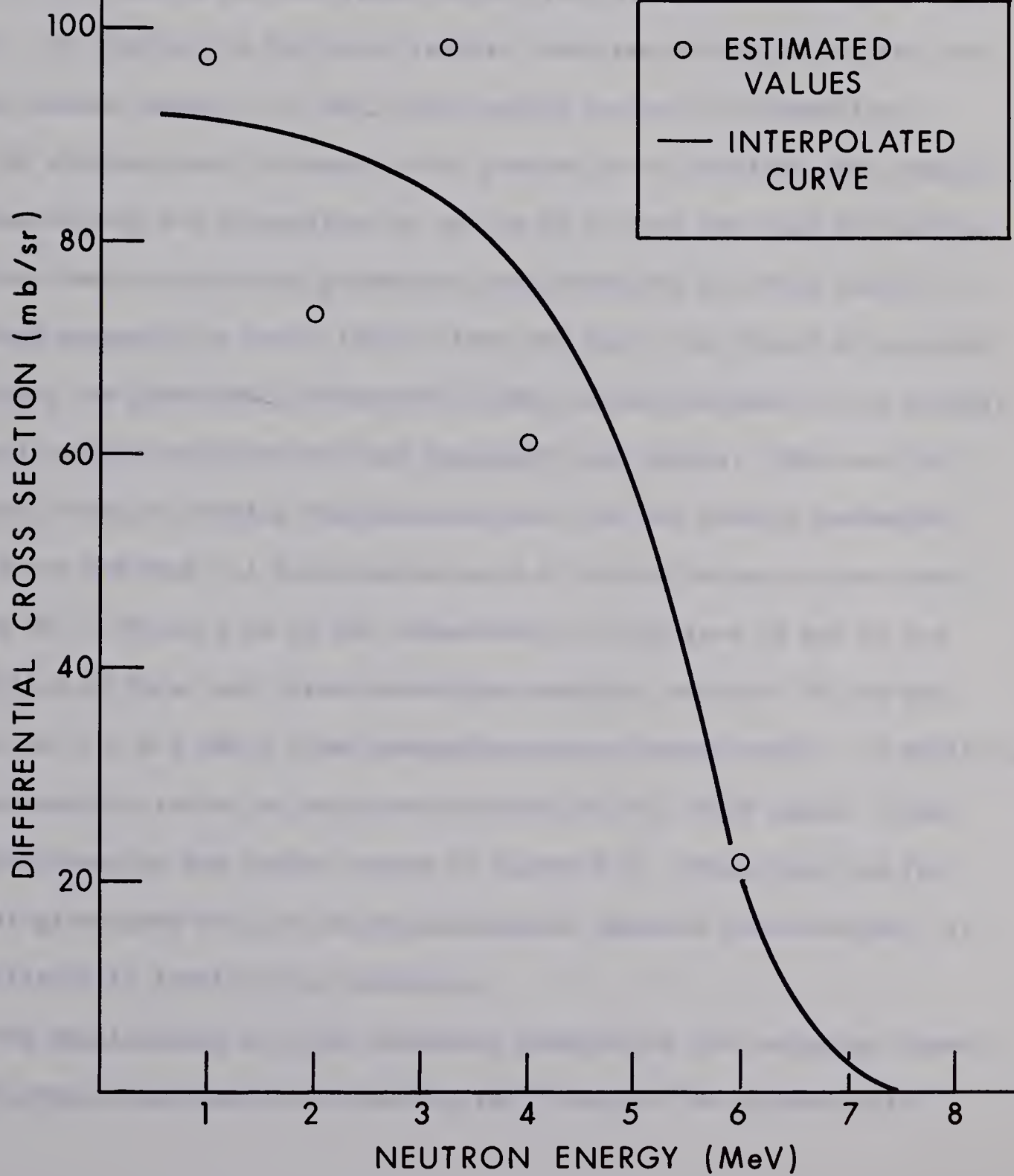


Figure 2-11 Neutron compound elastic cross sections on calcium. This figure is taken directly from Wilmore (Wi 64)

NEUTRON COMPOUND ELASTIC
CROSS SECTIONS ON CALCIUM



calculate the compound nucleus effects and test these arguments is now underway.

Calculations have been performed (Le 64) to estimate the contribution of compound processes to the $^{40}\text{Ca}(d,p)^{41}\text{Ca}$ angular distributions. It was found, particularly for the ground state, that the contribution was negligible. In contrast to the (d,n) results, this may be because of the much higher proton energy (> 13 MeV) that results in the (d,p) reaction.

An alternate way to approach the problem is to consider that compound nucleus effects are unimportant as in the (d,p) case and that the average neutron elastic scattering parameters are inadequate for this case. It has been suggested by Perey (Pe 67) that the best fits should be obtained by fixing the geometrical parameters (radii and diffuseness) of an average set and varying only the real and imaginary well depths. This was the approach taken in fitting the distributions with the neutron parameters from Perey and Buck. A simultaneous grid of V_n and W_n was carried over ranges 30 to 70 and 2 to 30 MeV respectively. This gave 55 MeV as the best value of V_n at all three bombarding energies, and $W_n = 12, 16$ and 18 MeV at 5.0, 6.0 and 6.5 MeV bombarding energy respectively. In addition, a spectroscopic factor of unity was obtained in all three cases. These fits are shown as the dashed curves in figure 2-4. Other than the fact that it gives good fits to the experimentally observed distributions, it is difficult to justify this procedure.

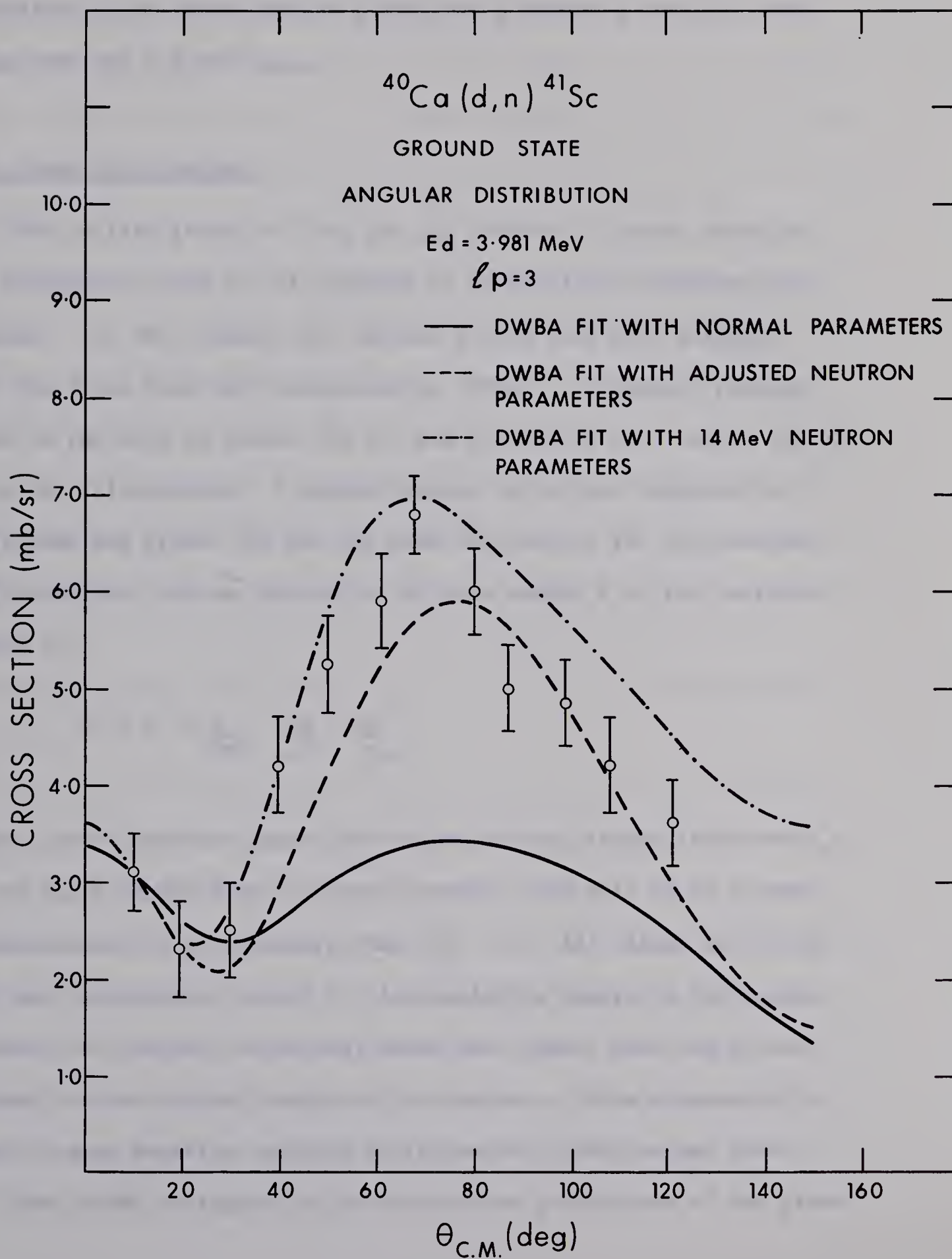
The implications of these parameter changes for the outgoing channel were further investigated by studying the $^{40}\text{Ca}(d,n)^{41}\text{Sc}$ ground state

angular distribution obtained by Macefield (Ma 61) at a bombarding energy of 3.981 MeV. The solid curve shown in figure 2-12 is a DWBA fit with the 6.0 MeV dueteron elastic scattering parameters, and the neutron parameters suggested by Perey and Buck, whereas the dashed curve is a calculation with the real part of the neutron potential equal to 55 MeV and the imaginary part equal to 16 MeV. The predicted cross section at zero degrees for the solid curve was 2.02 mb/sr, and for the dashed curve 1.36 mb/sr. It is seen that these values are too low compared with the experimental data (figure 2-12). This may simply be an expression of the fact that the proper deuteron elastic parameters are not being used. In addition, it may indicate that the cross sections quoted by Macefield are in error. The latter seems probable since it is suggested by Macefield that an error of 40% may exist because of possible target non-uniformities. Consequently, both curves in figure 2-12 have been normalized to the 10° data point. The resulting fits to the experimental data seem to support the adjusted parameters.

The additional curve shown in figure 2-12 was calculated with the 6.0 MeV deuteron elastic scattering parameters (Le 67) and the 14 MeV neutron parameters also presented by Rosen (Ro 66). This parameter set is given in Table 2-3. Of interest are the large values for the imaginary parameters, particularly 11 MeV for W_n and 0.98 fm for a'_n . It is probably these parameters that give rise to the peaking of the cross section of approximately 70° in agreement with the experimental data. This agreement with the 3.981 MeV distribution is probably only



Figure 2-12 Ground state angular distribution of neutrons from the reaction $^{40}\text{Ca}(\text{d},\text{n})^{41}\text{Sc}$ at a deuteron bombarding energy of 3.981 MeV. The experimental points are from Macefield (Ma 61). The curves shown with the data are DWBA calculations from the present work



fortuitous since these neutron parameters produced a poor fit when tried with the 6.0 MeV data.

2.5 Plane Wave Analysis

The excited states of ${}^4\text{Sc}$ are all unbound to proton emission, and therefore, could not be analyzed by an available distorted wave program. For this reason, the unbound states have been analyzed with the Plane Wave Born Approximation (PWBA). A computer program based on the work of Lubitz (Lu 57) was written by W.K. Dawson (Da 65) to do the calculations. A simple Coulomb correction suggested by MacFarlane and French (Ma 60) has been included in the calculations. The correction involves replacing the wave number k of the captured proton by

$$\bar{k}^2 = k^2 + \frac{A}{A+1} \frac{2M}{h^2} \frac{Ze^2}{r_0}$$

where A and M are the target and nucleon masses, respectively and r_0 is the usual interaction or cut-off radius. For this to be a good approximation, it is necessary that $\bar{k}r > 1$. All values of $\bar{k}r$ in this work are greater than 2.0. A singularity exists in the normal (without the coulomb correction) plane wave theory when the Q value is equal to the binding energy of the deuteron. This singularity is moved to more negative energies by inclusion of the Coulomb term.

The curves in figure 2-5 to 2-9 are the predictions of the plane

wave theory. In most cases, a single fit is shown for a particular ℓ value since the spin and parity of most levels seen in this study are known. In some cases, however, a number of fits are shown to point out the ambiguity that exists in determining both the cut-off radius and the ℓ value.

Figures 2-5 to 2-9 show the fits that were obtained for the transition to the excited states of ^{41}Sc at the bombarding energies 5.0, 6.0 and 6.5 MeV. Butler fits to the ground state were calculated for the purpose of finding relative reduced widths.

A cut-off radius of 4.6 fermis was chosen as giving the best fit to the data. Some individual cases, however, gave better fits for a larger radius. This is seen for instance in figure 2-7 where a radius of 5.2 fermis gave the best fit to the 2.415 MeV level at 6.0 MeV bombarding energy. The choice of a cut-off radius is thus somewhat uncertain.

Fits for the transitions to the two excited states at 1.718 and 2.415 MeV have been tried for $\ell = 1$ momentum transfer only (figures 2-5 and 2-7). Bock (Bo 65) finds excellent agreement in fitting $\ell = 1$ curves to transitions to these states as observed in the $^{40}\text{Ca}(^3\text{He},d)^{41}\text{Sc}$ reaction. The present results seem to confirm this assignment of $\ell = 1$.

Fits for the transition to the 2.096 MeV level were found for $\ell = 1$, 2 and 3, and are shown in figure 2-6. The data supports a somewhat uncertain assignment of $\ell = 2$ consistent with that found in a recent $^{40}\text{Ca}(^3\text{He},d)^{41}\text{Sc}$ experiment by Bock (Bo 65).

Figure 2-8A shows fits for $\ell = 0, 1$ and 2 transitions to the 2.719 MeV level. Figure 2-8B shows fits to this same data that are obtained when the Coulomb correction is removed. Of particular interest here is the exceptionally good agreement that is obtained for the $\ell = 1$ transition with a cut-off radius equal to 6.0 fermis. No clear cut assignment of $\ell = 1$ can, however, be made for this transition since the curves for $\ell = 0$ and 2 are insufficiently different. Alternatively figure 2-8A indicates the distinct differences that exist between the three ℓ values when the Coulomb term is included. A more positive assignment of $\ell = 0$ can thus be made for this transition. This is a more likely assignment than $\ell = 1$ since the mirror level at 2.68 MeV in ^{41}Ca has also been shown to be $\frac{1}{2}^+$ (Bo 65). A rather unpleasant feature of the $\ell = 0$ calculations that appears with the inclusion of the Coulomb term, and at large r_0 is a peaking of the distribution at backward angles. This effect is beginning to be evident as well for the $\ell = 1, 3.463$ MeV transitions (figure 2-9) with a cut-off radius equal to 5.9 fermi.

A tentative assignment of $\ell = 1$ can be made for the 3.463 MeV transition shown in figure 2-9. An exceptionally good fit is obtained for the $\ell = 1$ calculation without the Coulomb correction, but again the $\ell = 0$ and 2 calculations are not sufficiently different to allow an unambiguous assignment. With the Coulomb term included and with a cut-off radius equal to 4.6 fermis, both $\ell = 0$ and 2 gives quite unacceptable fits. From figure 2-9, it is obvious that a cut-off radius of 4.6 fermis does not reproduce the quality of fit observed for lower excited states,

however, a radius of 5.9 fermis reproduces at least the observed forward angle stripping.

Relative reduced widths (Ma 60) have been extracted from the plane wave analysis at 6.0 MeV bombarding energy, and are presented in Table 2-4.

Table 2-4 Relative reduced widths from a plane wave analysis of the $^{40}\text{Ca}(d,n)^{41}\text{Sc}$ data at 6.0 MeV bombarding energy

Excitation Energy (MeV) of ^{41}Sc Level	Relative Reduced Width θ^2
0	1.0
1.718	2.7
2.415	0.42
2.719	1.1
3.463	5.4

2.6 DWBA Fitting of Unbound States

It has been pointed out before that the excited states of ^{41}Sc are all unbound to proton emission and therefore, could not be analyzed by an available distorted wave program. The theory for a program which can treat unbound levels has been outlined by Huby and Mines (Hu 65) and has been used in calculations for the unbound 5.08 MeV state in ^{17}O observed in the reaction $^{16}\text{O}(d,p)^{17}\text{O}$ (Al 67).

In the absence of such a program, it has been usual to use an available distorted wave program with the binding energy adjusted to just bind the captured particle in a Woods-Saxon potential well. This procedure was adopted by Sheppard (Sh 64) and Bock (Bo 65) in a study of the $^{40}\text{Ca}(^3\text{He},d)^{41}\text{Sc}$ reaction and is also used here for a study of the $^{40}\text{Ca}(d,n)^{41}\text{Sc}$ reaction. The calculations for the present work were carried out with a DWBA program obtained from Hutton.* This program was used since the binding energy is a readily adjustable parameter whereas it is not in Smith's program.

The procedure of adjusting the binding energy is at best a crude approximation. For the first excited state, it may be justified on the basis of the lifetime of the state. Youngblood (Yo 65) has reported the lifetime of this state to be $(5.2 \pm 1.5) \times 10^{-13}$ sec (Yo 65) which is quite long compared to the 10^{-21} sec expected for the direct reaction. One can thus argue that the captured particle is indeed, bound during the time that the direct reaction takes place. It is not possible to evaluate the assumption that higher excited state can be considered bound since lifetimes have not been measured. However, states at about 6.0 MeV excitation in ^{41}Sc have an energy width of 50 to 250 KeV as seen in the $^{40}\text{Ca}(p,\gamma)^{41}\text{Sc}$ reaction (Sh 64), which is an indication that proton emission is still somewhat inhibited by the Coulomb barrier.

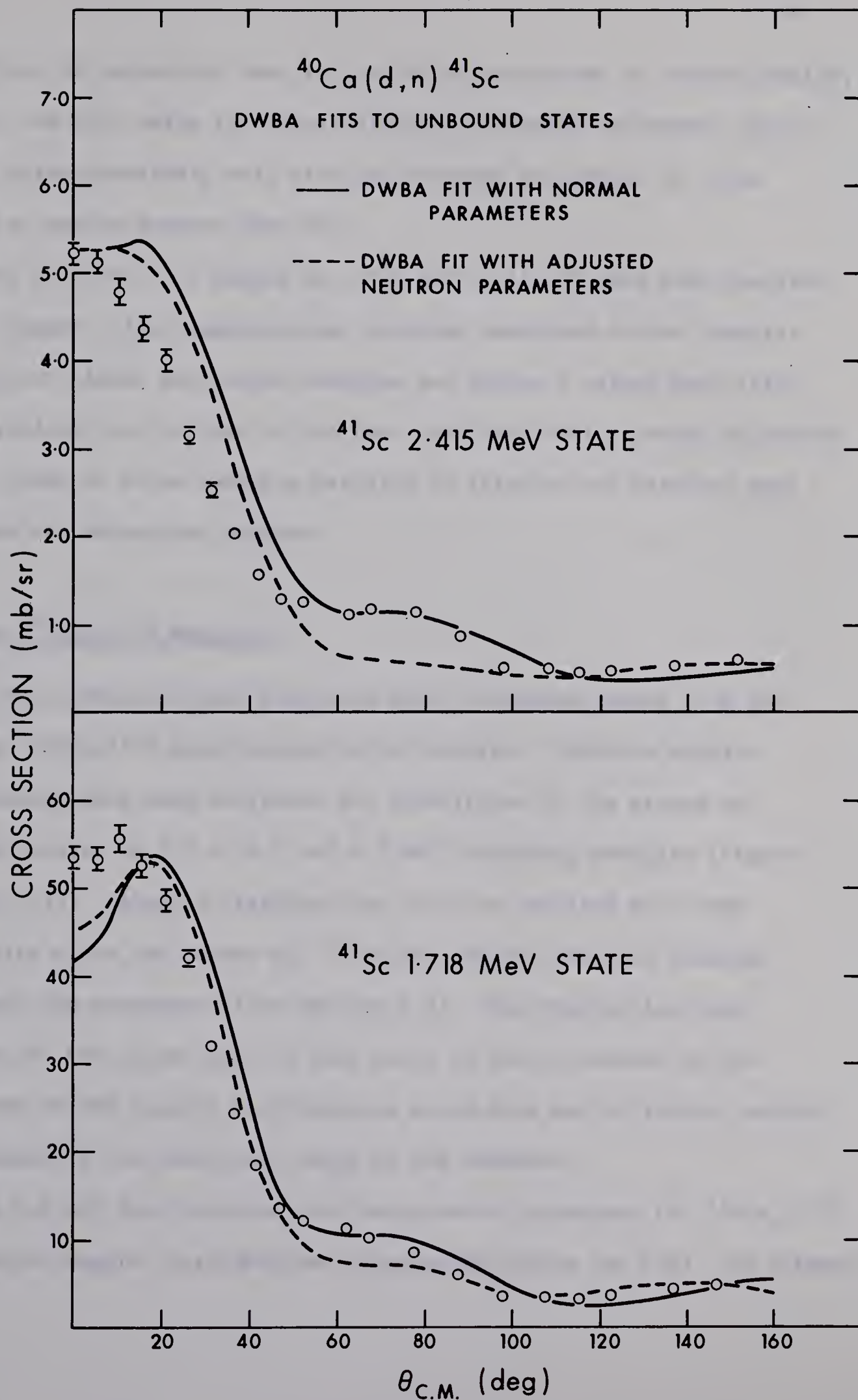
Sheppard (Sh 64) has used a binding energy of 1.0 MeV for calculation

* L. Hutton, Dept. of Theoretical Physics, University of Liverpool, Liverpool, England.

of stripping patterns for unbound levels excited in the $^{40}\text{Ca}(^3\text{He},d)^{41}\text{Sc}$ reaction. In the present experiment, a binding energy of 0.2 MeV was used for initial attempts at fitting transitions to unbound levels. It was found that the shape of the angular distributions are not influenced much by the value of the binding energy used. The predicted cross sections and consequently, the spectroscopic factors did, however, change as the binding energy was varied. When plotted as a function of binding energy, the spectroscopic factors decreased almost linearly with decreasing binding energy. Indeed, as the binding energy approached 0.2 MeV, the variation was well approximated by a straight line. There is a temptation to extrapolate linearly to the correct binding energy for the state in question. If this is done, it gives 0.95 as the spectroscopic factor for the first excited state of ^{41}Sc at 1.718 MeV and 0.04 for the state at 2.415 MeV, or a total strength of 0.99 for the two components of the $2P_{\frac{3}{2}}$ single-particle strength. The present values are also in good agreement with 0.91 and 0.09 found by Bock (Bo 65) in the analysis of the $^{40}\text{Ca}(^3\text{He},d)^{41}\text{Sc}$ reaction at 18.05 MeV bombarding energy. No justification can be given for this approach as it is purely spectralative.

Figure 2-13 shows fits for the states at 1.719 and 2.415 MeV obtained with the binding energy set equal to 0.2 MeV. The solid curves were obtained with the deuteron elastic scattering parameters from Leighton (Le 67) and the neutron parameters from Perey and Buck (Ro 66). The dashed curves were calculated with the neutron real and imaginary well depths equal to 55 and 16 MeV, respectively, as discussed in Section 2.4.

Figure 2-13 DWBA fits to the $^{40}\text{Ca}(d,n)^{41}\text{Sc}$ transitions leading to the unbound levels at 1.718 and 2.415 MeV in ^{41}Sc . The transferred proton is assumed to be bound to the target nucleus with a binding energy of 0.2 MeV. Each curve has been normalized to the data at the maximum calculated value



Neither set of parameters seem to fit the distributions at forward angles, however, the fits using the normal elastic scattering parameters (solid curves) agree remarkably well with the observed variations in cross section at angles greater than 60° .

Only the two $\lambda = 1$ states at 1.718 and 2.415 MeV have been analyzed in this manner, since computational problems developed in the computer program when higher excitation energies and higher λ values were tried. These problems were related to the fact that the binding energy adjustment was too large to allow adequate matching of interior and exterior wave functions at the nuclear surface.

2.7 The $^{16}\text{O}(\text{d},\text{n})^{17}\text{F}$ Reaction

It has previously been mentioned that contaminant peaks from the reaction $^{16}\text{O}(\text{d},\text{n})^{17}\text{F}$ were present on all spectra. Relative angular distributions have been extracted for transitions to the ground and 0.500 MeV states of ^{17}F at 6.0 and 6.5 MeV bombarding energies (figures 2-14 and 2-15). Angular distributions could be obtained with some reliability since the amount of ^{16}O on the targets remained constant throughout the experiment (see Section 2.2). The observation that oxidation of the target did not take place is also evidenced by the smoothness of the angular distributions since data was collected randomly with respect to the laboratory angle of the detector.

The 6.0 MeV distributions were extracted to accompany the $^{16}\text{O}(\text{d},\text{n})^{17}\text{F}$ polarization angular distributions measured by Gedcke (Ge 67b). An attempt

Figure 2-14 Centre of mass angular distributions for neutrons leading to the ground state of ^{17}F from the reaction $^{16}\text{O}(\text{d},\text{n})^{17}\text{F}$ at bombarding energies of 6.0 and 6.5 MeV. The curves shown with the 6.0 MeV data are DWBA fits. Error bars are shown where they exceed the size of the experimental points

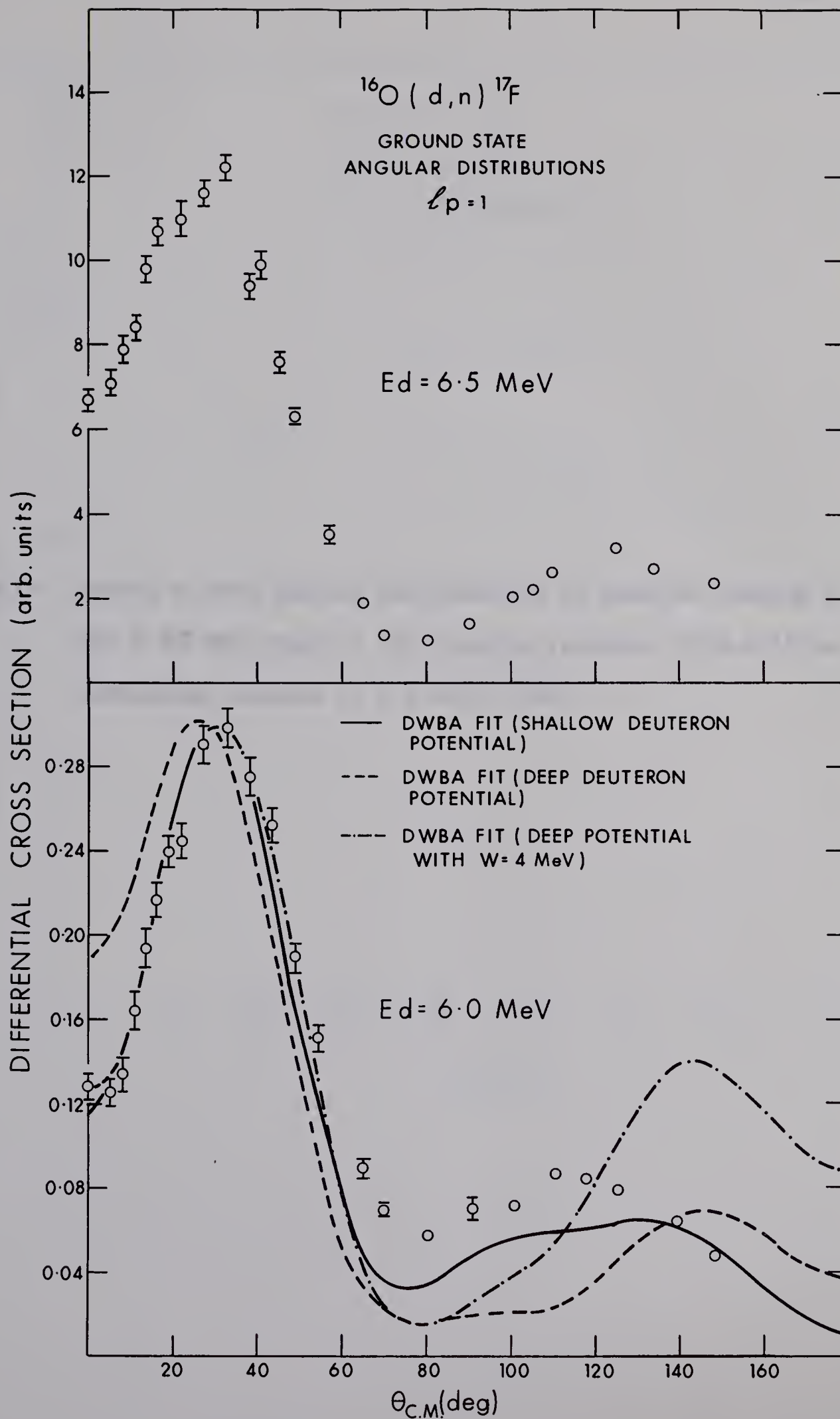
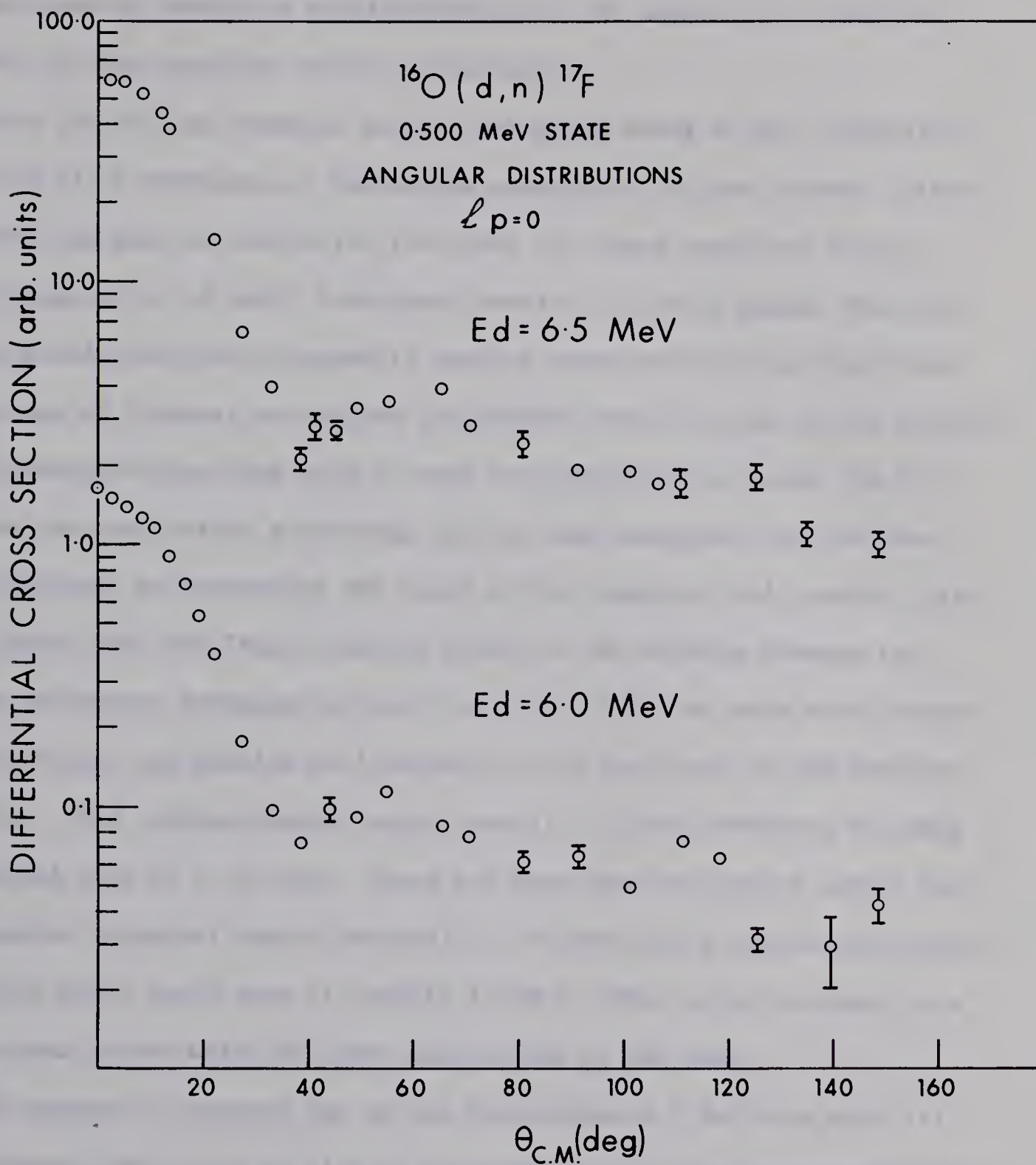


Figure 2-15 Centre of mass angular distributions of neutrons leading to the 0.500 MeV state of ^{17}F from the reaction $^{16}\text{O}(\text{d},\text{n})^{17}\text{F}$ at bombarding energies of 6.0 and 6.5 MeV



has been made by Gedcke to simultaneously fit the angular distributions observed in this reaction and the polarization.

Alty (Al 67) has recently made an extensive study of the $^{16}\text{O}(\text{d},\text{d})^{16}\text{O}$ and $^{16}\text{O}(\text{d},\text{p})^{17}\text{O}$ reactions at bombarding energies of 11 and 12 MeV. Little structure was seen in excitation functions for these reactions over an energy range 10 to 13 MeV. From their results, it would appear that the optical model condition of smoothly varying cross sections was fulfilled.

It was of interest to analyze the present data in terms of the optical model parameters from this work to test the contention of Perey (Pe 67), that one can use elastic scattering data at high energies, for the same target nucleus, by decreasing the value of the imaginary well depth. Also, it was hoped that the (d,n) reaction might aid in choosing between two sets of parameters presented by Alty (Al 67). These two sets were characterized by deep and shallow well depths for the real part of the deuteron potential. The shallow depths ranged from 31 - 55 MeV, whereas, the deep ones ranged from 75 - 157 MeV. There has been some indication lately that the deuteron potential should be equal to the sum of the neutron and proton potentials which would make it roughly 110 MeV. This is in contrast to a value around 50 MeV which has been used widely in the past.

The method of approach was to fit the present 6.0 MeV data with all the parameter sets found by Alty in the analysis of 12 MeV deuteron elastic scattering without adjusting any parameters. The best fit to the data was obtained with a parameter set from the shallow potentials. In particular, this set had real and imaginary well depths of 55.33 and 3.85 MeV, respec-

tively. This fit is shown as the solid curve in figure 2-14. The calculated distribution has been normalized to data at the forward maximum. It is seen that this first maximum is fairly well reproduced. As well, the shape, but not the amplitude of the secondary maximum at 110° is reproduced.

The dashed curve shown in figure 2-14 was calculated with a deep deuteron potential. The set with a real depth equal to 109.57 MeV was chosen since this corresponded closely to the potential used for the $^{40}\text{Ca}(d,n)^{41}\text{Sc}$ analysis (Table 2-2). This fit is characterized by a poor reproduction of both the main and secondary stripping maxima.

Next, a number of the parameter sets from Alty (Al 67) were tried and the imaginary well depth stepped from 2 to 20 MeV in each case. In general, only very minor improvements were seen for the shallow potential sets. However, marked improvements were observed when W for the deep potential sets was reduced below that found by Alty (Al 67). An example of the quality of fit observed is shown by the dot-dashed curve shown in figure 2-14. The deuteron well depth is again 109.57, but now the imaginary depth has been reduced from 9.18 to 4 MeV. Excellent reproduction of the forward maximum was observed even to a small rise in the cross section at zero degrees. However, even poorer agreement than with the unchanged imaginary depth is observed for the secondary maximum at 110° .

In answer to the questions posed, it appears that the results from high energy elastic scattering can be used at lower energies, but should

only be expected to reproduce the main features of the stripping pattern. In addition, it is not possible to choose without ambiguity between the shallow and deep deuteron potentials. It would seem that a DWBA analysis of this kind has not enough information content to decide on the proper deuteron potential.

2.8 Discussion

A considerable amount of experimental data has been extracted from studies of the $^{40}\text{Ca}(d,n)^{41}\text{Sc}$ reaction at deuteron bombarding energies of 5.0, 6.0 and 6.5 MeV. Analysis of this data in terms of a Distorted Wave Program was limited to the ground state transition since excited states are unbound to proton emission. Considerable spectroscopic information could be extracted from this data if a program were available that adequately described stripping to unbound levels. One could, for instance, establish whether the total $2P_{\frac{3}{2}}$ strength is contained in two levels at 1.718 and 2.415 MeV as suggested by Bock (Bo 65) and whether the state at 3.463 MeV carries an appreciable fraction of the $2P_{\frac{1}{2}}$ strength. Of considerable interest also would be a determination of the strengths of the $\ell = 2$ level at 2.096 MeV, and the $\ell = 0$ level at 2.719 MeV. This could give information on the extent to which ^{40}Ca can be considered a good closed shell nucleus since in the extreme single particle model even parity states should not occur in low-lying level structure of ^{41}Sc . Attempts have been made to extract spectroscopic information from these unbound levels by adjusting the binding energy of the captured particle. This information is, however, open to

question because of the approximations required to do the calculations.

Attempts to describe the experimental data in terms of the Butler Plane Wave Theory have met with only partial success in the present study. It has been demonstrated that for unbound states Butler theory, without a Coulomb term, is inadequate to determine even the orbital angular momentum of the transferred particle. The inclusion of an approximate Coulomb term was seen to remove some of this ambiguity but at the expense of poorer fits in the backward angles. The inadequacies of this theory emphasize the need for a proper DWBA program for fitting transitions to unbound levels.

In the present work, the ability of the Distorted Wave Theory to describe the angular distribution of neutrons leading to the ground state of ^{41}Sc was examined. It was assumed that the appropriate deuteron and neutron elastic scattering parameters should adequately predict the features of the experimentally measured (d,n) stripping patterns. It was found that this was an inadequate approach to the analysis of the data. It is possible that compound nucleus contributions to the observed cross sections are responsible for some of the disagreement. Also, the average neutron parameters may be inadequate to describe all cases of neutron elastic scattering. A likely reason for the poor agreement between observed and calculated $\ell = 3$ angular distribution has very recently been pointed out by two authors (Jo 67, Al 67a). An observation was made that spin dependent effects in $\ell = 3$ transitions to levels with spin $\frac{7}{2}^-$ cause the distributions to be smoothed out in the region around $70 - 90^\circ$. This is not observed for $\ell = 3$ transitions to levels with spin $\frac{5}{2}^-$, instead

a minimum is observed around $70 - 90^\circ$. The observed lack of a minimum in the present ground state angular distributions may be due to this fact alone. As such, it represents the inability of present DWBA theories to take into account the experimentally observed spin dependent features of stripping angular distributions. Johnson (Jo 67) has proposed that inclusion of the D component of the deuteron internal wave function (normally neglected in DWBA theory to simplify calculations) gives rise to corrections to the direct reaction theory of (d,p) and (p,d) reactions which depend strongly on the angular momentum of the transferred neutrons. For an orbital angular momentum transfer of 3, the corrections are large and give important contributions to the spin dependence observed in the reactions $^{56}\text{Fe}(p,d)^{55}\text{Fe}$ and $^{57}\text{Ni}(p,d)^{56}\text{Ni}$. It would be interesting to extend these calculations to the (d,n) reaction and determine the extent to which the D state of the deuteron is important in the reaction $^{40}\text{Ca}(d,n)^{41}\text{Sc}$.

CHAPTER 3

THE $^{42}\text{Ca}(\text{d},\text{n})^{43}\text{Sc}$ REACTION

3.1 Introduction

The study of the $1f_{7/2}$ shell has been extended, in this chapter, to the nucleus ^{43}Sc . The ground states of most of the calcium, scandium and titanium isotopes have been described by assuming active nucleons only in the $1f_{7/2}$ shell. The excited states arising from several particles in this shell usually extend over a region of several MeV in energy. Excited states arising from particles in the 2P shell occur in the same region, so that configuration mixing can be expected even in low-lying states.

In previous work, the energy-level structure of ^{43}Sc has been studied with the reactions $^{43}\text{Ca}(\text{p},\text{n})^{43}\text{Sc}$ (Mc 60, Mc 67), $^{40}\text{Ca}(\alpha,\text{p})^{43}\text{Sc}$ (La 63, Cu 66), $^{46}\text{Ti}(\text{p},\alpha)^{43}\text{Sc}$ (Pl 65), $^{42}\text{Ca}(\text{p},\gamma)^{43}\text{Sc}$ (Br 65) and $^{42}\text{Ca}(^3\text{He},\text{d})^{43}\text{Sc}$ (Sc 66).

In the present work, levels in ^{43}Sc have been studied with the $^{42}\text{Ca}(\text{d},\text{n})^{43}\text{Sc}$ reaction which is expected to preferentially excite states consisting largely of a single proton coupled to the target ground state. The results of this experiment are compared with those from the $^{42}\text{Ca}(^3\text{He},\text{d})^{43}\text{Sc}$ reaction where a single proton is also transferred to the target nucleus. Results have been analyzed in terms of the distorted wave theory of direct reactions to determine the orbital angular momentum of the transferred proton and spectroscopic factor for a number of excited states in ^{43}Sc .

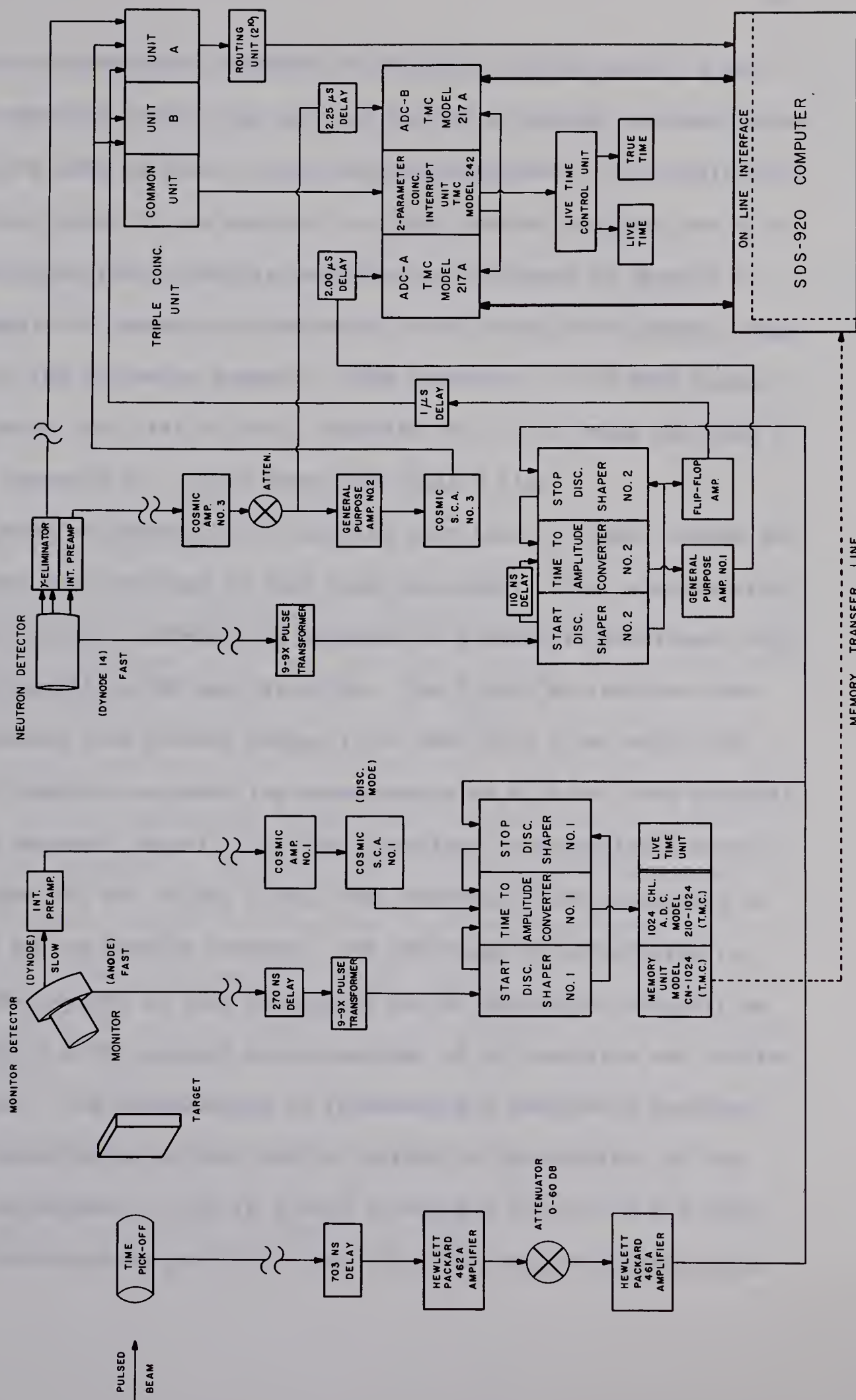
3.2 Experimental Method

The experiment was performed with the University of Alberta 5.5 MeV Van de Graaff accelerator and associated Mobley Compression System, both of which have been described in Chapter 1.

A block diagram of the time of flight electronics is shown in figure 3-1. The system is essentially the same as that described in Chapter 2, except for a number of features added to improve the system. A routing signal was added to route those events called gamma-rays into the first half of the kicksorter and those events called neutrons into the second half. This enables one to check on the stability of gamma-ray elimination throughout the experiment and if desired, determine the gamma-ray rejection efficiency for later efficiency corrections. Two general purpose amplifiers (Ge 66), which eliminated baseline shifts with counting rate, were added to the system. With the old system (Chapter 2), an average baseline shift of 0.1% could be expected at a count rate of approximately 500 cps. This resulted from the fact that a unipolar pulse from the time converter was fed through a capacitor to the ADC. The general purpose amplifiers gave instead, a symmetrical bipolar pulse provided by single delay line clipping. Count rate in the new system, with respect to baseline line shift, is limited only by the ADC (approximately 20,000 cps).

It was observed throughout a number of experiments that the largest correction for walk occurred at the lowest neutron energies. The walk

Figure 3-1 Block diagram of the time of flight electronics used in data gathering for the $^{42}\text{Ca}(d,n)^{43}\text{Sc}$ reaction



routine was subsequently modified to take this into account. A non-linear correction routine was written (Da 66) to sample the small pulse heights from ADCB in finer steps than the large ones. To do this, the signal from dynode 11 was applied to a 1024 channel analyzer and a 56 by 64 two dimensional analysis performed as indicated in Chapter 2. The 56 amplitude channels corresponded to the whole 1024 channel range of ADCB in the following manner: ADCB channels 0 - 255 were equally divided among the first 32 bins, channels 256 to 511 among the next 16 bins and channels 512 - 1023 among the final 8 bins.

The neutron detectors for both the main time of flight system and the monitor were the same as that used previously. The relative efficiency of the main detector was measured in a separate experiment with the reactions $D(d,n)^3\text{He}$ and $T(p,n)^3\text{He}$. The $T(p,n)^3\text{He}$ reaction gave the efficiency from cut-off energy (1.05 MeV) to 3.0 MeV while the $D(d,n)^3\text{He}$ reaction extended the measurements to 8.25 MeV (see Appendix I for the measured curve). For both reactions, the published angular distribution (Br 60, Go 60, Go 61) were reproduced and normalized to the yield in the monitor counter. The advantage of normalizing to the monitor counter is that background can be subtracted uniquely as contrasted to a BF_3 counter where neutrons of all energies and origins are counted. The disadvantage of reproducing a previously measured angular distribution is that one is limited by the accuracy of the original experiment. This is quoted as being $\pm 4\%$ for the $D(d,n)^3\text{He}$ angular distributions and 5% for the $T(p,n)^3\text{He}$ angular distributions.

Absolute efficiencies were obtained by normalizing the relative efficiency curve to an absolute efficiency measurement at 2.82 MeV by Burbank (Bu 67). The error in the measurement of absolute efficiency is estimated to be $\pm 5\%$.

A target[†], 200 $\mu\text{g}/\text{cm}^2$ enriched to 86.4% in ^{42}Ca was used in the present experiment. The target was supplied in the form of calcium metal evaporated onto 0.005" gold and covered with a layer of 50 $\mu\text{g}/\text{cm}^2$ thick gold to reduce oxidation.

3.3 Experimental Results

Figure 3-2 shows $^{42}\text{Ca}(d,n)^{43}\text{Sc}$ excitation curves for the low lying states of ^{43}Sc measured at 30° to the incident beam. These measurements were taken to discover whether or not the optical model condition of smoothly varying cross sections was fulfilled. It was determined that the least amount of structure in the yield curves occurred between 4.8 and 5.2 MeV. Subsequent angular distribution measurements were carried out at 5.15 MeV. Figure 3-3 shows the yield to an intense state at 6.155 MeV in ^{43}Sc . This state has been tentatively identified (Sc 66) as the isobaric analog of the $2P_{\frac{3}{2}}$ level in ^{43}Ca at 2.048 MeV. An interesting feature of this yield curve is a broad resonance between 5.0 and 5.5 MeV that is not obvious in other states. Some of this variation may be due

[†] Purchased from A.E.R.E., Harwell, England.

Figure 3-2 $^{42}\text{Ca}(\text{d},\text{n})^{43}\text{Sc}$ excitation functions for several low-lying states in ^{43}Sc taken at 30° to the incident beam. The number with each curve represents the ^{43}Sc excitation energy in MeV. All curves are plotted on the same scale to show relative variations

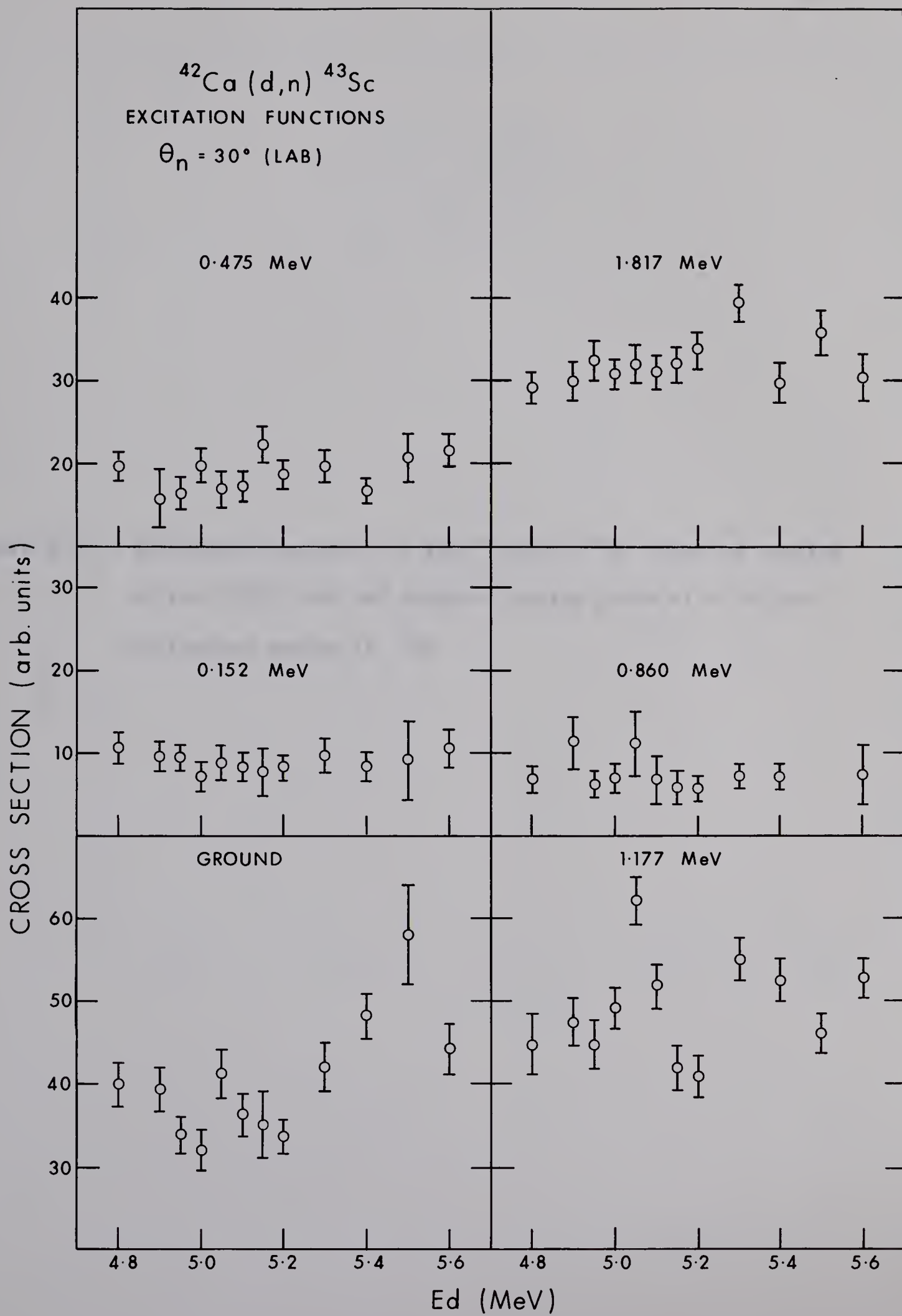
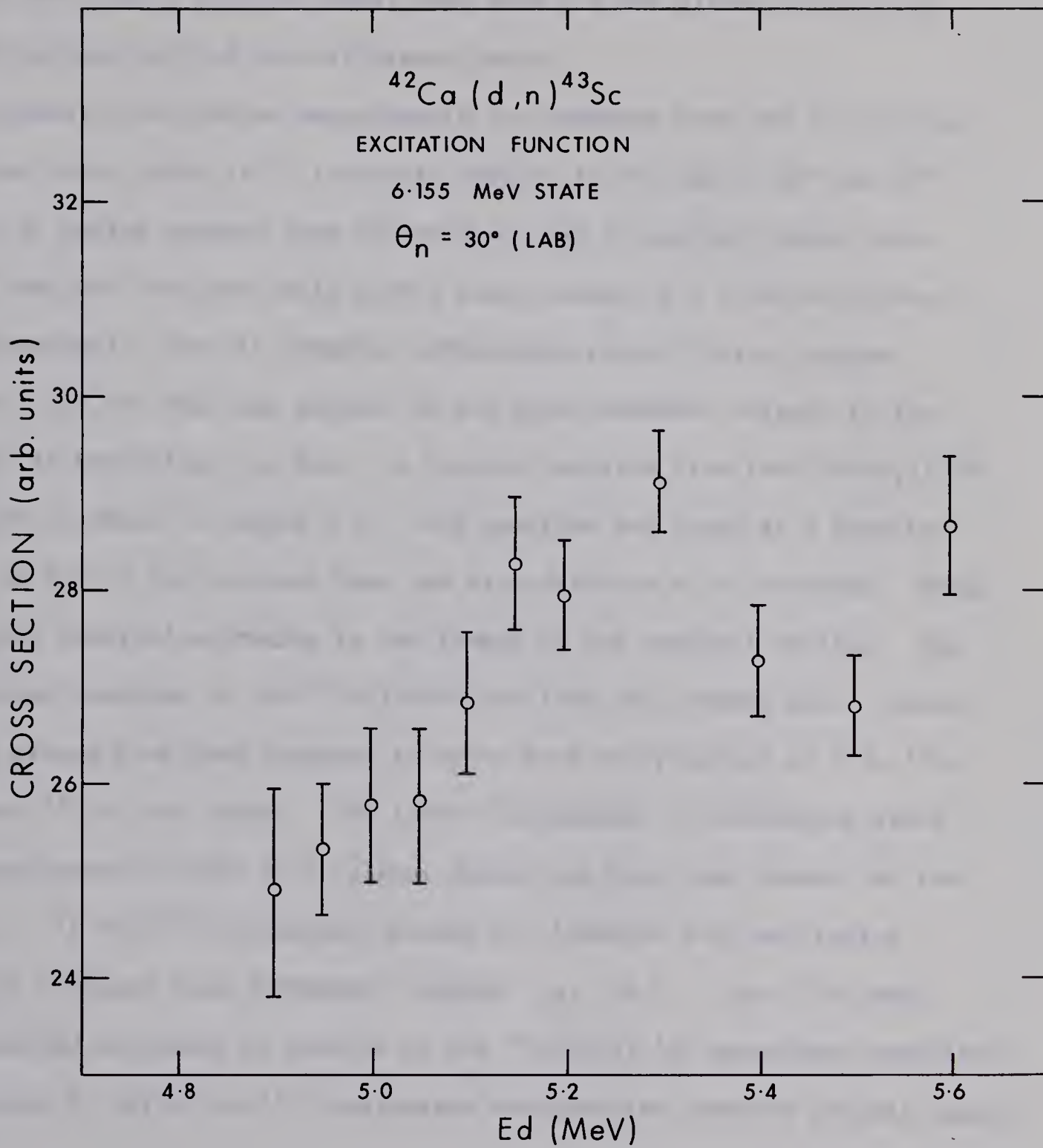


Figure 3-3 Excitation function for the $^{42}\text{Ca}(\text{d},\text{n})^{43}\text{Sc}$ reaction leading to the ^{43}Ca 2.048 MeV isobaric analog state at 6.155 MeV excitation energy in ^{43}Sc



to the fact that a neutron energy less than 1.6 MeV places this on the more uncertain part of the efficiency curve.

Angular distribution measurements for neutrons from the ^{43}Sc states observed, were taken at 5° intervals from 0° to 70° and at 80° and 90° . Yields at angles greater than 90° were too low to warrant taking data. (More than one hour per angle with a beam current of 2 μ amp would have been required). This is somewhat unfortunate since it is at angles greater than 90° that one expects to see spin-dependent effects in the angular distributions (Le 64a). A typical spectrum from the $^{42}\text{Ca}(d,n)^{43}\text{Sc}$ reaction is shown in figure 3-4. This spectrum was taken at a detector angle of 15° to the incident beam and at a distance of 6.00 meters. Peaks have been labelled according to the levels in the residual nucleus. The excitation energies of the ^{43}Sc levels are from the present work. Contaminant groups have been observed to arise from the presence of ^{16}O , ^{12}C , ^{40}Ca and ^{32}S on the target. The latter contaminant is surprising since the manufacturer claims that sulphur should not have been present on the target. ^{17}F and ^{13}N contaminant groups are labelled with excitation energies obtained from AJZENBERG - SELOVE (Aj 59). The ^{41}Sc peaks are labelled according to results of the $^{40}\text{Ca}(d,n)^{41}\text{Sc}$ experiment described in Chapter 2, while the ^{33}Cl excitation energies are from the present experiment.

Table 3-1 shows the Q values obtained for the various transitions to states in ^{43}Sc . The method of finding Q values has been outlined in Chapter 2. This included determination of the time calibration of the spectrometer

Figure 3-4 A semi-log plot of a time of flight spectrum for the reaction $^{42}\text{Ca}(\text{d},\text{n})^{43}\text{Sc}$. Peaks are labelled according to the excitation energies of levels in the residual nucleus. Unless otherwise indicated, the excitation energies are for levels in ^{43}Sc . A time calibration of 0.275 ns/channel was found for this spectrum. A deuteron bombarding energy of 5.15 MeV was used. This spectrum was taken at 15° and 6.00 meters

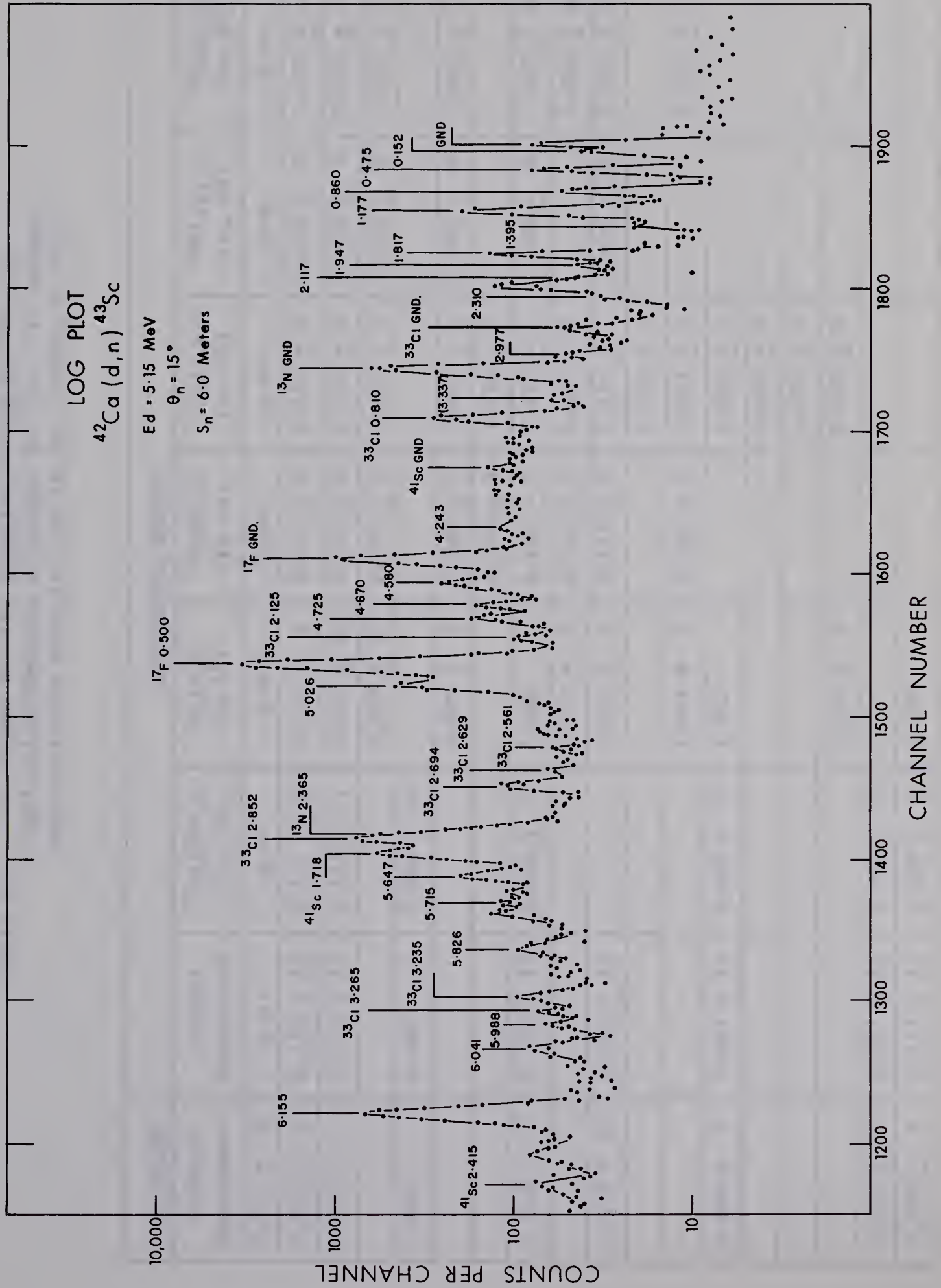


Table 3-1 Q values for the reaction $^{42}\text{Ca}(\text{d},\text{n})^{43}\text{Sc}$ and
Excitation Energies of Levels in ^{43}Sc . (Q values
and excitation energies are in MeV, errors in KeV).

Q VALUE		EXCITATION ENERGY						
Present Experiment	Present Experiment	$^{42}\text{Ca}(^3\text{He},\text{d})$ (Sc 66)	$^{40}\text{Ca}(\alpha,\text{p})$ (Cu 66)	$^{40}\text{Ca}(\alpha,\text{p})$ (Ph 66)	$^{40}\text{Ca}(\alpha,\text{p})$ (Sc 67)	$^{46}\text{Ti}(\text{p},\alpha)$ (Pl 65)	$^{43}\text{Ca}(\text{p},\text{n})$ (Mc 67)	
$2.713 \pm \underline{\hspace{0.5cm}}$	g.s.	g.s.	g.s.	g.s.	g.s.	g.s.	g.s.	
$2.561 \pm \underline{\hspace{0.5cm}}$	0.152 ± 13	$0.152 \pm \underline{\hspace{0.5cm}}$	$0.145 \pm \underline{\hspace{0.5cm}}$	$0.151 \pm \underline{\hspace{0.5cm}}$	$0.152 \pm \underline{\hspace{0.5cm}}$	$0.151 \pm \underline{\hspace{0.5cm}}$	$0.152 \pm \underline{\hspace{0.5cm}}$	
$2.238 \pm \underline{\hspace{0.5cm}}$	0.475 ± 12	$0.475 \pm \underline{\hspace{0.5cm}}$	$0.474 \pm \underline{\hspace{0.5cm}}$	$0.472 \pm \underline{\hspace{0.5cm}}$	$0.473 \pm \underline{\hspace{0.5cm}}$	$0.479 \pm \underline{\hspace{0.5cm}}$	$0.476 \pm \underline{\hspace{0.5cm}}$	
			$0.853 \pm \underline{\hspace{0.5cm}}$	$0.849 \pm \underline{\hspace{0.5cm}}$	$0.844 \pm \underline{\hspace{0.5cm}}$	$0.856 \pm \underline{\hspace{0.5cm}}$	$0.855 \pm \underline{\hspace{0.5cm}}$	
$1.854 \pm \underline{\hspace{0.5cm}}$	$0.860 \pm \underline{\hspace{0.5cm}}$	$0.856 \pm \underline{\hspace{0.5cm}}$						
			$0.885 \pm \underline{\hspace{0.5cm}}$	$0.880 \pm \underline{\hspace{0.5cm}}$	$0.882 \pm \underline{\hspace{0.5cm}}$	$0.884 \pm \underline{\hspace{0.5cm}}$	$0.881 \pm \underline{\hspace{0.5cm}}$	
				$1.158 \pm \underline{\hspace{0.5cm}}$	$1.156 \pm \underline{\hspace{0.5cm}}$			
$1.536 \pm \underline{\hspace{0.5cm}}$	$1.177 \pm \underline{\hspace{0.5cm}}$	$1.180 \pm \underline{\hspace{0.5cm}}$	1.180	$1.181 \pm \underline{\hspace{0.5cm}}$	$1.178 \pm \underline{\hspace{0.5cm}}$	$1.188 \pm \underline{\hspace{0.5cm}}$	$1.175 \pm \underline{\hspace{0.5cm}}$	
			$1.337 \pm \underline{\hspace{0.5cm}}$	$1.341 \pm \underline{\hspace{0.5cm}}$	$1.335 \pm \underline{\hspace{0.5cm}}$		$1.347 \pm \underline{\hspace{0.5cm}}$	
$1.318 \pm \underline{\hspace{0.5cm}}$	$1.395 \pm \underline{\hspace{0.5cm}}$		$1.410 \pm \underline{\hspace{0.5cm}}$	$1.414 \pm \underline{\hspace{0.5cm}}$	$1.418 \pm \underline{\hspace{0.5cm}}$	$1.426 \pm \underline{\hspace{0.5cm}}$	$1.424 \pm \underline{\hspace{0.5cm}}$	
					$1.426 \pm \underline{\hspace{0.5cm}}$			
			$1.644 \pm \underline{\hspace{0.5cm}}$	$1.644 \pm \underline{\hspace{0.5cm}}$	$1.647 \pm \underline{\hspace{0.5cm}}$		$1.644 \pm \underline{\hspace{0.5cm}}$	
$0.896 \pm \underline{\hspace{0.5cm}}$	$1.817 \pm \underline{\hspace{0.5cm}}$	$1.812 \pm \underline{\hspace{0.5cm}}$	1.812		$1.810 \pm \underline{\hspace{0.5cm}}$			
					$1.827 \pm \underline{\hspace{0.5cm}}$			
					$1.877 \pm \underline{\hspace{0.5cm}}$			
			$1.912 \pm \underline{\hspace{0.5cm}}$		$1.928 \pm \underline{\hspace{0.5cm}}$			
$0.766 \pm \underline{\hspace{0.5cm}}$	$1.947 \pm \underline{\hspace{0.5cm}}$	$1.962 \pm \underline{\hspace{0.5cm}}$						
$0.596 \pm \underline{\hspace{0.5cm}}$	$2.117 \pm \underline{\hspace{0.5cm}}$	$2.100 \pm \underline{\hspace{0.5cm}}$	2.100					

Table 3-1 (Continued) Q values for the reaction $^{42}\text{Ca}(d,n)^{43}\text{Sc}$ and higher Excitation Energies of Levels in ^{43}Sc . (Q values and excitation energies are in MeV, errors in KeV).

Q VALUE		EXCITATION ENERGY						
Present Experiment		Present Experiment	⁴² Ca(³ He,d) (Sc 66)	⁴⁰ Ca(α,p) (Cu 66)	⁴⁰ Ca(α,p) (Ph 66)	⁴⁰ Ca(α,p) (Sc 67)	⁴⁶ Ti(p,α) (Pl 65)	⁴³ Ca(p,n) (Mc 67)
0.403 ± 5		2.310 ± 11	2.294 ± 5					
			2.679 ± 15					
-0.264 ± 7		2.977 ± 12	2.992 ± 15					
			3.337 ± 15					
			3.462 ± 15					
-0.917 ± 4		3.630 ± 11	3.618 ± 15					
-0.970 ± 4		3.683 ± 11	3.673 ± 15					
-1.298 ± 9		4.011 ± 13	3.992 ± 10					
-1.530 ± 2		4.243 ± 10	4.238 ± 8					
-1.666 ± 4		4.379 ± 11	4.380 ± 10					
-1.867 ± 12		4.580 ± 16	4.565 ± 10					
-1.957 ± 2		4.670 ± 10	4.663 ± 10					
-2.012 ± 2		4.725 ± 10	4.713 ± 10					
-2.185 ± 3		4.898 ± 11	4.896 ± 10					
-2.313 ± 1		5.026 ± 10	5.025 ± 8					
			5.266 ± 9					
-2.798 ± 2		5.511 ± 10	5.495 ± 10					
-2.934 ± 2		5.647 ± 10	5.634 ± 10					
-3.002 ± 2		5.715 ± 10						
-3.113 ± 2		5.826 ± 10	5.818 ± 10					
-3.275 ± 2		5.988 ± 10						
-3.328 ± 2		6.041 ± 10						
-3.442 ± 1		6.155 ± 10	6.156 ± 9					
			6.282 ± 10					

in terms of zero degree spectra from the reaction ${}^9\text{Be}(d,n){}^{10}\text{B}$. Small baseline shifts in the spectrometer were corrected for by noting the shift of the ${}^{13}\text{N}$ and ${}^{17}\text{F}$ peaks on each spectrum away from that calculated on the basis of the ${}^9\text{Be}(d,n){}^{10}\text{B}$ calibration. Observed time shifts were usually less than 0.5 ns. Excitation energies for the ${}^{43}\text{Sc}$ levels were computed on the basis of the Q value of 2.713 ± 0.010 MeV for the ground state transition determined in the present work. These are also shown in Table 3-1 and are compared to recent work with various other reactions. The errors quoted for the Q values listed in Table 3-1 arise from a one cm uncertainty in the flight path of 6.00 meters; the uncertainty in the time calibration of the spectrometer, the uncertainty in determining peak positions and the uncertainty in determining the time correction for baseline shifts. In most cases, the largest uncertainty is the peak position. The additional error in the excitation energy arises from an estimated 8 KeV spread due to target thickness, an error of 3 KeV in determining beam energy and 3 KeV spread in energy from the transverse momentum imparted to the beam by the Mobley RF system.

Contaminant peaks from the reaction ${}^{32}\text{S}(d,n){}^{33}\text{Cl}$ overlap possible peaks due to the levels at energies 2.679, 3.462 and 5.266 MeV seen in the ${}^{42}\text{Ca}({}^3\text{He},d){}^{43}\text{Sc}$ reaction (Sc 66). A ${}^{43}\text{Sc}$ level at 3.337 seen in the $({}^3\text{He},d)$ reaction has also been tentatively identified in the present study, but was obscured at a large number of angles by the ${}^{13}\text{N}$ ground state peak, and consequently could not be identified unambiguously. The level is, however, indicated in brackets on the spectrum in figure 3-4.

A level seen at 1.395 ± 0.014 MeV in the present experiment is probably the new level in ^{43}Sc at 1.410 ± 0.005 MeV reported by Cujec (Cu 66). It would appear that none of the other new levels seen by Cujec at 1.337, 1.644, 1.879 and 1.912 MeV are excited in the present reaction.

Phillips (Ph 66) reports a level at 1.158 ± 0.003 MeV for which no evidence could be seen in the present experiment. With a spin $(\frac{3}{2}, \frac{5}{2})$ and possible positive parity, this state would be excited only weakly in the (d,n), and is most likely obscured by the very intense $\frac{3}{2}^-$ state at 1.177 ± 0.011 MeV.

A literature search revealed that two levels at 5.715 ± 0.010 , and 5.988 ± 0.010 had not been previously reported. Neutron peaks corresponding to these two states were observed at a minimum of ten angles. This provided good kinematic identification of the peaks as originated from the $^{42}\text{Ca}(d,n)^{43}\text{Sc}$ reaction. All remaining states have been reported before. In general, all excitation energies obtained from the present work agree very well with the previously published values.

^{32}S has been identified as a contaminant on the ^{42}Ca target used in the present experiment. As mentioned before, sulphur should not occur as a natural contaminant. Its presence on the target probably resulted from evaporation of a natural sulphur target into the vacuum system by the previous group to use the accelerator. A number of transitions to states in ^{33}Cl have been identified for which Q values and excitation energies are presented in Table 3-2. Excitation energies are based on the ground

Table 3-2 Q values for the $^{32}\text{S}(\text{d},\text{n})^{33}\text{Cl}$ reaction and Excitation Energies of Levels in ^{33}Cl . (Q values and excitation energies are in MeV, errors in KeV).

Q VALUE	EXCITATION ENERGY					
	Present Experiment	$^{32}\text{S}(\text{d},\text{n})$ (Mi 53)	$^{32}\text{S}(\text{d},\text{n})$ (Ma 60a)	$^{32}\text{S}(\text{}^3\text{He},\text{d})$ (Gr 66)	$^{32}\text{S}(\text{}^3\text{He},\text{d})$ (Mo 67)	$^{32}\text{S}(\text{p},\gamma)$ (Le 58)
0.046 ± 4	g.s.	g.s.	g.s.	g.s.	g.s.	
-0.764 ± 2	0.810 ± 10	0.76 ± 70	0.88 ± 70	0.816 ± 4	0.810 ± 9	0.806 ± 4
		1.89			1.978 ± 14	
-2.079 ± 4	2.125 ± 11		2.11 ± 60			
					2.351 ± 9	
-2.515 ± 4	2.561 ± 11		2.53 ± 60			
-2.583 ± 5	2.629 ± 11					
-2.648 ± 0	2.694 ± 10			2.675 ± 4	2.686 ± 8	
						2.85 ± 20
-2.806 ± 1	2.852 ± 10	2.84 ± 60	2.82 ± 60	2.835 ± 4	2.848 ± 9	2.86 ± 20
-3.189 ± 3	3.235 ± 11					
-3.219 ± 2	3.265 ± 10					
					4.119 ± 10	
		4.22 ± 80				

state Q value of 0.046 ± 0.010 MeV obtained in the present experiment. Published excitation energies obtained from various other reactions are also presented in Table 3-3 for comparison. Good agreement is found with the previous results. It is interesting to note that the errors quoted for previous (d,n) work are a factor of 5 to 6 greater than those presented here. Previously unreported ^{33}Cl levels have been seen at 2.629 ± 0.011 , 3.235 ± 0.011 and 3.219 ± 0.010 MeV. These levels are very weak in the present reaction so that the assignment to ^{33}Cl is somewhat uncertain.

3.4 Analysis of the Angular Distributions

The results of the angular distribution measurements are shown in figures 3-5 to 3-9. The error bars shown here arise from statistical errors and background subtraction. Peak areas were found by the program "Anneliese" described in Chapter 2. Absolute cross sections were calculated by using the target thickness quoted by the manufacturer. The error in target thickness estimated by the manufacturer is $\pm 10\%$. This error has not been included with the angular distributions. Peak cross sections for transitions to the low lying states of ^{43}Sc were observed to be less than 1 mb/sr. Reliable angular distributions could only be extracted for a small number of these states. Numerical values for the cross sections are listed in Appendix II. The solid curves shown in figures 3-5 to 3-7 are DWBA calculations performed with a program written

Figure 3-5 Centre of mass angular distribution for neutrons leading to the ground state of ${}^4_3\text{Sc}$ from the reaction ${}^{42}_{20}\text{Ca}(\text{d},\text{n}){}^{43}_{21}\text{Sc}$ at a deuteron bombarding energy of 5.15 MeV. The curve shown with the data is from a DWBA calculation for an ℓ -transfer value of 3

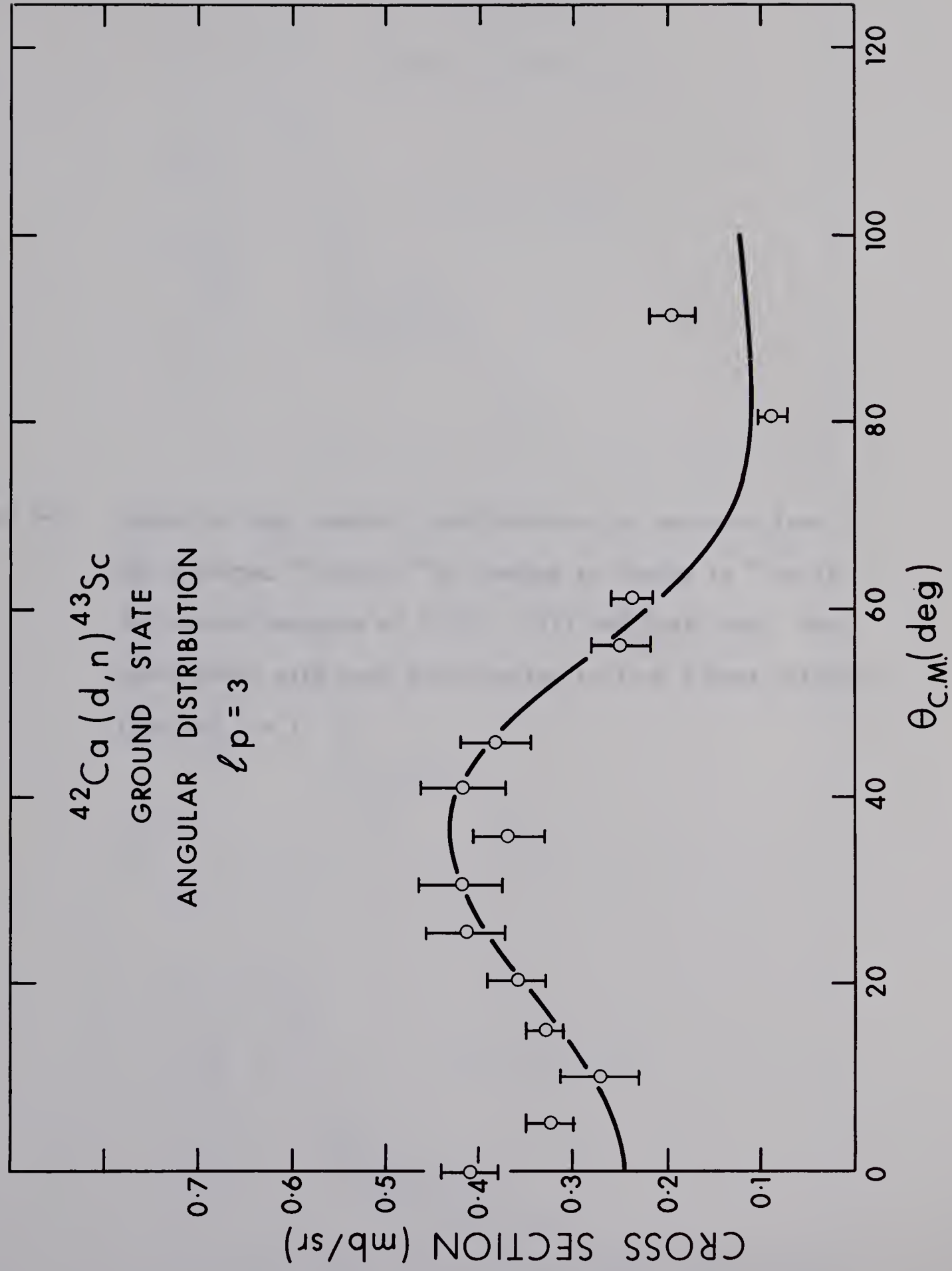
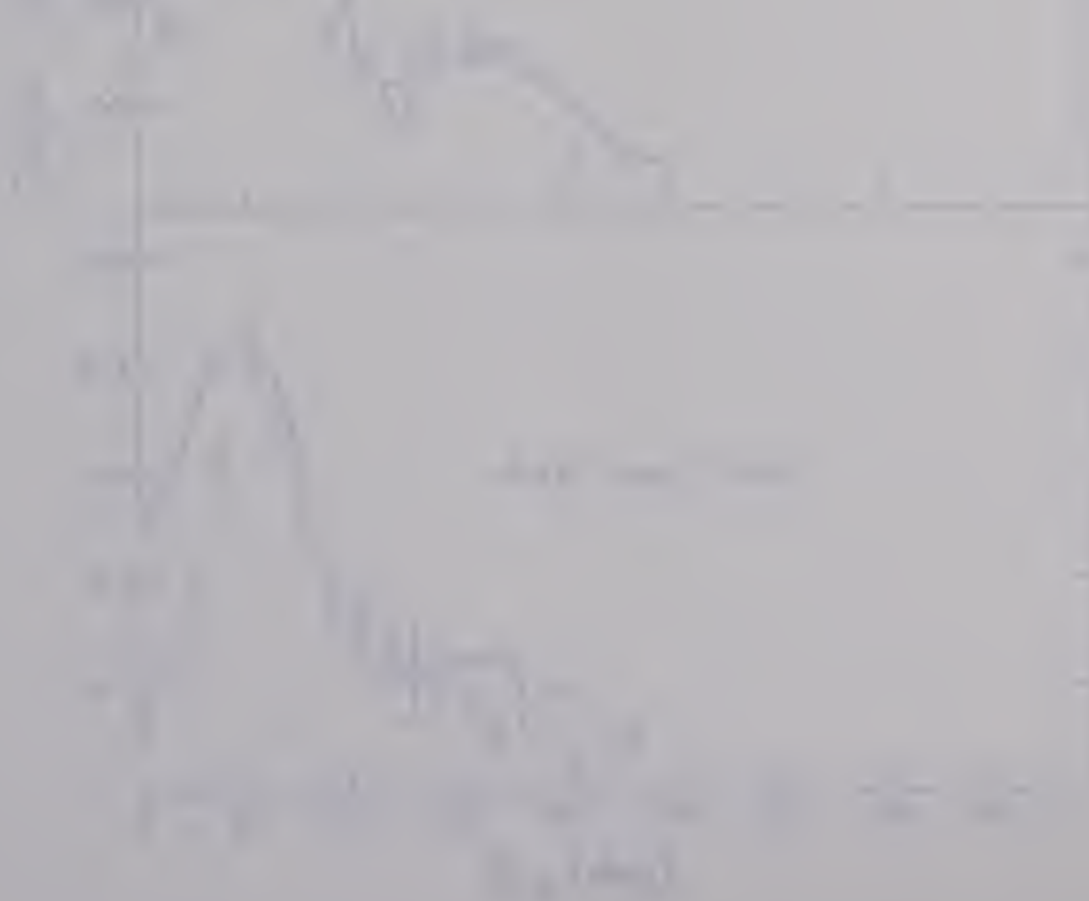




Figure 3-6 Centre of mass angular distributions for neutrons from the reaction $^{42}\text{Ca}(d,n)^{43}\text{Sc}$ leading to states in ^{43}Sc at excitation energies of 0.475, 1.177 and 1.817 MeV. The curve shown with each distribution is from a DWBA calculation for $\ell = 1$



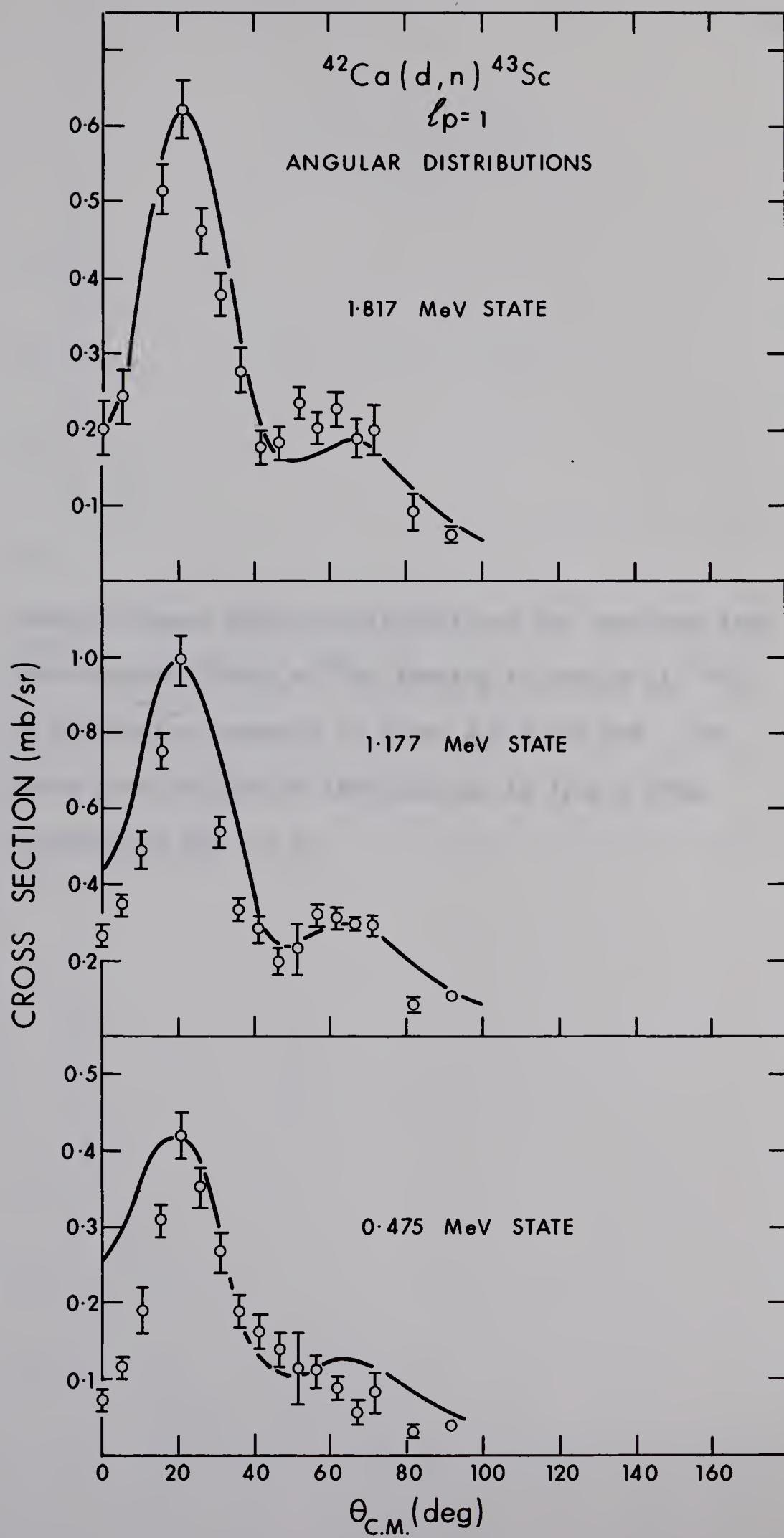


Figure 3-7 Centre of mass angular distributions for neutrons from the reaction $^{42}\text{Ca}(d,n)^{43}\text{Sc}$ leading to states in ^{43}Sc at excitation energies of 0.860 and 1.947 MeV. The curve shown with each distribution is from a DWBA calculation for $\ell = 0$

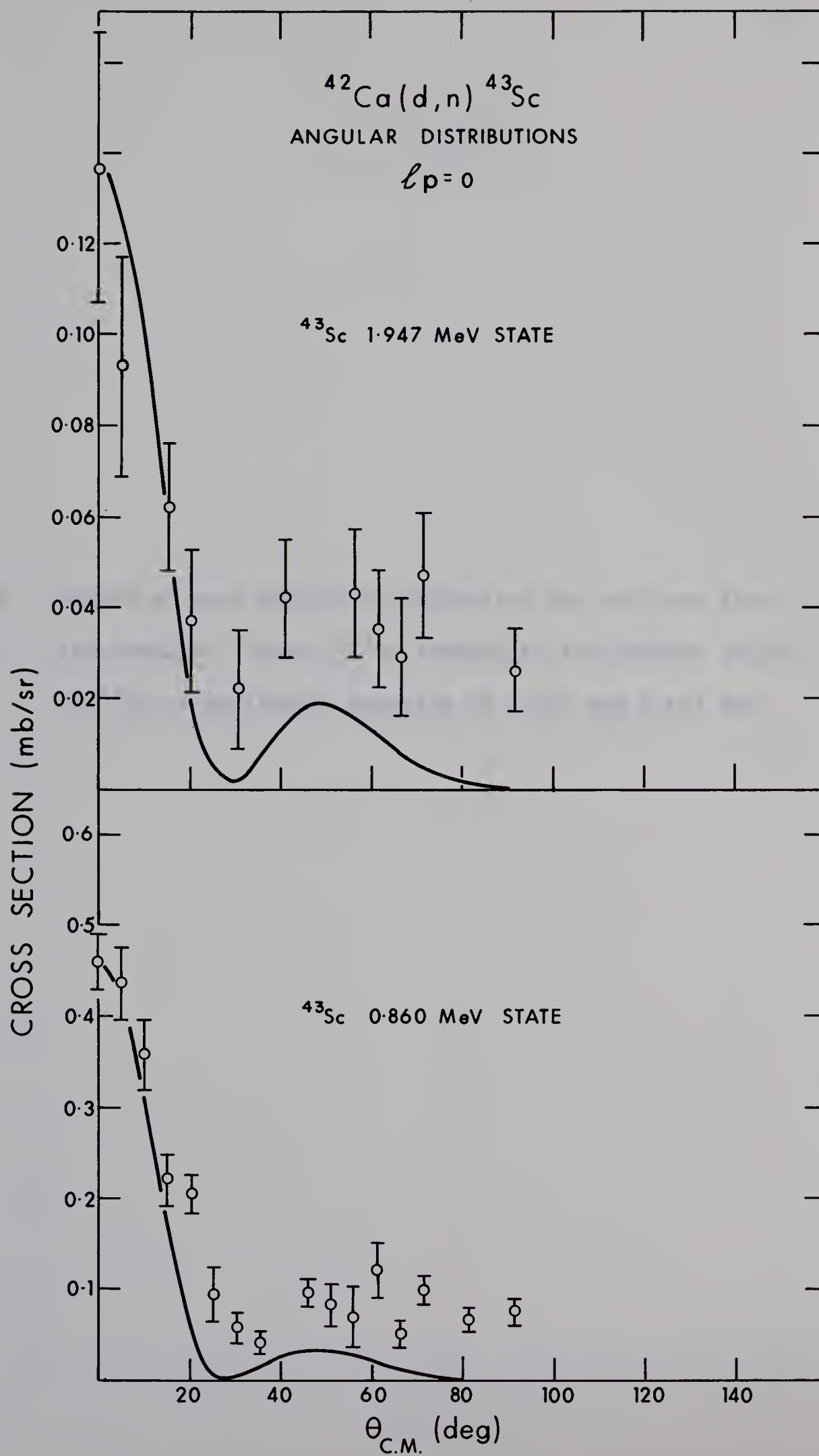


Figure 3-8 Centre of mass angular distributions for neutrons from the reaction $^{42}\text{Ca}(d,n)^{43}\text{Sc}$ leading to two unbound states in ^{43}Sc at excitation energies of 5.026 and 5.647 MeV

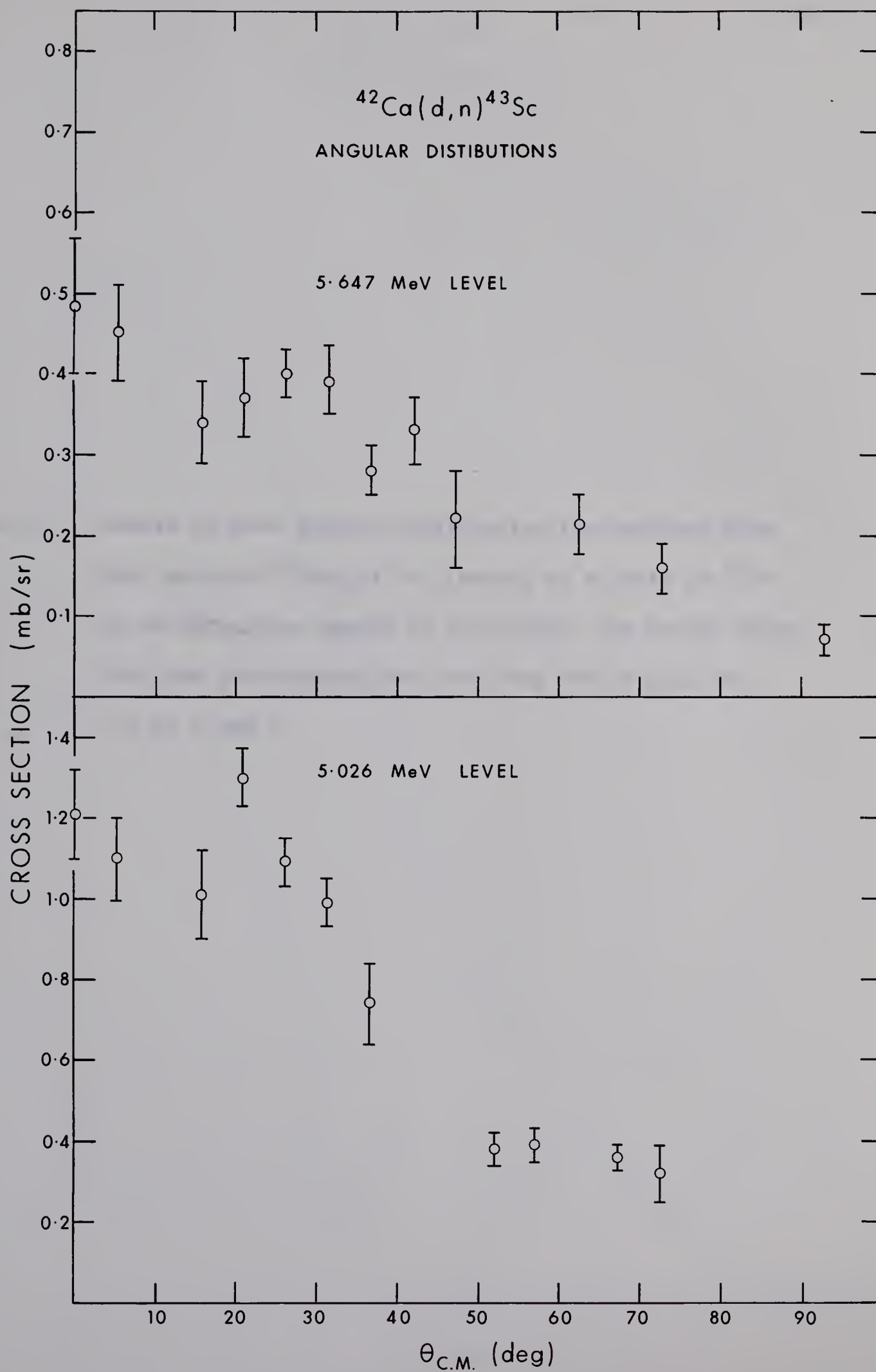
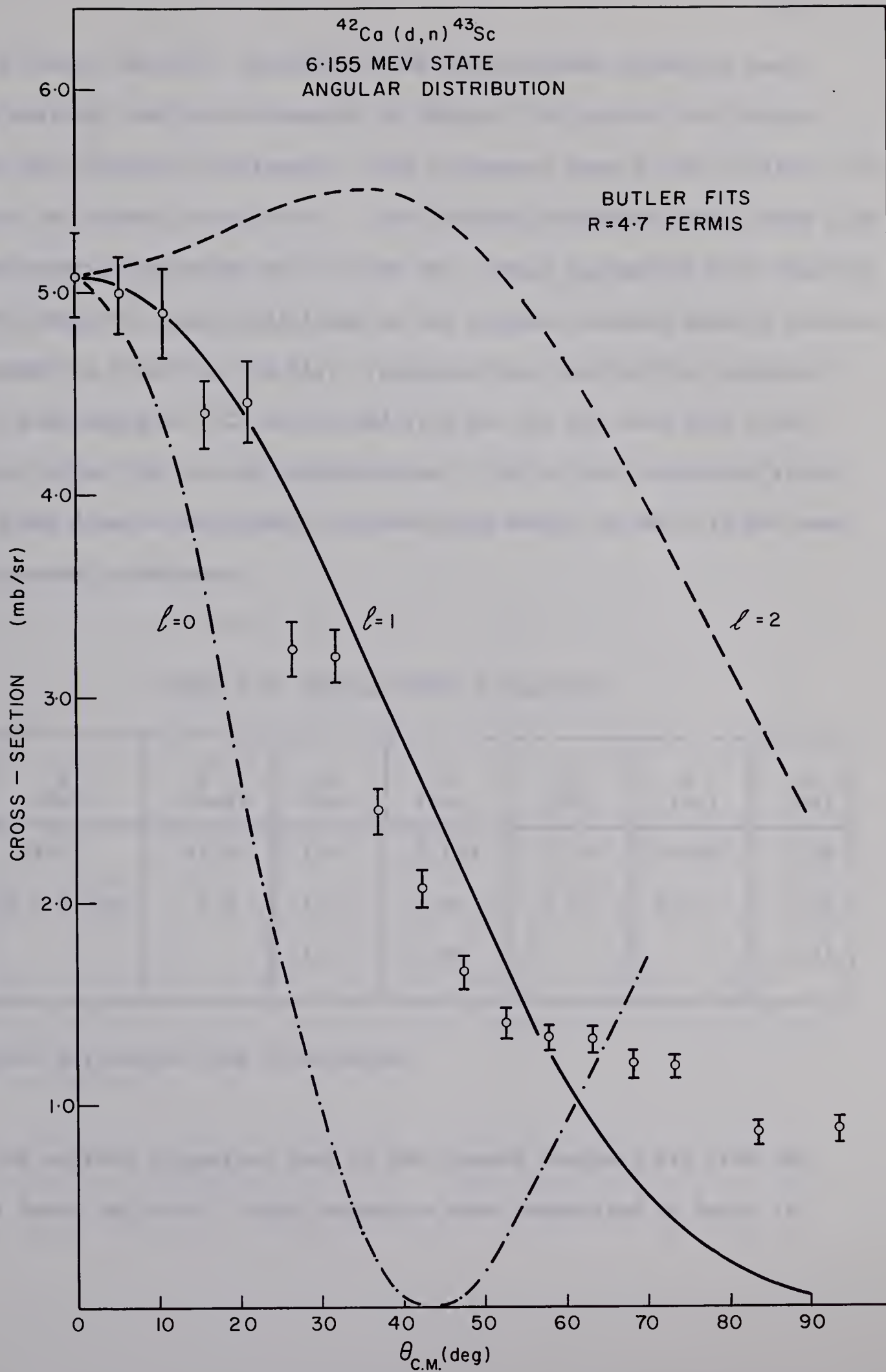


Figure 3-9 Centre of mass angular distribution for neutrons from the reaction $^{42}\text{Ca}(d,n)^{43}\text{Sc}$ leading to a state in ^{43}Sc at an excitation energy of 6.155 MeV. The curves shown with the experimental data are from Butler fits for $\ell = 0, 1$ and 2



by W. R. Smith (Sm 65). The form of the optical model potential used in the analysis has been presented in Chapter 2 as part of the discussion of the $^{40}\text{Ca}(d,n)^{41}\text{Sc}$ results. The parameters used in the $^{42}\text{Ca}(d,n)^{43}\text{Sc}$ analysis are present in Table 3-3. The deuteron parameters were taken from 7.0 MeV elastic scattering on ^{42}Ca (Do 66). These parameters were observed to give almost the same predictions as the average deuteron elastic scattering parameters from ^{40}Ca (Ba 64). Parameter sets derived from deuteron elastic scattering on ^{42}Ca at 9.0 and 12.0 MeV (Er 66) were also tried, but gave poorer fits to the distributions. This is not surprising since the 7.0 MeV data is the closest in bombarding energy to the 5.15 MeV used in the present experiment.

Table 3-3 Optical Model Parameters.

Particle	V (MeV)	W^\dagger (MeV)	r_o (fm)	a (fm)	r_o' (fm)	a' (fm)	r_c (fm)
d	113.2	12.9	1.0	0.753	1.50	0.659	1.25
n	48 - 0.29E	9.6	1.27	0.66	1.27	0.47	1.25
p			1.25	0.65			1.25

† surface derivative type of potential

The neutron parameters used in the present analysis are from the work of Perey and Buck. These parameters were summarized by Rosen at

the Karlsruhe Conference on Polarization, Sept., 1965 (Ro 66).

The proton wave function for the bound particle was calculated in a Woods-Saxon potential well with radius $r_0 = 1.25$ fm and diffuseness $a = 0.65$ fm. The proton potential had no imaginary part but did include a derivative type of spin-orbit potential with a depth of 6.0 MeV. With these parameters well depths of 58.0, 63.0, 45.6, 61.8, 60.6 and 43.8 MeV resulted from fitting data for the ground, 0.475, 0.860, 1.177, 1.817 and 1.947 MeV states of ^{43}Sc respectively.

The DWBA fit for the ground state transition (figure 3-5) clearly supports an angular momentum transfer of 3. This is consistent with a spin and parity assignment of $\frac{7}{2}^-$ deduced from the observed β decay to ^{43}Ca (Li 54) and from a measurement of its magnetic moment (Co 66). An interesting feature of this angular distribution is a peaking of the distribution at 0° which is reminiscent of the distributions observed for the $^{40}\text{Ca}(d,n)^{41}\text{Sc}$ ground state transition. In this case, however, the DWBA theory fails to predict the existence of this forward maximum. An absolute spectroscopic factor of 0.15 was calculated for the transition to the ^{43}Sc ground state. This is considerably below the value of 0.68 observed by Schwartz (Sc 66) in the $^{42}\text{Ca}(^3\text{He},d)^{43}\text{Sc}$ reaction. This probably indicates a larger error in target thickness than that quoted by the manufacturer.

Levels at 0.475, 1.177 and 1.817 MeV show angular distributions characteristic of stripping with $\ell = 1$. These distributions are shown

in figure 3-6. An additional $\ell = 1$ transition seen at 2.100 in the $(^3\text{He}, d)$ reaction (Sc 66) (2.117 MeV in the present experiment) was too weak to give a recognizable stripping pattern. It is expected that the $p_{\frac{1}{2}}$ states will lie at excitation energies of about 4 MeV, and it is consequently assumed that these three levels all have $J^\pi = \frac{3}{2}^-$. With this assumption, absolute spectroscopic factors of 0.033, 0.066 and 0.036 were observed for the 0.475, 1.177 and 1.817 MeV states respectively. Normalization of these values to the 0.68 observed in the $(^3\text{He}, d)$ reaction (Sc 66) for the ground state transition gives 0.15, 0.29 and 0.16. This is then in very good agreement with the values of 0.12, 0.29 and 0.12 observed for these states in the $(^3\text{He}, d)$ reaction (Sc 66). The sums of spectroscopic factors, S_i , should be equal to 1.0 if all components of the single particle state are included. In ^{43}Sc the spectroscopic factor for the isobaric analog states will be

$$S_T = \frac{3}{2} = 1 / (2T_0 + 1) = \frac{1}{3} ,$$

and the sum of the normal low lying states with one unit of isobaric spin less than the analog states should have a total spectroscopic factor

$$S_T = \frac{1}{2} = 1 - 1 / (2T_0 + 1) = \frac{2}{3} .$$

The sum of the observed $2P_{\frac{3}{2}}$ single particle strength in ^{43}Sc with $T = \frac{1}{2}$ is 0.60. This indicates that approximately 90% of the $2P_{\frac{3}{2}}$ single particle strength is contained in the levels at 0.475, 1.177 and 1.817 MeV.

Two levels at 0.860 and 1.947 MeV show angular distributions characteristic of stripping with $\ell = 0$, as shown in figure 3-7. This leads to assignments of $J^\pi = \frac{1}{2}^+$ for these levels. It has been surmised by Schwartz (Sc 66) that an assignment of $\frac{1}{2}^+$ to a level at 0.860 (0.856 MeV in the $(^3\text{He}, d)$ reaction) was in contradiction to an assignment of $(\frac{5}{2}, \frac{9}{2})$ to a level at 0.849 and $\frac{5}{2}^+$ to a level at 0.880 by Phillips (Ph 66). It has been shown recently, however, that there are actually three levels in this region at excitation energies 0.846, 0.857 and 0.878 MeV (Br 67). The 0.860 level observed in the present experiment showed no appreciable broadening in any of the spectra indicating that transitions to the additional two states are very weak (< 0.05 mb/sr peak cross-section). Assignment of $J^\pi = \frac{1}{2}^+$ to the levels at 0.860 and 1.947 MeV leads to spectroscopic factors of 0.024 and 0.0043 respectively, or normalized to a ground state value of 0.68 (Sc 66) these values become 0.11 and 0.02. The value of 0.11 for the 0.860 MeV state is in good agreement with the value of 0.13 observed for the $S_{\frac{1}{2}}$ hole state in the $^{42}\text{Ca}(d, p)^{43}\text{Ca}$ reaction (Do 66). No previous assignment could be found for the state at 1.947 MeV. The assignment of $\frac{1}{2}^+$ in the present experiment is somewhat tentative because of the low cross section (0.14 mb/sr peak) and the associated large errors.

The ground state of ^{43}Sc is actually overlapped by a state at 0.152

MeV excitation energy. A separation of the ground and this excited state was carried out with the fitting program "Anneliese" but yielded an angular distribution with no recognizable pattern for the 0.152 MeV state. This could be remedied in a future experiment by demanding better statistics for the 0.152 MeV state.

A number of intense states have been observed in the $^{42}\text{Ca}(d,n)^{43}\text{Sc}$ reaction at energies 5.026, 5.647 and 6.155 MeV. Angular distributions for the 5.026 and 5.647 MeV states are shown in figure 3-8. Both of these states are unbound to proton emission and thus do not exhibit the familiar stripping pattern observed for bound states. It has been suggested by Schwartz (Sc 66) that the level at 5.026 MeV may be a major component of the $P_{\frac{1}{2}}$ single particle strength.

3.5 Isobaric Analog States in ^{43}Sc

Schwartz (Sc 66) has tentatively identified two states in ^{43}Sc at 4.238 ± 0.008 and 6.156 ± 0.009 MeV as being the isobaric analogs of the ground, and 2.048 MeV states of ^{43}Ca , respectively. The identification of the ground state analog was based on an observed $\ell = 3$ stripping pattern and an expected excitation energy of 4.172 MeV calculated by McCullen (Sc 66). In the present reaction, a similar state has been observed at 4.243 ± 0.010 MeV. However, the transition was too weak to be identified unambiguously as arising from $\ell = 3$ stripping.

No justification has been given by Schwartz (Sc 66) for the identification of a state at 6.156 ± 0.009 MeV as the $(J^\pi, T) = (\frac{3^-}{2}, \frac{3}{2})$

analog of the $2P_{\frac{3}{2}}$ state found in ^{43}Ca at an excitation energy of 2.048 MeV. One might surmise that this is the correct identification, since the $^{42}\text{Ca}(^3\text{He},d)^{43}\text{Sc}$ cross section is large in keeping with a strong $^{42}\text{Ca}(d,p)^{43}\text{Ca}$ transition to the level at 2.048 MeV in ^{43}Ca (En 62).

In the present $^{42}\text{Ca}(d,n)^{43}\text{Sc}$ reaction, a strong transition has been observed to a level at 6.155 ± 0.010 MeV in ^{43}Sc . A peak cross section of 5.2 mb/sr makes this the most intense transition observed in the experiment. The excitation energy is in excellent agreement with the value of 6.156 ± 0.009 MeV found by Schwartz (Sc 66). More positive identification of the ℓ value can be made than in the $(^3\text{He},d)$ study. Figure 3-9 shows the experimentally observed distribution plotted together with the predictions of the Butler theory for $\ell = 0, 1$ and 2 angular momentum transfer. A coulomb correction discussed in Chapter 2 has been included. These calculations support an assignment of $\ell = 1$ for the transition consistent with the previously suggested $J^\pi = \frac{3}{2}^-$ for the 6.155 MeV state.

3.6 Summary

Angular distributions, characteristic of a single particle transfer, have been observed in the (d,n) reaction leading to a number of levels in ^{43}Sc . A $J^\pi = \frac{7}{2}^-$ assignment for the ground state of ^{43}Sc (Li 54, Co 66) was confirmed by an observed $\ell = 3$ stripping pattern. A tentative $J^\pi = \frac{3}{2}^-$ assignment (Sc 66) to three levels in ^{43}Sc located approximately 90% of the $2P_{\frac{3}{2}}$ single particle strength. Two intense transitions to unbound

levels in ^{43}Sc were observed at excitation energies of 5.026 and 5.647 MeV. These levels probably carry the major part of the $2P_{\frac{1}{2}}$ single particle strength. One of the levels (5.026 MeV) has previously been seen in the $^{42}\text{Ca}(^3\text{He},d)^{43}\text{Sc}$ reaction (Sc 66) where the shape of the angular distribution indicates that the state might carry part of the $2P_{\frac{1}{2}}$ strength. Levels which can be identified as $2S_{\frac{1}{2}}$ hole states have been observed at excitation energies of 0.860 and 1.947 MeV in ^{43}Sc . No previous J^π assignment had been made for the 1.947 MeV level.

Isobaric analog states corresponding to the ground state and 2.048 MeV state of ^{43}Ca first seen in the $^{42}\text{Ca}(^3\text{He},d)^{43}\text{Sc}$ reaction (Sc 66) have been identified in the (d,n) reaction. The angular momentum transfer for the 2.048 MeV analog (6.155 MeV excitation energy in ^{43}Sc) has been established on the basis of Butler Plane Wave fits.

Results agree fairly well with a shell model study of the ^{43}Sc nucleus by Flowers (Fl 67) except for a level at 1.817 MeV, assigned $J^\pi = \frac{3}{2}^-$ in the present work. This level is required to be $\frac{1}{2}^-$ to obtain the proper level structure as calculated by Flowers (Fl 67). A rough calculation of the isobaric spin splitting in ^{43}Sc as indicated by French (Fr 64) gives the T_z component of the 6.155 MeV isobaric analog state to be the level at 1.817 MeV. This requires that the level at 1.817 MeV have a $J^\pi = \frac{3}{2}^-$ assignment in agreement with the present experiment.

CHAPTER 4

THE $^{48}\text{Ca}(\text{d},\text{n})^{49}\text{Sc}$ REACTION

4.1 Introduction

The nucleus ^{49}Sc has one proton more than the nucleus ^{48}Ca , whose ground state has been known for some time to be doubly magic. Early study of the β -decay of ^{49}Ca indicated low-lying ^{49}Sc levels at 3.1, 4.1 and 4.7 MeV excitation (Ok 56, Ma 56). It was suggested at that time that the ground state and first two excited states might be interpreted rather simply as the $1f_{\frac{7}{2}}$, $2p_{\frac{3}{2}}$ and $1f_{\frac{5}{2}}$ single particle states, respectively.

This chapter reports on properties of the ^{49}Sc nucleus observed in the reaction $^{48}\text{Ca}(\text{d},\text{n})^{49}\text{Sc}$. Angular distributions for each resolved neutron group are presented and compared to the predictions of the Distorted Wave Born Approximation to establish the ℓ -transfer value for the captured proton and to obtain the desired spectroscopic information. Components of the $2p_{\frac{3}{2}}$, $1f_{\frac{5}{2}}$ and $2p_{\frac{1}{2}}$, expected to be fragmented by residual interactions, are tentatively identified and discussed. Comparisons are made between recent $^{48}\text{Ca}(^3\text{He},\text{d})^{49}\text{Sc}$ results (Ar 64, Ar 65, Er 66) and those from the present reaction.

Considerable interest has been expressed lately in a number of ^{49}Ca isobaric analog states seen at excitation energies above 11.6 MeV in ^{49}Sc . Properties of these levels have been extensively studied with the $^{48}\text{Ca}(\text{p},\text{p})^{48}\text{Ca}$ (Jo 66) and the $^{48}\text{Ca}(\text{p},\gamma)^{49}\text{Sc}$ (Ch 67) reactions. The ^{49}Ca ground state analog has been identified in the present study and some of its experimental properties are discussed.

4.2 Experimental Method

The time of flight electronics was the same as that shown in figure 3-1. The time resolution and gamma ray rejection efficiency of the spectrometer were improved by the use of a cylindrical (3 1/2" diameter x 3/4" length) NE 218^{*} liquid scintillator (Re 66) and an RCA C70133 phototube. A time resolution of approximately 0.7 ns (FWHM) was achieved in the experiment. With a flight path of 6.325 meters, this represented an energy resolution of 34 KeV for 5 MeV neutrons. The system was also improved by using a 2048 rather than a 1024 channel analog to digital converter for ADCA. This change accompanied an increase in the time range of the spectrometer from 300 to 600 nanoseconds, and a decrease in the time calibration from 0.276 to 0.222 ns/ch. This had the effect of giving better peak definition which helped considerably in the analysis of the data with peak fitting program "Anneleise". In addition, it allowed a wider energy range for the spectrometer. In particular, this meant that one could include the gamma ray peak without losing any neutron peaks of interest.

Spectra were obtained by bombarding an enriched ^{48}Ca target[†] with

* Nuclear Enterprises Ltd., Winnipeg, Manitoba, Canada.

† The target, 200 $\mu\text{g}/\text{cm}^2$ thick, enriched to 84.6% ^{48}Ca was supplied in the form of calcium metal evaporated onto 0.005" gold and covered with a layer of 50 $\mu\text{g}/\text{cm}^2$ thick gold to reduce oxidation by A.E.R.E., Harwell, England.

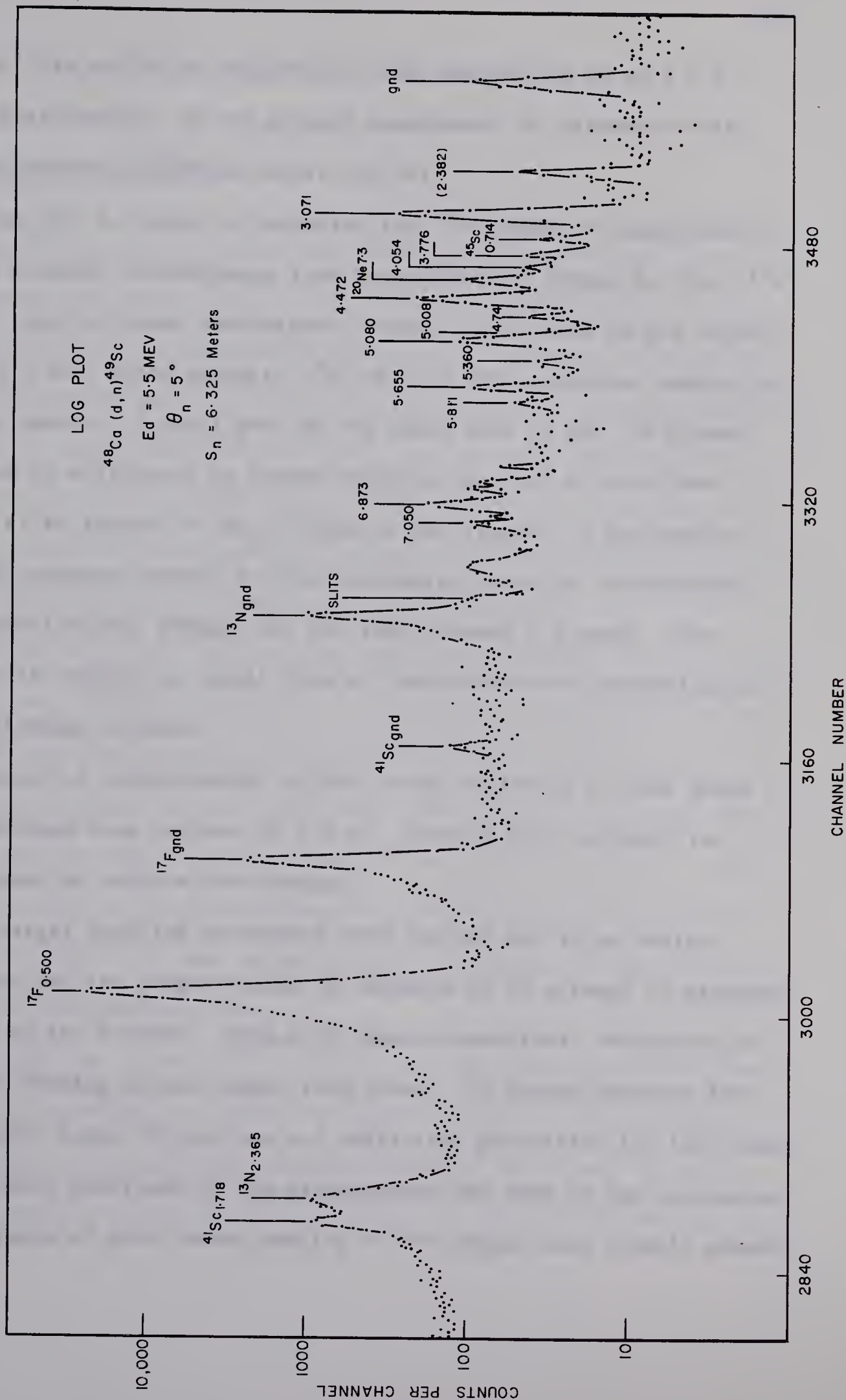
deuterons of energies 5.5 and 6.0 MeV. The bombarding energies were measured with a 90° analyzing magnet. The magnet was calibrated shortly after the experiment and the calibration was found to be the same as that of a year before (Chapter 2).

The absolute efficiency of the neutron detector from a neutron cut-off energy of 1.41 MeV to 14.0 MeV was calculated by a computer program which takes into account double scattering from hydrogen, single scattering from carbon and detector resolution (Appendix I). It is estimated that the absolute efficiency is accurate to better than $\pm 5\%$ especially at neutron energies above 5 MeV. The relative efficiency should then be good to at least $\pm 1\%$.

Angular distributions were measured at 5° intervals from 0° to 45° , at 10° intervals from 45° to 75° and at 95° , 110° and 120° . A typical spectrum from the $^{48}\text{Ca}(d,n)^{49}\text{Sc}$ reaction is shown in figure 4-1. This spectrum was taken at a bombarding energy of 5.5 MeV, a flight path of 6.325 meters and at a detector angle of 5° to the incident beam. Peaks have been labelled according to the levels in the residual nucleus. The excitation energies of the ^{49}Sc levels are from the present work. Contaminant groups have been observed to arise from the presence of ^{40}Ca , ^{16}O , ^{12}C and ^{19}F on the target. The ^{41}Sc peaks are labelled according to the results of the $^{40}\text{Ca}(d,n)^{41}\text{Sc}$ experiment presented in Chapter 2. Remaining contaminant groups are labelled with excitation energies obtained from AJZENBERG-SELOVE (Aj 59).

The identification of the 7.3 MeV contaminant group from the

Figure 4-1 A semi-log plot of a time of flight spectrum from the reaction $^{48}\text{Ca}(\text{d},\text{n})^{49}\text{Sc}$. Peaks are labelled according to the excitation energies of levels in the residual nucleus. Unless otherwise indicated, excitation energies are for levels in ^{49}Sc . A time calibration of 0.222 ns/channel was found for this spectrum. A deuteron bombarding energy of 5.5 MeV was used. This spectrum was taken at 5° and 6.325 meters



reaction $^{19}\text{F}(\text{d},\text{n})^{20}\text{Ne}$ is supported by the observation of an $\ell = 0$ angular distribution, in the present experiment; in agreement with that tabulated by AJZENBERG-SELOVE (Aj 59).

A log plot is shown to emphasize the ^{49}Sc peaks in comparison to the much stronger contaminants from transitions to levels in ^{41}Sc , ^{17}F and ^{13}N . None of these contaminants caused any trouble in the experiment at 5.5 MeV, since states in ^{49}Sc up to 7 MeV excitation energy lie higher in energy. A small peak on the right side of the ^{13}N ground state peak is attributed to carbon deposits on a set of gold beam defining slits located 30 cm in front of the target. A noticeable amount of asymmetry exists for the low energy peaks in the spectrum. This is particularly evident for the very intense ^{17}F peaks. The asymmetry is thought to result from an inadequate walk correction and target thickness effects.

A charge of approximately 12,000 μC was collected at each angle with an average beam current of 2.8 μA . Even at this current, the target showed no serious beam damage.

All target handling procedures were carried out in an helium atmosphere and the target stored in nitrogen in an attempt to minimize oxidation of the calcium. Even with these precautions; oxidation and subsequent flaking of the target took place. It became apparent that the 50 $\mu\text{g}/\text{cm}^2$ layer of gold was not sufficient protection for the target. This was later confirmed by the manufacturer who came to the conclusion that the layer of gold caused peeling of the target once a small amount

of flaking had taken place.

4.3 Experimental Results

The results of the angular distribution measurements at 5.5 MeV are shown in figures 4-2 to 4-6. The error bars shown here arise from statistical errors and background subtraction. Absolute cross-sections were calculated by using the target thickness quoted by the manufacturer. The error in target thickness estimated by the manufacturer is $\pm 10\%$. Peak cross sections for the $^{48}\text{Ca}(d,n)^{49}\text{Sc}$ reaction were observed to be less than 1 mb/sr for all states. Reliable angular distributions could only be extracted for the more intense of these.

Q values for the $^{48}\text{Ca}(d,n)^{49}\text{Sc}$ transitions observed in the present experiment are listed in Table 4-1. The method of obtaining Q values and determining their errors has been outlined in Chapters 2 and 3. This included determination of the time calibration of the spectrometer in terms of zero degree spectra from the reaction $^9\text{Be}(d,n)^{10}\text{B}$. Small baseline shifts in the spectrometer were corrected for by noting the shift of the gamma ray peak on each spectrum relative to that on the $^9\text{Be}(d,n)^{10}\text{B}$ reference spectrum.

A ground state Q value of 7.404 ± 0.010 MeV was observed for the ground state transition. This is in good agreement with the value of 7.396 ± 0.009 MeV calculated from the $^{48}\text{Ca}(p,\gamma)^{49}\text{Sc}$ Q value listed by Mattauch (Ma 65). A ground state Q value of 4.150 ± 0.012 MeV has been

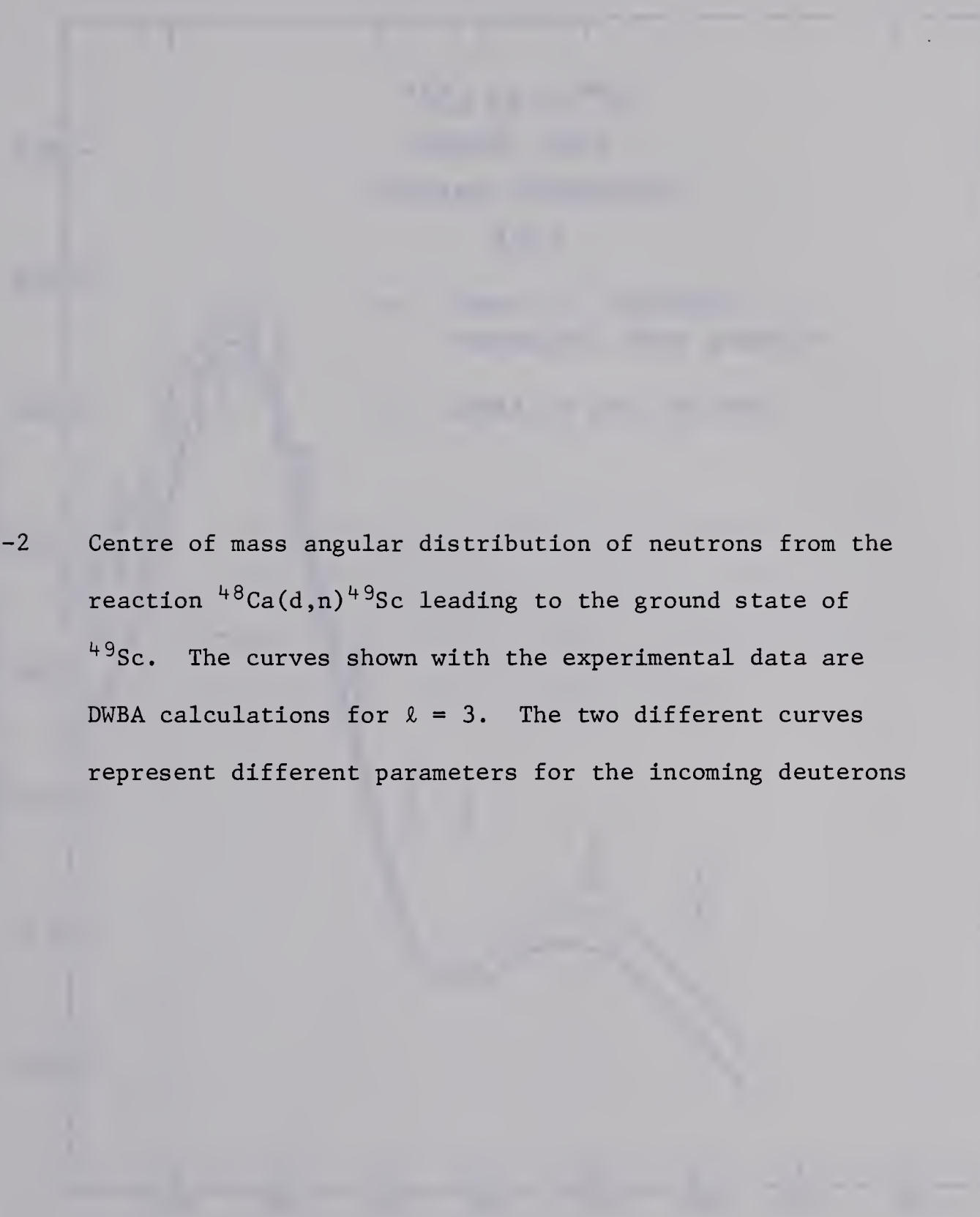
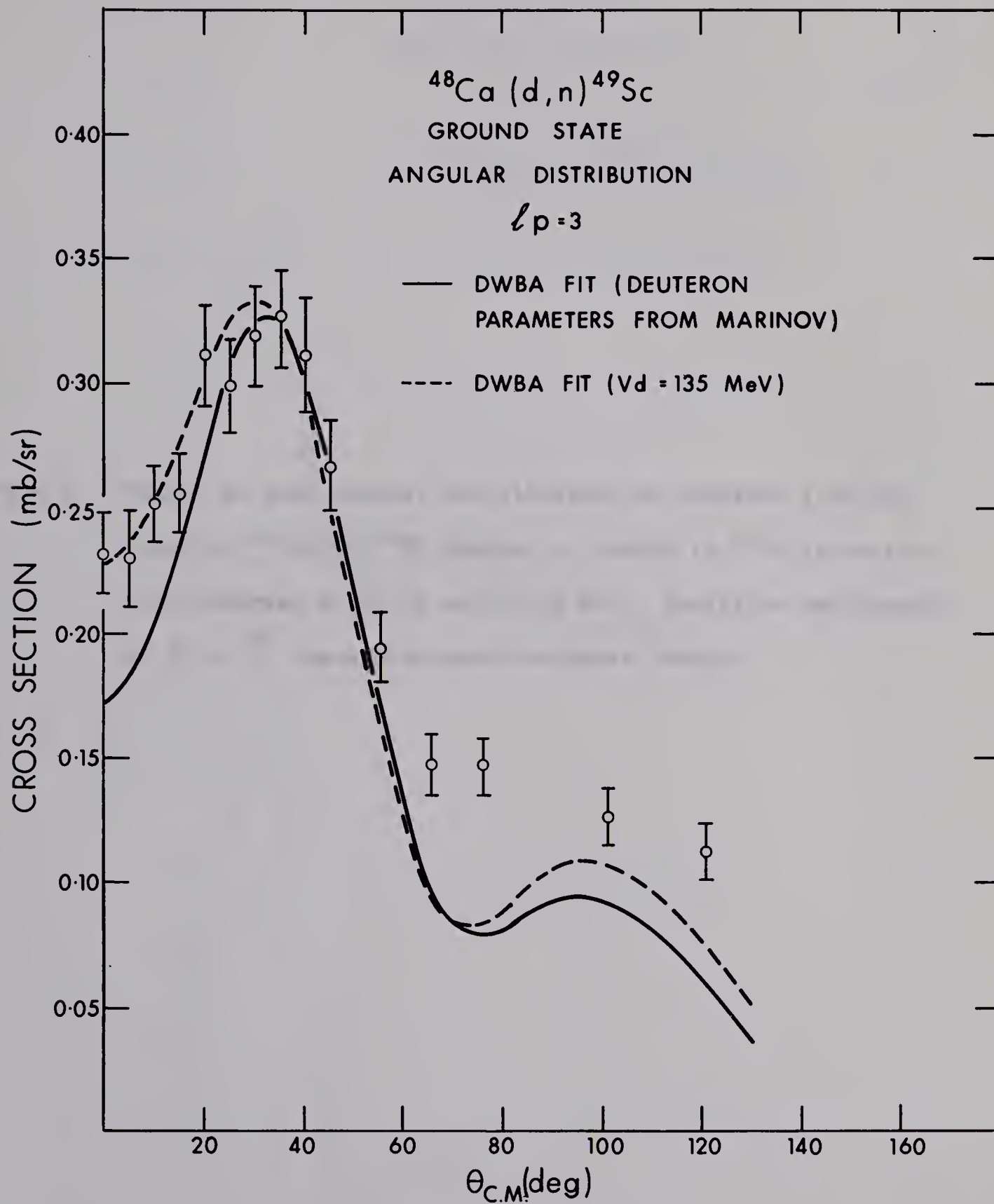


Figure 4-2 Centre of mass angular distribution of neutrons from the reaction $^{48}\text{Ca}(d,n)^{49}\text{Sc}$ leading to the ground state of ^{49}Sc . The curves shown with the experimental data are DWBA calculations for $\ell = 3$. The two different curves represent different parameters for the incoming deuterons



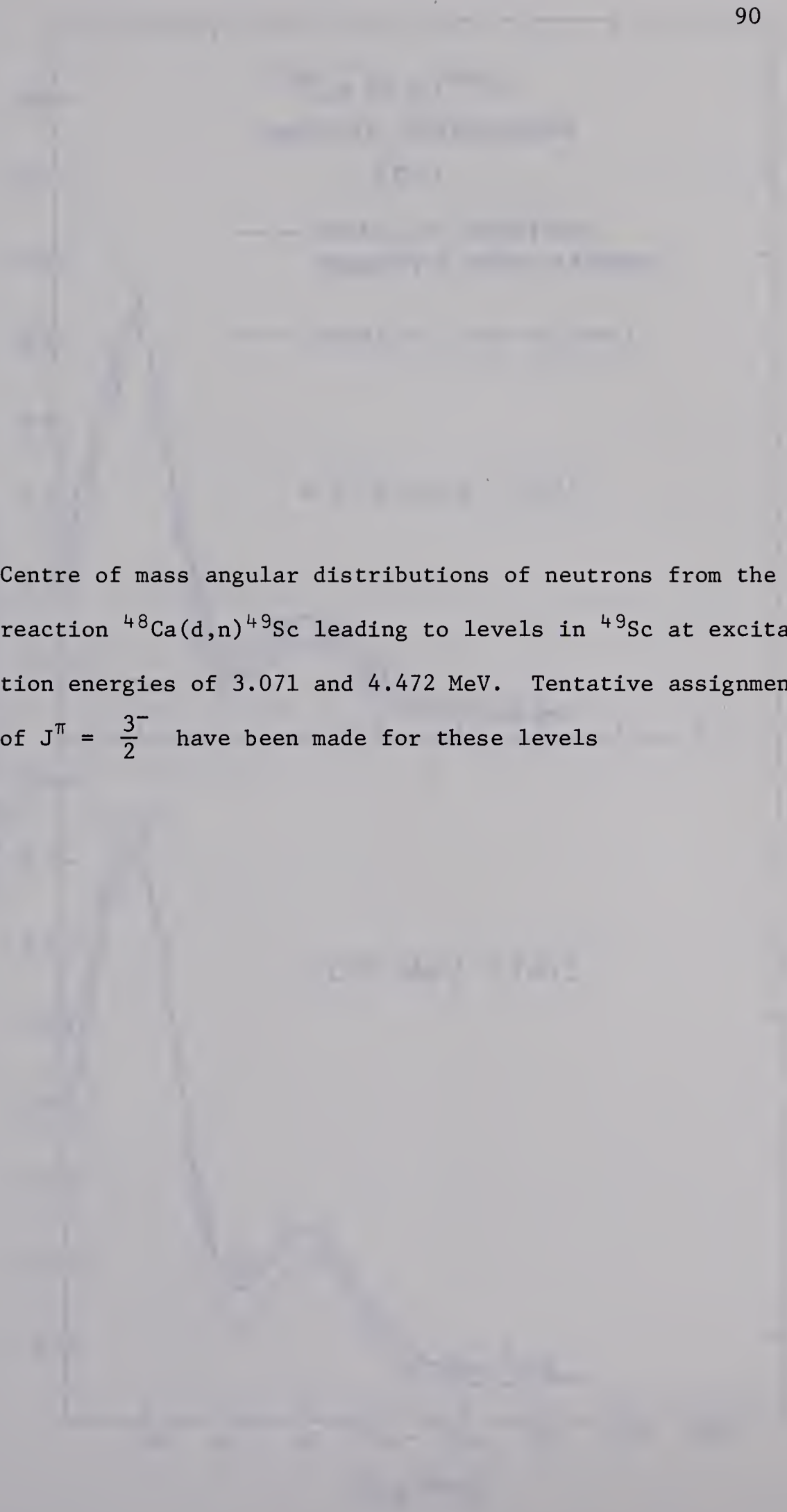


Figure 4-3 Centre of mass angular distributions of neutrons from the reaction $^{48}\text{Ca}(d,n)^{49}\text{Sc}$ leading to levels in ^{49}Sc at excitation energies of 3.071 and 4.472 MeV. Tentative assignments of $J^\pi = \frac{3}{2}^-$ have been made for these levels

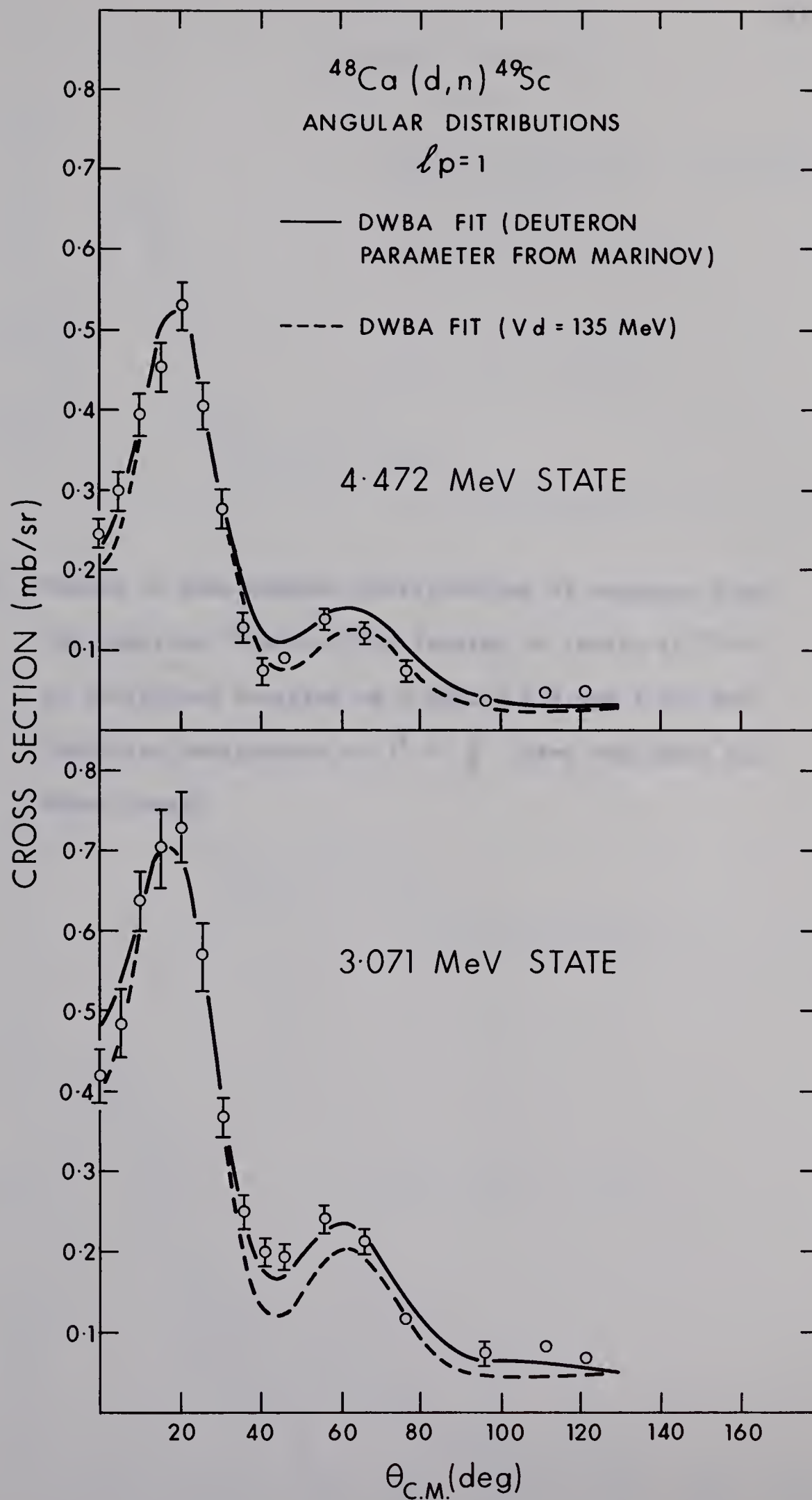


Figure 4-4 Centre of mass angular distributions of neutrons from the reaction $^{48}\text{Ca}(d,n)^{49}\text{Sc}$ leading to levels in ^{49}Sc at excitation energies of 5.008, 5.655 and 7.050 MeV. Tentative assignments of $J^\pi = \frac{1}{2}^-$ have been made for these levels

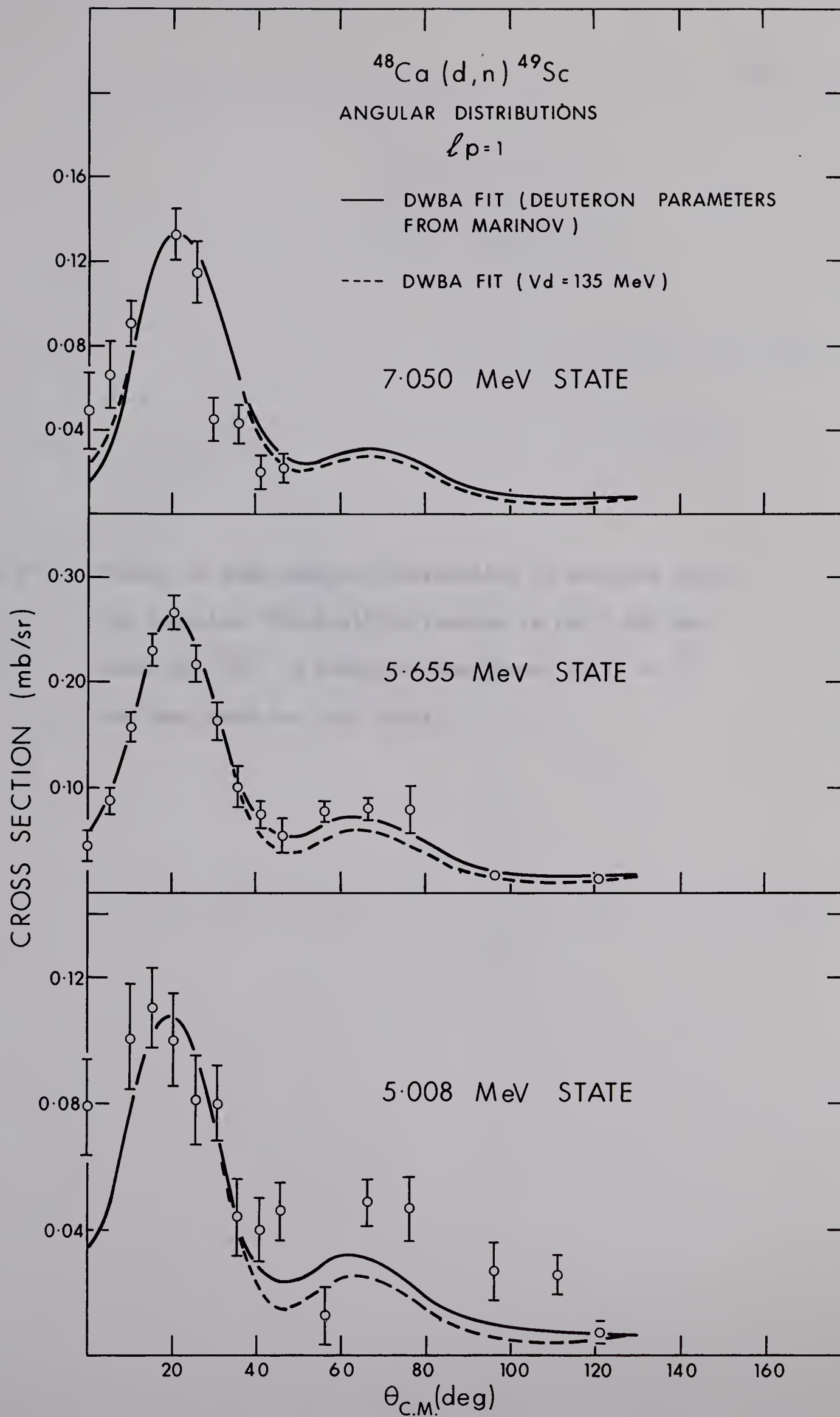
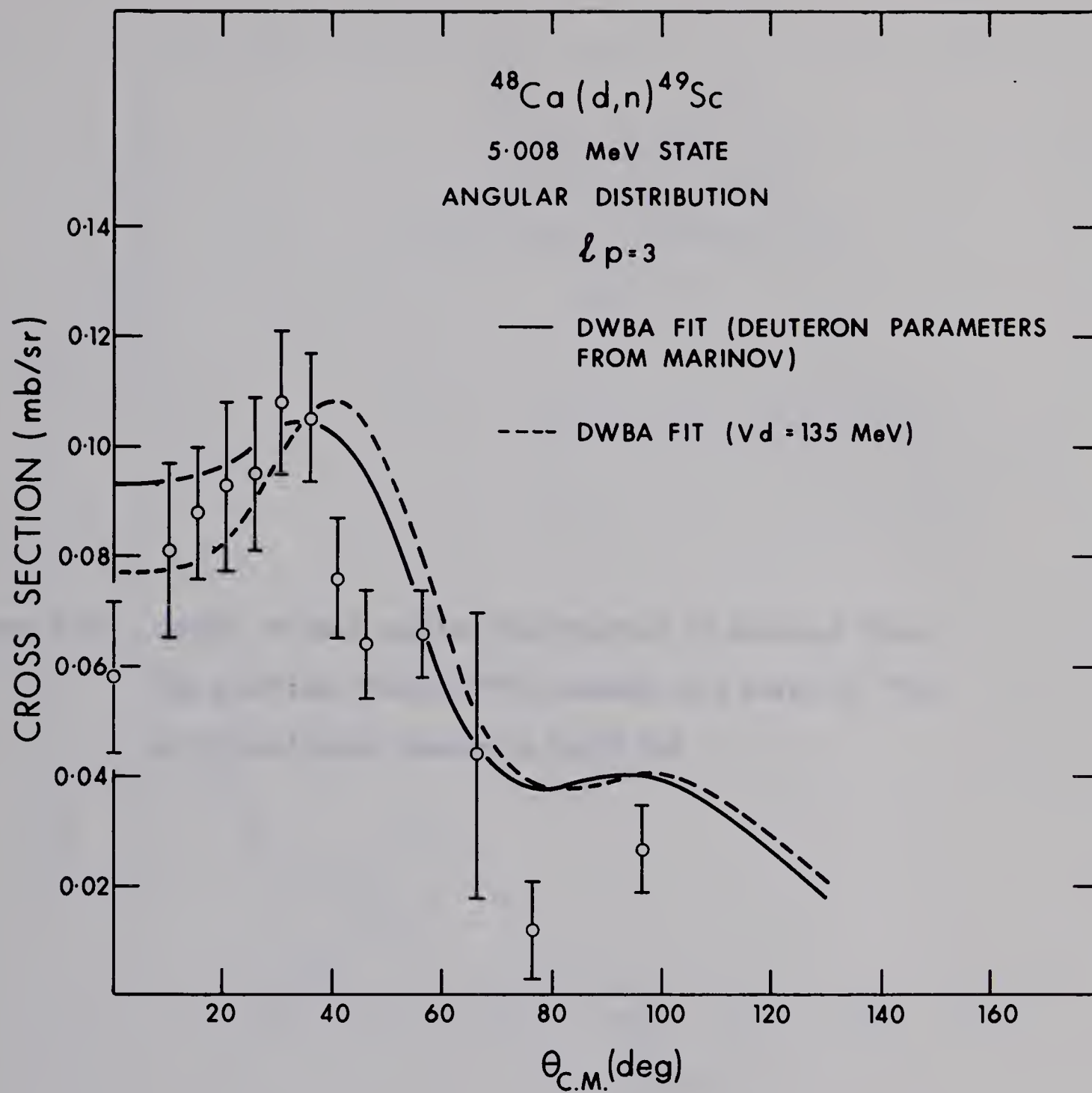


Figure 4-5 Centre of mass angular distribution of neutrons from the reaction $^{48}\text{Ca}(d,n)^{49}\text{Sc}$ leading to the 5.080 MeV level in ^{49}Sc . A tentative assignment of $J^\pi = \frac{5^-}{2}$ has been made for this level



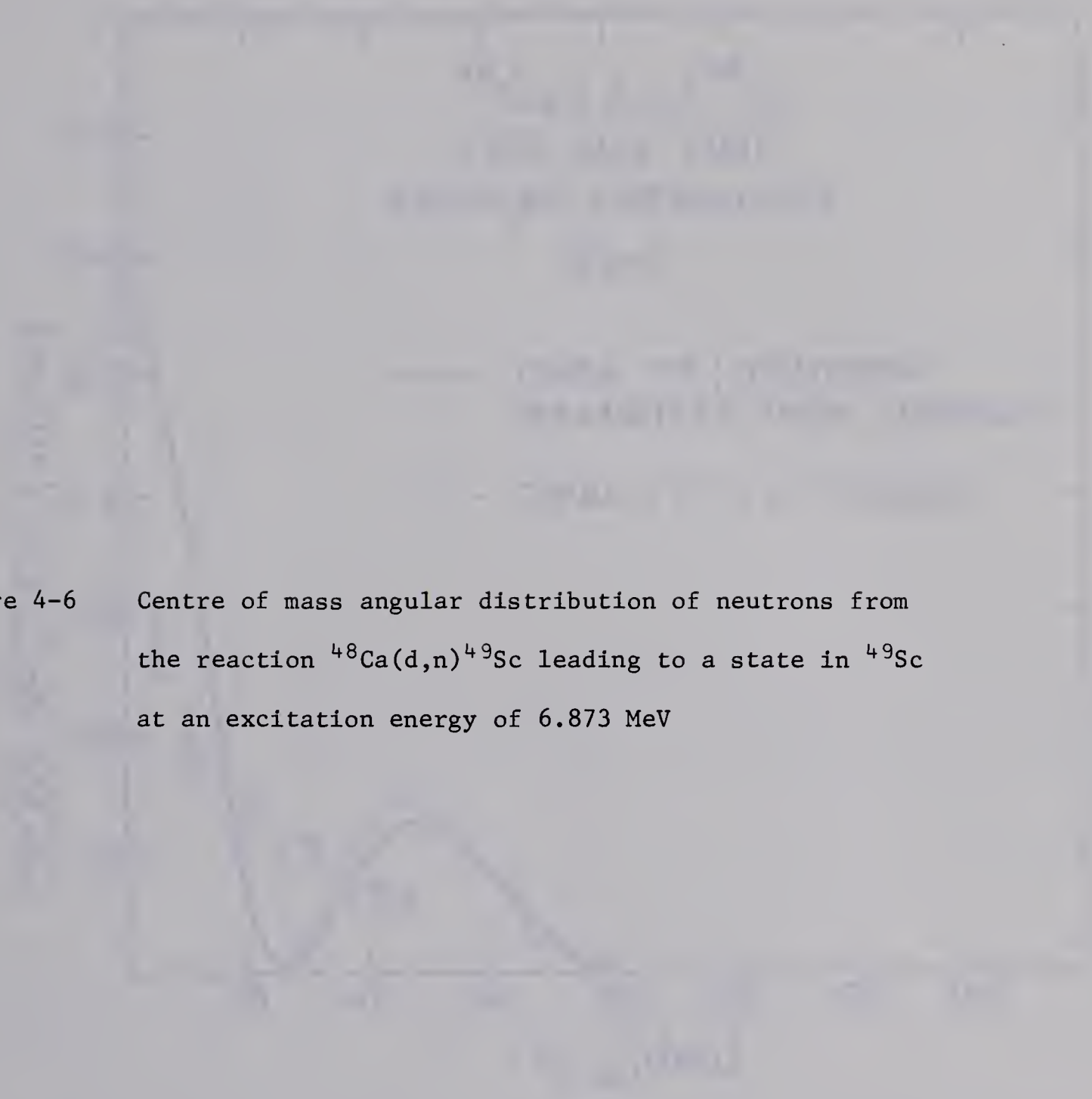


Figure 4-6 Centre of mass angular distribution of neutrons from the reaction $^{48}\text{Ca}(d,n)^{49}\text{Sc}$ leading to a state in ^{49}Sc at an excitation energy of 6.873 MeV

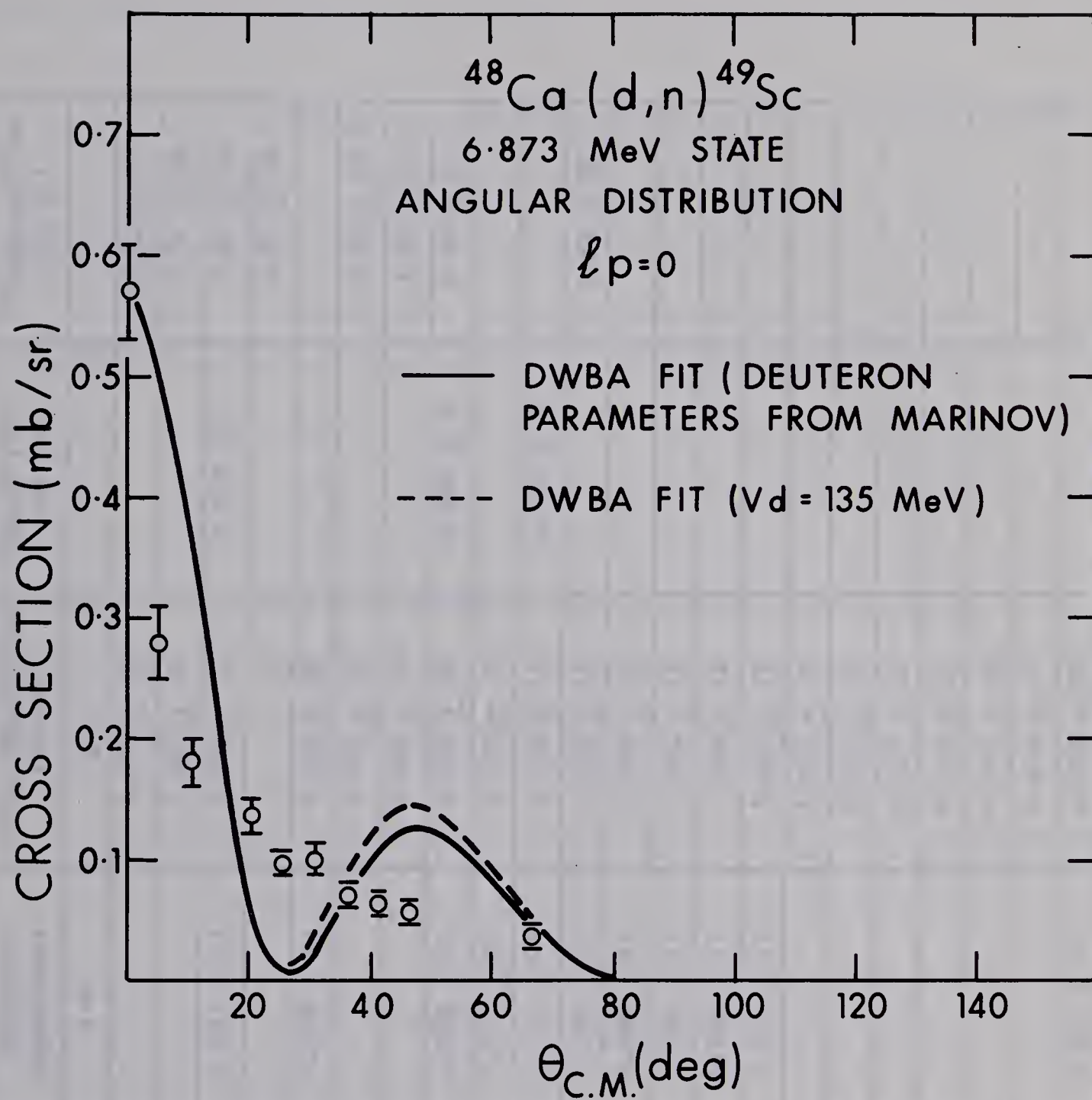


Table 4-1 Q values for the $^{48}\text{Ca}(\text{d},\text{n})^{49}\text{Sc}$ reaction and Excitation Energies of Levels in ^{49}Sc . (Q values and excitation energies are in MeV, errors in KeV).

Q VALUE	EXCITATION ENERGY			
	Present Experiment	$^{48}\text{Ca}(\text{}^3\text{He},\text{d})^{49}\text{Sc}$ (Er 66)	$^{49}\text{Ca}(\beta^-)^{49}\text{Sc}$ (Ch 65)	$^{48}\text{Ca}(\text{p},\gamma)^{49}\text{Sc}$ (Du 66)
$7.404 \pm \underline{\quad}$ 4	g.s.	g.s.		
		$2.233 \pm \underline{10}$		$2.22 \pm \underline{20}$
		$2.382 \pm \underline{10}$		$2.34 \pm \underline{20}$
$4.333 \pm \underline{\quad}$ 3	$3.071 \pm \underline{11}$	$3.092 \pm \underline{5}$	$3.079 \pm \underline{1}$	$3.10 \pm \underline{30}$
				$3.50 \pm \underline{30}$
$3.628 \pm \underline{\quad}$ 8	$3.776 \pm \underline{13}$	$3.819 \pm \underline{10}$		
		$3.923 \pm \underline{10}$		$3.93 \pm \underline{50}$
		$4.004 \pm \underline{10}$		$3.96 \pm \underline{50}$
$3.350 \pm \underline{\quad}$ 4	$4.054 \pm \underline{11}$	$4.080 \pm \underline{10}$	$4.065 \pm \underline{3}$	$4.10 \pm \underline{50}$
$2.932 \pm \underline{\quad}$ 2	$4.472 \pm \underline{10}$	$4.507 \pm \underline{5}$		
$2.657 \pm \underline{\quad}$ 19	$4.747 \pm \underline{22}$	$4.756 \pm \underline{12}$	$4.732 \pm \underline{3}$	
$2.396 \pm \underline{\quad}$ 6	$5.008 \pm \underline{12}$	$5.035 \pm \underline{12}$		$4.96 \pm \underline{50}$
$2.324 \pm \underline{\quad}$ 5	$5.080 \pm \underline{11}$	$5.100 \pm \underline{12}$		
$2.044 \pm \underline{\quad}$ 6	$5.360 \pm \underline{12}$	$5.392 \pm \underline{12}$		
$1.749 \pm \underline{\quad}$ 3	$5.655 \pm \underline{11}$	$5.686 \pm \underline{12}$		
$1.593 \pm \underline{\quad}$ 4	$5.811 \pm \underline{11}$	$5.836 \pm \underline{12}$		
		$6.024 \pm \underline{12}$		
		$6.210 \pm \underline{12}$		
		$6.434 \pm \underline{12}$		
		$6.555 \pm \underline{12}$		
		$6.742 \pm \underline{12}$		
		$6.836 \pm \underline{12}$		
$0.531 \pm \underline{20}$	$6.873 \pm \underline{22}$	$6.903 \pm \underline{12}$		
		$7.044 \pm \underline{12}$		
$0.354 \pm \underline{\quad}$ 3	$7.050 \pm \underline{11}$	$7.081 \pm \underline{12}$		

observed by Erskine (Er 66) for the $^{48}\text{Ca}(^3\text{He},d)^{49}\text{Sc}$ reaction which leads to a ground state Q value of 7.419 MeV for the $^{48}\text{Ca}(d,n)^{49}\text{Sc}$ reaction. This value is also in agreement with the present result.

Excitation energies for the ^{49}Sc levels seen in the present experiment are also listed in Table 4-1. Results from several other published works are presented for comparison. It is interesting to note that the ^{49}Sc excitation energies obtained in the present experiment are consistently lower than those obtained by Erskine (Er 66). In most cases, the differences disappear if the 15 KeV difference between the present ground state Q value and that calculated from the $(^3\text{He},d)$ reaction is taken into account. The results of the present experiment agree more closely with the measurements of Chilosi (Ch 65) (Table 4-1); especially for the level at 3.071 ± 0.011 MeV. Chilosi reports an excitation energy of 3.079 ± 0.001 MeV for this level which is in considerable disagreement with value of 3.092 ± 0.005 MeV reported from a study of the $^{48}\text{Ca}(^3\text{He},d)^{49}\text{Sc}$ reaction (Er 66). Subtracting 15 KeV from the $(^3\text{He},d)$ value gives 3.077 MeV in good agreement with the value of 3.079 from Chilosi. This evidence strongly supports the present ground state Q value and lends weight to present excitation energies as being correct.

No evidence could be given for existence of a state at 3.50 MeV reported from a study of gamma rays in the $^{48}\text{Ca}(p,\gamma)^{49}\text{Sc}$ reaction (Du 66). In the present reaction, this possible state was obscured by a contaminant group from the reaction $^{44}\text{Ca}(d,n)^{45}\text{Sc}$ (0.714 MeV excitation energy in ^{45}Sc (Sc 66)).

4.4 Analysis of the Angular Distributions

The solid curves shown with the angular distributions in figures 4-2 to 4-6 are DWBA calculations performed with a program written by W.R. Smith (Sm 65). The form of the optical model potentials used in the analysis have been shown in Chapter 2 as part of the discussion of the $^{40}\text{Ca}(d,n)^{41}\text{Sc}$ reaction. The parameters used in the $^{48}\text{Ca}(d,n)^{49}\text{Sc}$ analysis are presented in Table 4-2.

Table 4-2 Optical Model Parameters.

Particle	V (MeV)	W (MeV)	r_o (fm)	a (fm)	r_o' (fm)	a' (fm)	r_c (fm)
d	127.6	13.9	0.962	0.772	1.427	0.564	1.25
n	48 - 0.29E	9.6	1.27	0.66	1.27	0.47	1.25
p			1.25	0.65			1.25

Neutron parameters are from Perey and Buck (see Ro 66) and have been discussed in Chapters 2 and 3.

Several sets of deuteron parameters were tried in arriving at those shown in Table 4-2. The first tried was the average set derived from ^{40}Ca deuteron elastic scattering by Bassel (Ba 64). This set was of interest since it had been used previously by Erskine (Er 66) in an analysis of the $^{48}\text{Ca}(^3\text{He},d)^{49}\text{Sc}$ reaction. Decidedly better fits were

obtained with the ^{48}Ca deuteron elastic scattering data from Marinov (Ma 66). This, of course, is not surprising since elastic scattering on the target nucleus should indeed give better optical model parameters than elastic scattering on a nucleus eight mass units away. The elastic scattering data of Marinov was at bombarding energies 9.0 and 12.0 MeV. The method of adjusting the imaginary potential to apply the results of high energy elastic scattering to low energy stripping described in Chapter 2 was adopted in the present analysis. A number of parameter sets are presented in the report by Marinov all of which were tried in the analysis of the $^{48}\text{Ca}(d,n)^{49}\text{Sc}$ data. Of these, the parameter set shown in Table 4-2 gave the best fits to the angular distributions. It is interesting to note that Marinov obtained this parameter set by starting with the ^{40}Ca parameters of Bassel (Ba 64) first tried in this analysis. The parameters used are from 9.0 MeV scattering of deuterons on ^{48}Ca , so that the extrapolation to 5.5 MeV is not large. It was found that the best fits to the angular distributions did not come when the imaginary potential was varied, but when it was kept at the value found in the elastic scattering analysis. It is possible that the bombarding energy difference of 3.5 MeV between the present experiment and the 9.0 MeV elastic scattering data is not sufficient to see a difference. For example, a large difference may not be expected since the values of W_d in the results of Marinov decrease by less than 2 MeV in going from 12 to 9 MeV bombarding energy.

A disturbing feature of this set of parameters is the poor fit to

the main stripping peak of the ground state transition. In an attempt to produce a better fit to the experimental data, the real part of the deuteron potential was stepped from 120 to 150 MeV. The dashed curves in figures 4-2 to 4-6 are DWBA calculations with this potential equal to 135 MeV and with all other parameters the same as for the solid curves. This change in the real potential from 127.6 to 135.0 MeV may be regarded as representing a required energy increase in going from 9.0 to 5.15 MeV bombarding energy since the calculations do not take into account the non-locality of nuclear forces. An example of this energy dependence to duplicate the effects of non-local forces is given in the energy dependent term for the neutron potentials of Table 4-2. The effect of this potential change is to give better fits at forward angles for $\ell = 3$ transitions, and somewhat worse fits for $\ell = 1$ transitions, particularly at angles greater than 40° . In all cases, the curves are normalized at the same angle to point out the relative changes. As such, the change in potential does not reflect the changes in absolute cross sections that are present in the calculations. For instance, the cross section predicted for the ground state transition at 35° dropped from 3.28 to 2.57 mb/sr in changing from the unadjusted parameters to those with the real potential at 135.0 MeV. The ℓ value assignments indicated in figures 4-2 to 4-6 are consistent with the recent $^{48}\text{Ca}(^3\text{He},d)^{49}\text{Sc}$ results of Armstrong (Ar 64, Ar 65) and Erskine (Er 66). The spectroscopic factors given in Table 4-3 were obtained from the DWBA calculations

Table 4-3 Spectroscopic factors from the present study of the $^{48}\text{Ca}(\text{d},\text{n})^{49}\text{Sc}$ reaction compared to recent $^{48}\text{Ca}(^3\text{He},\text{d})^{49}\text{Sc}$ measurements and to the calculated values.

Single Particle State	Excitation Energy (MeV)	S With Unadjusted Parameters	$\sum S$ With Unadjusted Parameters	S With Deuteron Potential 135 MeV	$\sum S$ With Deuteron Potential 135 MeV	S ($^3\text{He},\text{d}$) (Er 66)	S ($^3\text{He},\text{d}$) (Ar 64)	S ($^3\text{He},\text{d}$) (Ar 65)	$\sum S$ Calculated (Ar 64)
$1f_{7/2}$	g.s.	1.0	1.0	1.0	1.0	1.0	1.0	0.91	1.0
$1f_{5/2}$	5.080	0.54	0.54	0.54	0.54	0.35	0.34	0.37	0.89
$2p_{3/2}$	3.071	0.69	1.08	0.59	0.89	0.68	0.61	0.60	0.89
	4.472	0.39		0.30		0.31	0.28	0.25	
$2p_{1/2}$	5.008	0.17	0.59	0.13	0.45	0.13	0.07	0.07	0.89
	5.655	0.32		0.24		0.30	0.24	0.27	
	7.050	0.10		0.08		0.10	0.10	0.14	
	6.873	0.13		0.11		0.07			

by assuming the ground state transition to have $J^\pi = \frac{7}{2}^-$ and to be of single particle strength. This required the cross sections calculated from the elastic scattering data of Marinov (Ma 66) to be divided by 10.05 and those calculated with the real potential adjusted to be divided by 7.90. The existence of a factor greater than unity could indicate that the program was calculating the absolute cross section incorrectly. However, this seems unlikely as the $^{40}\text{Ca}(d,n)^{41}\text{Sc}$ cross sections are calculated correctly. It is more likely that the target thickness quoted by the manufacturer is greatly in error.

The assignment of spins to states in ^{49}Sc indicated in Table 4-3 is necessarily uncertain since gamma ray correlation measurements have only been performed for the two lowest excited states at 2.22 and 2.34 MeV (Du 66). Both of these states were too weak to be considered in the present angular distribution analysis. In addition, it appears that the assignment of $\frac{3}{2}, \frac{5}{2}$ to the level at 2.34 MeV (Du 66) is incorrect. Erskine (Er 66) assigns $\frac{1}{2}^+$ to this level (2.382 MeV) as seen in the $^{48}\text{Ca}(^3\text{He},d)^{49}\text{Sc}$ reaction.

Erskine (Er 66) has made some reasonable tentative spin assignments on the basis of systematics and results from the β decay of ^{49}Ca to ^{49}Sc . The arguments for these assignments are presented here for the sake of completeness. One would expect $J^\pi = \frac{7}{2}^-$ for the ground state of ^{49}Sc (the $1f_{\frac{7}{2}}$ single particle state of the shell model). This is, in fact, the assignment from the $\ell = 3$ angular distribution and the lack of a β^-

transition which would proceed if this state had $J^\pi = \frac{5^-}{2}$. The next shell model state expected is the $2P_{\frac{3}{2}}$ state which is probably the state at 3.071 MeV. This assignment is supported by the $\ell = 1$ transition to this state with a large spectroscopic factor and a strong β^- transition. The next state (at 4.472 MeV) is excited with an $\ell = 1$ transition, which allows spin assignment of $\frac{1^-}{2}$ or $\frac{3^-}{2}$. Armstrong (Ar 65) suggests that the assignment should be $\frac{3^-}{2}$. This assignment is based on the J dependence of the angular distribution as seen in the $^{48}\text{Ca}(^3\text{He},d)^{49}\text{Sc}$ reaction. An assignment of $\frac{1^-}{2}$ appears to be a reasonable guess for all higher $\ell = 1$ states and $\frac{5^-}{2}$ for $\ell = 3$ states. This is reasonable since the total of $2P_{\frac{3}{2}}$ strength seems concentrated in the two levels at 3.071 and 4.472 MeV (Er 66, Ar 64, Ar 65 and the present results in Table 4-3). Remaining levels should then belong to the $2P_{\frac{1}{2}}$ shell. For instance, Armstrong (Ar 65) finds some evidence to support a J^π assignment of $\frac{1^-}{2}$ for the state at 5.655 MeV. In the present experiment, the transition to this state was characterized by an $\ell = 1$ stripping pattern (figure 4-4). The assumption of $\frac{5^-}{2}$ for higher $\ell = 3$ states is valid to the extent that ^{48}Ca is a good closed shell nucleus. Except for the ground state, no $\ell = 3$ transitions are observed in either the $(^3\text{He},d)$ or (d,n) reaction below 3 MeV excitation energy. Splitting of the $1f_{\frac{7}{2}}$ shell should be less than 3 MeV, so the ground state carries all of the $1f_{\frac{7}{2}}$ single particle strength. A number of $\ell = 3$ states have been seen in the $(^3\text{He},d)$ reaction (Ar 64, Er 66). An angular distribution could be extracted for only one

of these, the state at 5.080 MeV, since the intensity for the remaining states was too low.

The two sets of spectroscopic factors presented in Table 4-3 agree in general with the published data. It would appear that the spectroscopic factors calculated with the elastic scattering data from Marinov (Ma 66) agree with the results of Erskine (Er 66), while those calculated with the real part of the deuteron potential equal to 135 MeV agree more closely with the results presented by Armstrong (Ar 64). If the two states at 3.071 and 4.472 MeV have been identified correctly, the sum of the $\frac{3}{2}^-$ single particle strength is 1.08 for the unadjusted parameters and 0.89 for the adjusted parameters. The predicted sum of the strengths is 0.89 which clearly supports the latter set of parameters. The predicted strength of 0.89 for the single particle strength arises from the fact that only those states with isobaric spin, T , equal to $\frac{7}{2}$ are being considered. Two simple formulae have been presented in Chapter 3 which give the sum of the single particle strength expected to be with states of normal isobaric spin and with states with one unit of isobaric spin higher, the isobaric analog states. Since the target nucleus, ^{48}Ca , has isobaric spin 4, these sums are expected to be $\frac{8}{9}$ and $\frac{1}{9}$ respectively.

A re-analysis of the original ($^3\text{He},d$) data (Ar 64) by Armstrong (Ar 65) with the program TSALLY (Ba 62) does not change the conclusions presented here. The spectroscopic information from this work is presented in Table 4-3 for comparison.

The spectroscopic factor of 0.54 observed for the $\ell = 3$ transition

to the $\frac{5^-}{2}$, 5.080 MeV state is notable different from the previously measured value of 0.34. This may result, however, from the large uncertainty in extracting the angular distribution from the closely overlapping 5.008 MeV state. In general, neutron peaks for these two states were separated by only 3 or 4 channels in the observed spectra.

Only three of a possible seven or eight $2P_{\frac{1}{2}}$ levels (Ar 64, Ar 65, Er 66) were seen in the present experiment (Figure 4-4). These states are at excitation energies where the level density is high so that only the more intense neutron peaks could be extracted. The results of the present experiment suggest that 50% of the $2P_{\frac{1}{2}}$ single-particle strength is contained in levels at 5.008, 5.655 and 7.050 MeV.

An intense transition to a level at 6.873 MeV was observed to be characteristic of $\ell = 0$ stripping (figure 4-6). An assignment of $J^\pi = \frac{1^+}{2}$ is in agreement with that found by Erskine (Er 66), however, a spectroscopic factor of 0.13 disagrees, to some extent, with their measured value of 0.07.

4.5 Observation of the ^{49}Ca Ground State Analog in ^{49}Sc

The $^{48}\text{Ca}(d,n)^{49}\text{Sc}$ reaction was also studied at 6.0 MeV bombarding energy to observe a state reported to be the analog of the ^{49}Ca ground state (Jo 66, Ch 67). The state is expected to lie at 11.6 MeV excitation energy in ^{49}Sc as calculated from binding energy and Coulomb energy differences between ^{49}Ca and ^{49}Sc . It should have $J^\pi = \frac{3^-}{2}$ ($\ell = 1$ transi-

tion) as evidenced by the assignment of $\frac{3^-}{2}$ to the ground state of ^{49}Ca (En 62).

Evidence for this transition did not appear on the 5.5 MeV spectra since its neutron energy was too low (a high neutron cut-off energy was used to suppress low energy background). The 6.0 MeV study reported here was carried out with the same configuration for the time of flight system as had been used in the $^{40}\text{Ca}(d,n)^{41}\text{Sc}$ experiment. In particular, the neutron cut-off energy was 0.60 MeV.

Figure 4-7 shows a zero degree time of flight spectrum observed at a deuteron bombarding energy of 6.0 MeV and a distance of 6.0 meters. The peak on the side of the ^{13}N 3.51, 3.56 MeV doublet has been identified as the neutron group originating from the transition to the analog state. The state was observed at additional laboratory angles of 15° , 30° , 60° and 100° . Kinematic identification of this group leads to a Q value of -4.167 ± 0.002 MeV for the transition. On the basis of a ground state Q value of 7.404 ± 0.010 MeV, this gives 11.571 ± 0.010 as the excitation energy of the analog level in ^{49}Sc .

A rough angular distribution has been extracted from the data at the five angles and is shown in figure 4-8. No attempt has been made to analyze this data in terms of a stripping theory. Consequently, a laboratory angular distribution is presented to facilitate comparison with future experiments. Comparison to stripping theory is difficult since the state is unbound to proton emission making conventional stripping programs inadequate. Butler theory, which works for unbound levels,

Figure 4-7 A time of flight spectrum for the reaction $^{48}\text{Ca}(\text{d},\text{n})^{49}\text{Sc}$ taken at a deuteron bombarding energy of 6.0 MeV. The section of the spectrum showing the ^{49}Ca ground state analog has been selected. This state is seen to occur at an excitation energy of 11.571 MeV in ^{49}Sc

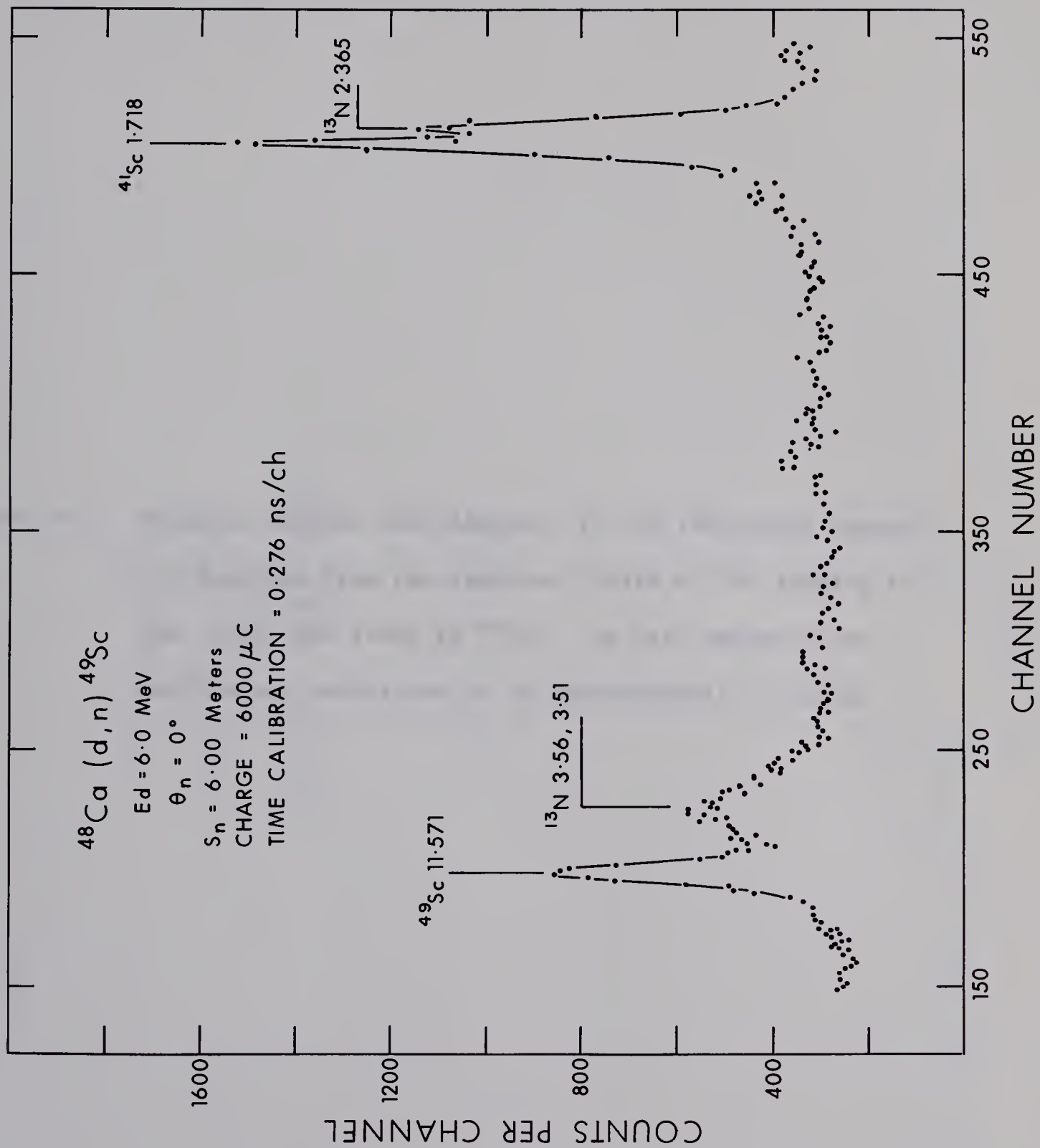
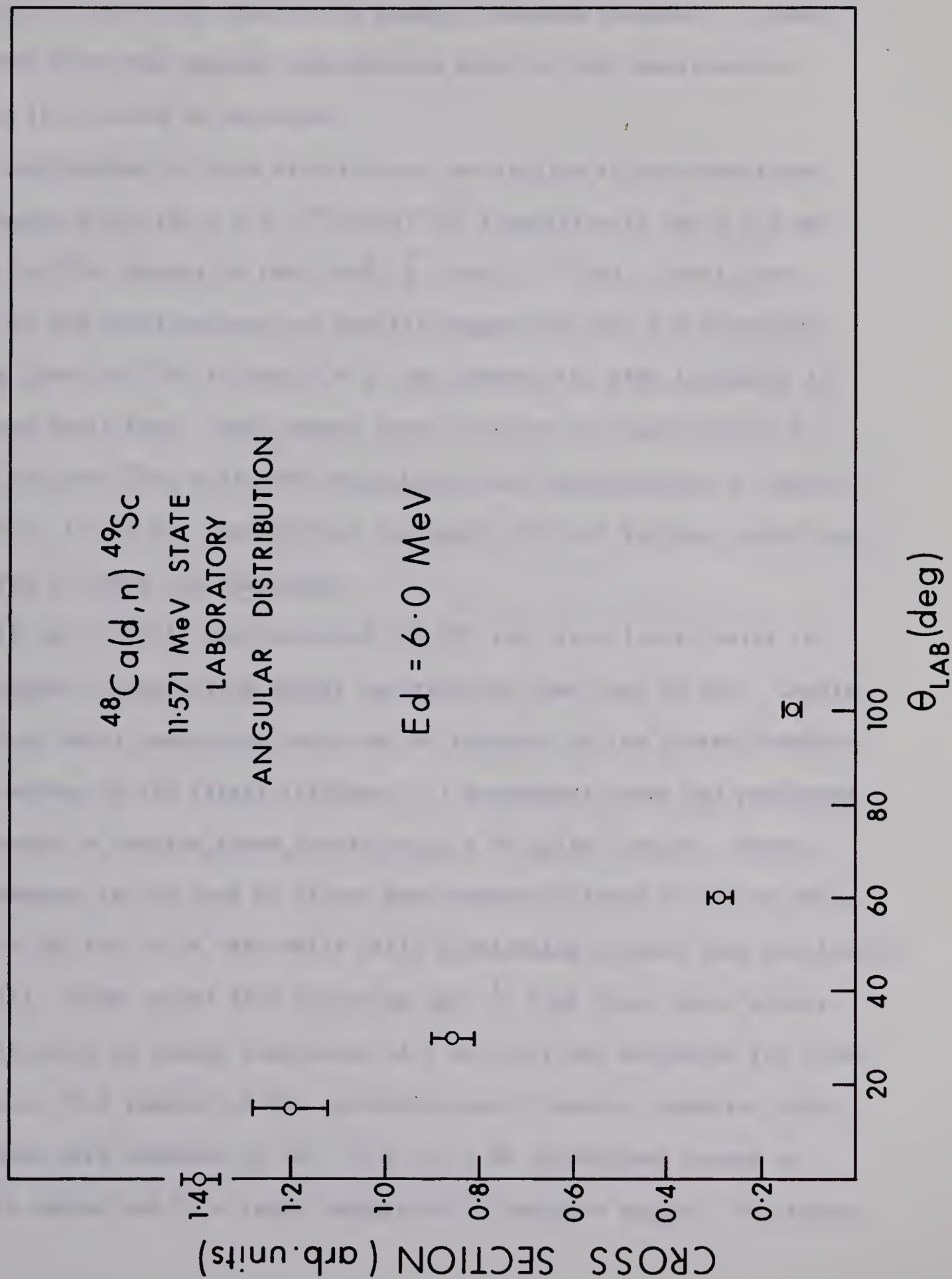


Figure 4-8 Relative angular distribution, in the laboratory system, for neutrons from the reaction $^{48}\text{Ca}(\text{d},\text{n})^{49}\text{Sc}$ leading to the 11.571 MeV state in ^{49}Sc . The zero degree cross section was calculated to be approximately 3.5 mb/sr



could do no more than confirm the angular momentum transfer. Of most interest from this angular distribution would be the spectroscopic factor if it could be extracted.

Two features of this distribution are similar to that described in Chapter 3 for the $\ell = 1$, $^{42}\text{Ca}(d,n)^{43}\text{Sc}$ transition to the 6.155 MeV level in ^{43}Sc (analog of the 2.048, $\frac{3^-}{2}$ level in ^{43}Ca). First, the shape of the distributions are similar suggesting that the transition to the level in ^{49}Sc is also $\ell = 1$, and second, the peak intensity in both are quite high. Zero degree cross sections of approximately 5.2 mb/sr for the ^{43}Sc , 6.155 MeV distribution and approximately 3.5 mb/sr for ^{49}Sc , 11.571 MeV distribution represent the most intense transitions observed in these two reactions.

It has recently been reported (Ch 67) that four levels exist in this region of excitation energy separated by less than 10 KeV. Levels with this small separation could not be resolved in the present experiment because of the target thickness. A subsequent study was performed to attempt to resolve these levels using a 50 $\mu\text{g}/\text{cm}^2$ target. Recent improvements in the time of flight spectrometer allowed a neutron threshold of 300 KeV to be used while still maintaining optimum time resolution (Ge 67d). With an RCA 8575 phototube and $\frac{1}{2}$ inch thick Naton plastic scintillator, an energy resolution of 5 to 6 KeV was estimated for 1 MeV neutrons. The results of the experiment were, however, negative since the peaks were obscured by the ^{13}N 3.51, 3.56 contaminant groups at forward angles and by a large background at backward angles. No cleaner

targets of this thickness were available, so the attempt to resolve these closely spaced levels was postponed.

4.6 Summary

Angular distributions have been observed in the (d,n) reaction leading to a number of states in ^{49}Sc . Spectroscopic information has been extracted, with the aid of the Distorted Wave theory, which is in good agreement with that found from the $^{48}\text{Ca}(^3\text{He},\text{d})^{49}\text{Sc}$ reaction (Ar 64, Ar 65, Er 66). A Q value of 7.404 ± 0.010 MeV measured for the $^{48}\text{Ca}(\text{d},\text{n})^{49}\text{Sc}$ reaction gives ^{49}Sc excitation energies which are generally lower than those found in the $^{48}\text{Ca}(^3\text{He},\text{d})^{49}\text{Sc}$ reaction (Er 66). The present excitation energies, however, agree with several precise measurements obtained from the study of gamma rays following the β decay of ^{49}Ca (Ch 65).

In ^{49}Ca ground state analog has been found to occur at an excitation energy of 11.571 ± 0.010 MeV in ^{49}Sc . A very strong transition to this state was observed in the $^{48}\text{Ca}(\text{d},\text{n})^{49}\text{Sc}$ reaction. An attempt to determine whether this state was actually composed of four closely spaced levels (Ch 67) was unsuccessful.

CHAPTER 5

CONCLUSIONS

Angular distributions characteristic of single particle transitions have been observed with the (d,n) reaction leading to a number of states in the nuclei ^{41}Sc , ^{43}Sc and ^{49}Sc . In ^{41}Sc and ^{49}Sc , both of which have been described as doubly magic plus one nucleon, departure from the simple shell model picture is observed. This is evidenced by a splitting of the $2P$ strength and the presence of low-lying even parity states. These departures from the simple shell model picture are possibly due to residual interactions and core excitations. A large splitting of the $1f_{\frac{7}{2}}$ and $2p_{\frac{3}{2}}$ strength is observed for ^{41}Sc and ^{49}Sc . Values of 1.75 and 3.53 MeV are found for ^{41}Sc and ^{49}Sc , respectively. In ^{43}Sc , however, components of $2P$ single particle strength are found as low as 0.475 MeV excitation energy and spread over a considerable range of energies. This probably results from configuration mixing of the three particles outside the closed ^{40}Ca core. The present results confirm similar observations made from studies of the ($^3\text{He},d$) reaction on these same three nuclei (Sh 64, Bo 65, Sc 66, Ar 64, Ar 65, Er 66).

This somewhat cursory study of nuclei in the $1f_{\frac{7}{2}}$ shell has stimulated a more extensive investigation into other features of this shell. Other groups in this laboratory are currently carrying out studies of the (d,p) and ($^3\text{He},n$) reactions on the stable calcium isotopes. Results from the

comparison of the reactions $^{40}\text{Ca}(d,n)^{41}\text{Sc}$ and $^{40}\text{Ca}(d,p)^{41}\text{Ca}$ have been presented by Leighton (Le 67a). From this study, it would appear that some families of deuteron parameters, characterized by large values for the imaginary well depth and small values for the imaginary diffuseness, can be discarded.

A number of the angular distributions observed in the present three reactions have been analyzed in terms of the Distorted Wave Theory for direct reactions. The most satisfactory fits to the data were observed for the $^{48}\text{Ca}(d,n)^{49}\text{Sc}$ reaction. It would also appear, from the $^{48}\text{Ca}(d,n)^{49}\text{Sc}$ results, that it is important to reproduce the main stripping maximum as well as possible if consistent spectroscopic information is to be extracted.

Average sets of neutron elastic scattering parameters have been presented by Perey and Rosen (Ro 66), which, it is suggested should work for all elastic scattering reactions regardless of mass. It would appear that this is indeed the case for the reactions $^{42}\text{Ca}(d,n)^{43}\text{Sc}$ and $^{48}\text{Ca}(d,n)^{49}\text{Sc}$, especially for stripping to the excited states in these nuclei. Poor agreement between calculations and data for the $^{40}\text{Ca}(d,n)^{41}\text{Sc}$ ground state transition gave rise to a number of proposals to explain the differences.

- (1) Compound nucleus process are important and should be taken into account.
- (2) average neutron elastic scattering parameters from Rosen (Ro 66) are inadequate to describe the stripping process.

- (3) the D state of the deuteron internal wave function should be included in the calculations.

It is becoming increasingly important in reaction theory to be able to treat stripping to unbound levels. Many reactions are now being studied where stripping to unbound levels forms an integral part of the data. The $^{40}\text{Ca}(\text{d},\text{n})^{41}\text{Sc}$ and $^{40}\text{Ca}(^3\text{He},\text{d})^{41}\text{Sc}$ reactions are just two of these. The formalism for such a program has been presented by Huby and Mines (Hu 65), but has not found wide application because of mathematical difficulties. In the past, it has been usual to analyze distributions to unbound levels in terms of the Butler Plane Wave theory. This has, however, proved to be an unreliable way of extracting nuclear structure information. In all three nuclei considered in the present study, additional information can be extracted with a program for fitting unbound levels. Of interest in ^{43}Sc and ^{49}Sc are isobaric analog states that have been calculated to carry appreciable portions of the single particle strength. It would be of considerable interest to be able to extract this information from the experimental data.

APPENDIX I

A FORTRAN IV PROGRAM FOR THE CALCULATION OF NEUTRON DETECTION EFFICIENCY

A1.1 Introduction

The main difficulty with using neutron detectors in nuclear spectroscopy experiments is the determination of detector efficiency versus neutron energy. Measurement of efficiencies can be long and tedious especially when absolute values are desired (Bu 67). It was for this reason that an attempt was made to calculate the efficiency.

In principal, the detection of neutrons with scintillators can be attributed to scattering from hydrogen and carbon. These are simple processes to calculate, so that determination of the efficiency to within a few percent should be possible. In the present calculations, double scattering from hydrogen, single scattering from carbon (Ha 58) and detector resolution have been included.

A1.2 Formalism for the Calculated Efficiency

Fig. A1-1 represents a cross section of a scintillator, showing the first and possible second proton collision of a neutron passing through it. The scintillator is approximated by an infinite slab of hydrocarbon L cm thick. Since the scintillator used was a disk 3.45 inches in diameter and 0.75 inch thick, a reduction in efficiency is to be expected due to neutron leakage out the sides. However, this should be a small effect for

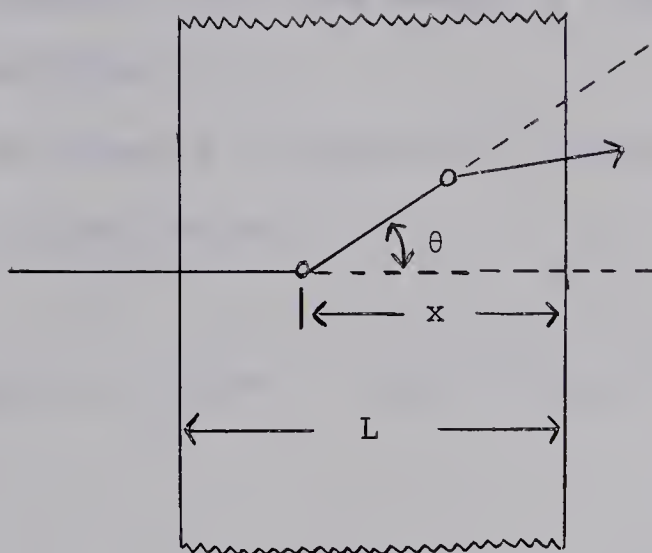


Figure A1-1 Scintillator cross section

the following reasons

1) The laboratory differential cross section for (n,p) scattering is proportional to the cosine of the neutron deflection angle, which insures predominantly forward scattering.

2) The energy of proton scattered neutrons is proportional to the square of the cosine of the neutron deflection angle, which means that the few neutrons scattered through large angles are slow, consequently having a greatly reduced mean free path in the hydrocarbon because of the rapidly rising (n,p) scattering cross section with decreasing neutron energy.

Hardy (Ha 58) gives the proton recoil spectrum in the form $P(K_p, E_0)$ where K_p is the fraction of the energy retained by the neutron after a proton collision i.e. $K_p = (E_0 - E_p) / E_0$ E_p is the proton recoil energy. E_0 is the maximum proton recoil energy and is equal to the laboratory neutron energy before scattering. In this representation, we may define $P(K_p, E_0)$ as the probability that an incident

neutron of energy E_0 will lose energy $(1 - K_p)E$ to one or two protons in the scintillator.

With the geometry of figure A1-1, the expression for $P(K_p, E_0)$ may be written as follows (Ha 58)

$$\begin{aligned}
 P(K_p, E_0) = & \int_0^L [\text{EXP} \{ - n(L-\kappa) \bar{\sigma}(E_0) \}] \frac{n\sigma(E_0)}{E_0} \\
 & \times \text{EXP} \{ - n\sigma(K_p E_0) \kappa / K_p^2 \} d\kappa \\
 & + \int_0^L [\text{EXP} \{ - n(L-\kappa) \bar{\sigma}(E_0) \}] \frac{n\sigma(E_0)}{E_0} \\
 & \times \int_{K_p}^1 [1 - \text{EXP} \{ - n\sigma(kE_0) \kappa / k^2 \}] \frac{dk}{k}
 \end{aligned}$$

where $\bar{\sigma}(E_0) = \sigma(E_0) + (n_c/n) \sigma_c(E_0)$

n, n_c - the hydrogen and carbon densities, in atoms per cm^3 .

$\sigma(E_0), \sigma_c(E_0)$ - the hydrogen and carbon neutron scattering cross sections; $\sigma(E_0)$ given by (Ba 57) and $\sigma_c(E_0)$ by (Hu 58)

Performing the integration over the scintillator width, which can be done explicitly, one obtains

$$P(K_p, E_0) = \frac{\sigma(E)}{E} \frac{K_p^{\frac{1}{2}}}{\sigma(K_p E) - \bar{\sigma}(E_p) K_p^2} \frac{1}{K_p^2} \{ q(K_p, E_0) - \bar{q}(E_0) \}$$

$$\begin{aligned}
& - \frac{\sigma(E_0)}{E_0} \frac{\bar{q}(E_0)}{\bar{\sigma}(E_0)} \log K_p \\
& + \frac{\sigma(E_0)}{E_0} \int_{K_p}^1 \frac{q(k, E_0) - \bar{q}(E_0)}{k \bar{\sigma}(E_0) - k^2 \sigma(kE_0)} dk
\end{aligned}$$

It is convenient for comparison to experiment to write the proton recoil spectrum in the form $P(E_p, E_0)$. The total area under the proton recoil spectrum in each representation must be the same so that we can write

$$P(E_p, E_0) dE_p = P(K_p, E_0) dK_p$$

$$P(E_p, E_0) = - \frac{P(K_p, E_0)}{E_0}$$

The above representations of the proton recoil spectrum assume an infinitely sharp detector resolution. It is assumed that a proton of definite energy stopping in the scintillator gives rise to a definite luminous output. In fact, however, this luminous output consists of a finite number of photons distributed statistically over a variety of wavelengths and produced by a finite number of discrete events in which energy is transferred from the proton to the scintillator and then to the radiation field. This implies that protons of a given energy give

rise to a distribution of luminous outputs rather than one discrete output. In addition, the pulse height observed at the output of the photomultiplier represents the finite number of electrons liberated from the photocathode by the photons emitted by the scintillator.

The net result of the statistical fluctuations in the scintillator and photomultiplier is that protons of a single energy produce a distribution of output pulse heights. This distribution is reasonably well represented by a Gaussian function whose width varies approximately as the square root of the pulse height (Ga 52).

The observed proton recoil spectrum can then be represented by a function $P'(E, E_0)$ which is obtained by folding the previous function $P(E_p, E_0)$ with the appropriate gaussian. E is now the observed or apparent proton energy. We may write

$P'(E, E_0)$ in the following form

$$P'(E, E_0) = \int_0^{E_0} P(E_p, E_0) G([E - E_p], W[E_p]) dE_p$$

where G is a gaussian whose standard deviation W is some function of E_p .

For purposes of calculation, we change to the K coordinate system. We have as before that

$$\begin{aligned} P'(K_E, E_0) &= P'(E, E_0) \frac{dE}{dK_E} \\ &= -E_0 P'(E, E_0) \end{aligned}$$

$$\text{where } K_E = \frac{E_O - E}{E_O}$$

$$P'(K_E, E_O)$$

$$= - E_O \int_1^0 - \frac{P(K_P, E_O)}{E_O} G \left(\left[E_O - E_O K_E \right] - \left[E_O - E_O K_P \right], \right. \\ \left. W \left[E_O - E_O K_P \right] \right) (- E_O d K_P)$$

The gaussian G in this expression can be written in the explicit form

$$G = \frac{1}{\frac{1}{\pi^2} W} \text{EXP} - \left[\frac{E_O (K_P - K_E)}{W} \right]^2$$

Finally the detector efficiency is given by

$$\xi(E_b, E_O) = E_O \int_0^{K_b} P'(K_E, E_O) dK_E$$

$$\text{where } K_b = \frac{E_O - E_b}{E_O}$$

A1.3 Experimental Aspects and Comparison to Calculations

The neutron detector efficiency has been calculated for a cylindrical NE 213 scintillator (3.45" dia. x 0.75" length) coupled to a Phillips XP 1040 photomultiplier.

The resolution of the detector system was measured by illuminating the photocathode with the output of a light pulser. The light output of the pulser was adjusted to give the range of pulse heights normally seen in a neutron time of flight experiment. The output of the photomultiplier was found to be adequately represented by a gaussian function. The following relationship between the FWHM of the gaussian and the average pulse height was found

$$\text{FWHM} = 2.50 * (\text{Average pulse Height})^{\frac{1}{2}}$$

For purposes of calculation, it is necessary to relate the pulse height to proton recoil energy. This is done most conveniently by looking at a ^{22}Na recoil spectrum (Sc 66a). The two thirds amplitude points on the Compton edges of the ^{22}Na recoil spectrum were assumed to correspond to the energies 0.341 and 1.066 MeV. To transform from electron to proton energies, one may use the following equations for NE 213 published by Batchelor et al (Ba 61)

$$L_p = 0.215 E_p + 0.028 E_p^2 \quad (0 < E_p < 8 \text{ MeV})$$

$$= 0.60 E_p - 1.28 \quad (8 < E_p < 14 \text{ MeV})$$

where L_p is the light output (equal to the electron energy in MeV)

E_p is the proton energy in MeV.

The lower cut-off energy, E_b , may also be found quite easily in terms of the ^{22}Na spectrum.

The absolute efficiency calculated with the present program is shown in figure A1-2 with the experimentally measured relative efficiency normalized at 5.0 MeV. The relative efficiency was measured for the detector configuration used in the $^{42}\text{Ca}(\text{d},\text{n})^{43}\text{Sc}$ experiment (Chapter 3). In particular, an NE 213 scintillator and an XP 1040 photomultiplier biased at a neutron energy of 1.05 MeV formed the detector combination.

Quite satisfactory agreement between the shapes of the two curves is obtained. Similar results have been obtained with other bias values, therefore, it is felt that the program can be used quite reliably to predict relative efficiencies. Burbank (Bu 67) finds some disagreement between the measured and absolute efficiencies which is presently being investigated by comparison with other experimentally measured absolute efficiency curves.

Calculations have been performed with a simpler theory in which the detector resolution was not included. In addition, single scattering from hydrogen and carbon were assumed to be the only important processes affecting the efficiency. This theory was found to underestimate the efficiency at the peak of the curve (neutron energy of 2.5 MeV in figure A1-2). At energies above 5.0 MeV values from this simple theory and from the present program were quite similar.

The present approach can possibly be improved by extending the scattering of the incoming particle to higher orders. This is the approach taken in Monte Carlo programs (Ba 61). One would expect better agreement between the calculated and experimental efficiencies at the peak of the efficiency curve if higher orders of scattering are

Figure A1-2 Absolute efficiency calculated with the present program compared with the relative efficiency for the XP 1040 detector and an NE 213 scintillator. The relative efficiency has been normalized to the calculated values at 5.0 MeV. Approximately 6% errors are associated with each point

EFFICIENCY FOR XP1040 DETECTOR
AND NE 213 SCINTILLATOR USED
IN $^{42}\text{Ca}(d,n)^{43}\text{Sc}$ EXPERIMENT

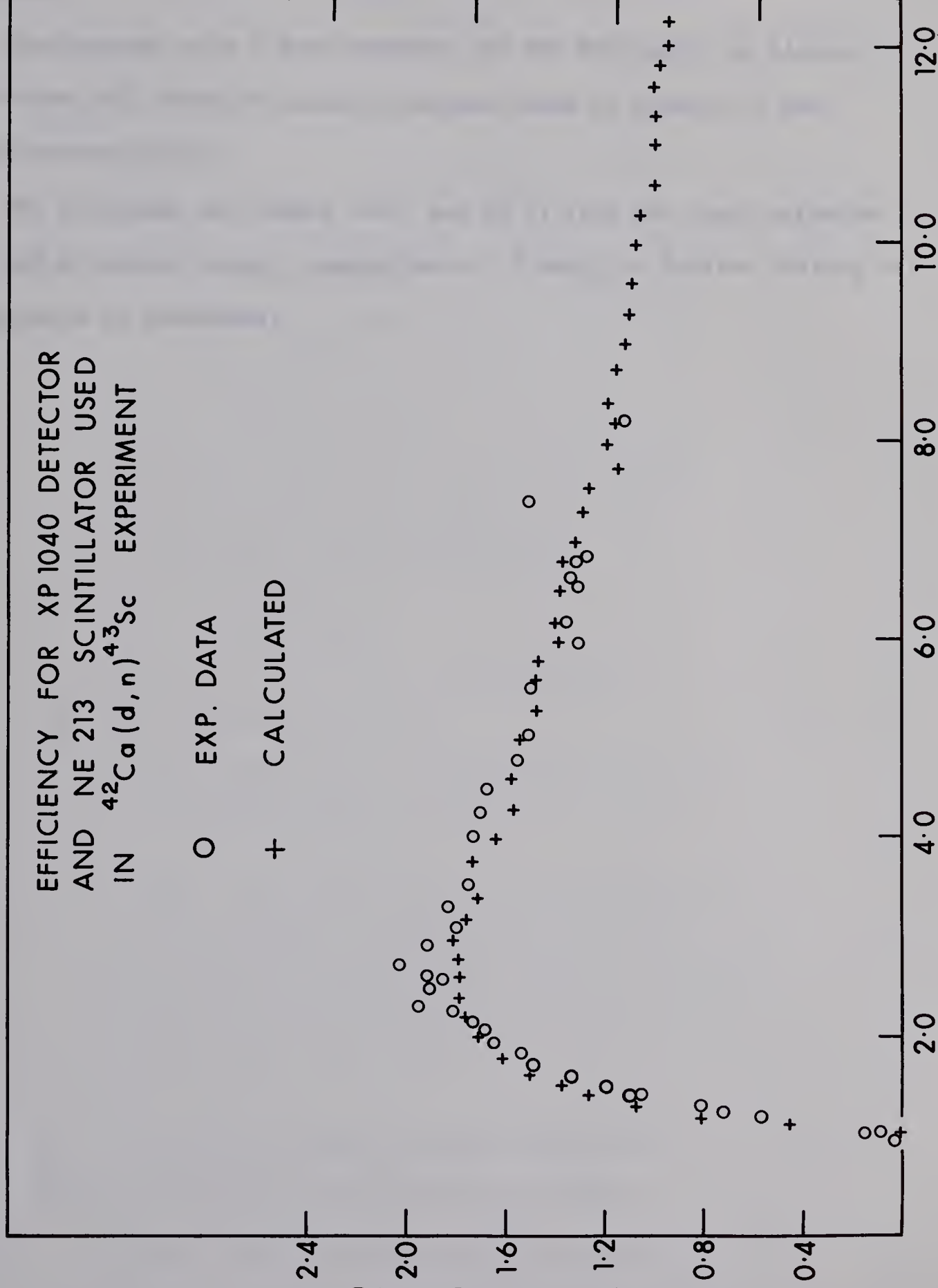
O EXP. DATA

+ CALCULATED

RELATIVE EFFICIENCY

NEUTRON ENERGY (MeV)

ABSOLUTE EFFICIENCY (%)



included.

The program is in a form suitable for the University of Alberta IBM System 360, Model 67 computer and was found to require 10 sec per efficiency point.

The following two tables (A1-1 and A1-2) give the input parameter list and a typical output, respectively. Finally, a Fortran listing of the program is presented.

Table A1-1 Program Input Parameters

Card No.	Program Symbol	Explanation	Format
1	VK, SMK	TITLE CARD	1X, 50H
2		<p><u>VK</u> is a dimensionless quantity relating the standard deviation of the gaussian used to approximate detector resolution and the position of this gaussian. In an actual experiment, the position of the gaussian is taken to mean the pulse height. For the XP 1040 photomultiplier used in the present experiments, the following expression was found</p> $\text{Gaussian FWHM} = \frac{1}{2.50 \times (\text{pulse height})^2}$ <p>thus $VK = 2.50/2.36$,</p> <p>the 2.36 relates the FWHM and the standard deviation of the gaussian.</p> <p><u>SMK</u> is the slope of the ^{22}Na calibration line obtained as described in the text. Units are electron energy (MeV) per channel. In the present experiment, this was found to be 0.0027 MeV/channel.</p>	2F10.0
3	E, DE, EMAX	<p><u>E</u> is the neutron energy at which the efficiency calculation is to begin,</p> <p><u>DE</u>, the increment in this energy and,</p>	3F5.2

Table A1-1 (continued)

Card No.	Program Symbol	Explanation	Format
		<u>EMAX</u> , the maximum value of the energy. For the NE 213 scintillator, this is limited to 14 MeV by the curves which relate electron and proton energies. It is also limited to 15 MeV as the highest value tabulated for the carbon cross sections. Units - MeV.	
4	EB	<u>EB</u> , neutron cut-off energy (MeV), in figure A1-2 found by extrapolating the sloping section of the curve to zero efficiency. Note E above can be less than EB	F5.2
5	AL, DN, DC	<u>AL</u> is the length of scintillator in CM. <u>DN</u> , number of hydrogen atoms/cm ³ in the scintillator. For NE 213 = 0.4888 x 10 ²³ atoms/cm ³ <u>DC</u> , number of carbon atoms/cm ³ in the scintillator. For NE 213 0.4030 x 10 ²³ atoms/cm ³	F5.2, 2E15.4

Table A1-2 Sample Output

NE 213 (Grandy) April 1967
 Length of crystal = 1.905 CM No of H atoms/CC = 0.4888E 23
 No of C atoms/CC = 0.4030E 23 EB = 1.050

Energy	Efficiency	Efficiency (Simple Theory)
0.8000	0.0000	-0.1020
1.0000	0.0102	-0.0148
1.2000	0.0584	0.0347
1.4000	0.0885	0.0651
1.6000	0.1037	0.0845
1.8000	0.1123	0.0972
2.0000	0.1183	0.1057
2.2000	0.1214	0.1113
2.4000	0.1227	0.1147
2.6000	0.1229	0.1163
2.8000	0.1218	0.1162
3.0000	0.1239	0.1191

The author wishes to acknowledge the contribution of D.A. Gedcke who was instrumental in the formulation of the present theory, particularly, in the section where the detector resolution was included. The interpolation routine used to extract the $n - {}^{12}\text{C}$ cross section is due to J.F. Easton and the general integration algorithm is from a DWBA program written by B.E.F. Macefield.

FORTRAN SOURCE LISTING

```

C    MAINLINE PROGRAM
      COMMON/TBG/AL, DN, DC
      COMMON/GRA/AKN, SMK, VK
      COMMON/PCA/PVAL(1001)
      DIMENSION RES(1001)
6    READ(5,8)
      WRITE(6,20)
      READ(5,111)VK, SMK
      READ(5,1) E, DE, EMAX
      READ(5,1) E B
      F1=0.01
      F2=0.01
      F3=0.01
      READ(5,7) AL, DN, DC
      WRITE(6,8)
      WRITE(6,9) AL, DN, DC
      WRITE(6,5) E B
      WRITE(6,3)
      J=(EMAX-E)/DE+1.49
      DO 2 J1=1, J
      AKB=(E-EB)/E
      CALL PCALC(E, F2, F3)
      NUM=1.0/F1+1.49
      AK=-3.0*G(E)/E
      DKB=F1*(AKB-AK)
      DO 30 JOB=1, NUM
      RES(JOB)=PII(AK, E, F3)
30   AK=AK+DKB
      CALL INTEG(RES, SUM, DKB, 1, NUM)
      EFF=SUM*E
      A=DN*SG(E)+DC*CSG(E)
      EAF=DN*SG(E)/A*(1.0-EXP(-A*AL))*(E-EB)/E
      WRITE(6,4) E, EFF, EAF
2    E=E+DE
      GO TO 6
1    FORMAT(5F5.2)
3    FORMAT(//10X, 6HENERGY, 7X, 10HEFFICIENCY, 5X, 25HEFFICIENCY(SIMPLE THE
10RY)/)
4    FORMAT(1X, 3F15.4, /)
5    FORMAT(6H    E B=, F9.3)
7    FORMAT(F5.2, 2E15.4)
8    FORMAT(1X, 50H
9    FORMAT(1X, 18HLENGTH OF CRYSTAL=, F6.3, 2X, 2HCM,
1    5X, 17HNO OF H ATOMS/CC=, E15.4,
2    5X, 17HNO OF C ATOMS/CC=, E15.4)
20   FORMAT(1H2)
111  FORMAT(2F10.0)
      END

```



```

FUNCTION P(TAK,E,TDK)
COMMON/TBG/AL, DN, DC
DIMENSION RES(1001)
AK=TAK
DK=TDK
IF(AK.LT.0.001) AK=0.001
IF(AK.GT.0.999) AK=0.999
IF(DK.LT.0.0001) DK=0.0001
NUM=(1.0-AK)/DK+1.49
ASG=SG(E)
SGB=ASG +(DC/DN)*CSG(E)
QBE=1.0-EXP(-DN*AL*SGB)
PH=SQRT(AK)
SGAK=SG(AK*E)
QAK=1.0-EXP(-DN*AL*SGAK/PH)
P1=PH*ASG/E*(QAK-QBE)/(SGAK-PH*SGB)
P3=-ASG*QBE*ALOG(AK)/(E*SGB)
BK=AK
DO 2 J=1, NUM
SQBK=SQRT(BK)
SGBK=SG(BK*E)
QBK=1.0-EXP(-DN*AL*SGBK/SQBK)
RES(J)=(QBK-QBE)/(BK*SGB-SQBK*SGBK)
BK=BK+DK
JT=J
IF(BK.GT.1.0) GO TO 3
2 CONTINUE
3 CALL INTEG(RES,SUM,DK,1,JT)
P2=SUM*ASG/E
P=P1+P2+P3
RETURN
END

```

```

FUNCTION G(E)
COMMON/GRA/AKB,SK,VK
EP=E
IF(EP.LT.0.001) EP=0.001
IF(EP.LE.8.0) GO TO 1
EE=0.60*EP-1.28
GO TO 2
1 EE=0.215*EP+0.028*EP**2
2 GE=SQRT(SK*EE)*VK
G=(-0.215+SQRT(0.0462+0.112*GE))/0.056
RETURN
END

```



```

FUNCTION SG(EN)
SG = 9.424778/(1.206*EN + (0.09415*EN + 0.000130*EN **2 - 1.860)
1**2) + 3.14159/(1.206*EN + (0.4223 + 0.130*EN )**2)
SG = SG*1.0E-24
RETURN
END

```

```

FUNCTION PII(AKE,E0,F3)
COMMON/ GRA/ AKB, SMK, VK
COMMON/ PCA/ PVAL(1001)
DIMENSION RES(1001)
AK = AKE
IF(AKE.LE.0.0) AK = 0.00
IR = 1
DAK = F3
DO 3 J = 1, 1001
AG = G(E0*(1.0-AK))
T = EXP(-(E0*(AK-AKE))/AG)**2)
INDEX = AK/F3 + 1.49
RES(INDEX) = PVAL(INDEX)*T/AG
IF(J.EQ.1) RREM = RES(INDEX)
GO TO (4,5),IR
4 AK = AK-DAK
IF(AK.LT.0.0.OR.RES(INDEX).LE.0.0001*RREM) GO TO 7
GO TO 3
7 AK = AK+DAK
IF(AKE.LE.0.0) AK = DAK
IR = 2
JL = INDEX
GO TO 3
5 AK = AK+DAK
IF(AK.GT.1.0.OR.RES(INDEX).LE.0.0001*RREM) GO TO 8
3 CONTINUE
8 CALL INTEG(RES,SUM,DAK,JL,INDEX)
PII = SUM*E0/1.77245
RETURN
END

```



```

SUBROUTINE PCALC(E,F2,F3)
COMMON/PCA/PVAL(1001)
IR=1
AK=0.0
PEND=P(1.0,E,0.0)
1 DK=(1.0-AK)*F2
J=AK/F3+1.49
GO TO(2,3),IR
2 PVAL(J)=P(AK,E,DK)
PTMP=PVAL(J)
IF((PVAL(J)-PEND)/PEND .LE.0.0001)IR=2
GO TO 4
3 PVAL(J)=(PEND+PTMP)/2.0
4 AK=AK+F3
IF(AK.GT.1.0) RETURN
GO TO 1
END

```

```

SUBROUTINE INTEG(F,V,H,N1,N2)
DIMENSION F(1001),A(6)
DATA A/0.31559193, 1.39217923,0.62397487, 1.24408069, 0.90990410,
1 1.01426918 /
NN1=N1
NN2=N2
V=0.0
DO 1 I=1,6
K=I-1+NN1
LL=NN2-K+NN1
V=(F(K)+F(LL))*A(I)+V
1 CONTINUE
LL=NN2-6
LLL=NN1+6
DO 2 I=LLL,LL
V=V+F(I)
2 CONTINUE
V=H*V
RETURN
END

```



```
FUNCTION CSG(E)
DIMENSION X(99),Y(99)
DATA X( 1),Y( 1)/0.00,4.70/
DATA X(02),Y(02)/0.01,4.75/
DATA X(03),Y(03)/0.10,4.55/
DATA X(04),Y(04)/0.15,4.35/
DATA X(05),Y(05)/0.20,4.20/
DATA X(06),Y(06)/0.30,3.95/
DATA X(07),Y(07)/0.40,3.65/
DATA X(08),Y(08)/0.50,3.40/
DATA X(09),Y(09)/0.60,3.20/
DATA X(10),Y(10)/0.70,3.00/
DATA X(11),Y(11)/0.80,2.85/
DATA X(12),Y(12)/0.90,2.73/
DATA X(13),Y(13)/1.00,2.85/
DATA X(14),Y(14)/1.10,2.50/
DATA X(15),Y(15)/1.20,2.38/
DATA X(16),Y(16)/1.30,2.27/
DATA X(17),Y(17)/1.40,2.17/
DATA X(18),Y(18)/1.50,2.07/
DATA X(19),Y(19)/1.60,2.00/
DATA X(20),Y(20)/1.70,1.93/
DATA X(21),Y(21)/1.80,1.85/
DATA X(22),Y(22)/1.90,1.78/
DATA X(23),Y(23)/2.00,1.73/
DATA X(24),Y(24)/2.10,1.70/
DATA X(25),Y(25)/2.20,1.60/
DATA X(26),Y(26)/2.40,1.55/
DATA X(27),Y(27)/2.60,1.60/
DATA X(28),Y(28)/2.70,1.65/
DATA X(29),Y(29)/2.80,1.80/
DATA X(30),Y(30)/2.85,2.00/
DATA X(31),Y(31)/2.90,2.40/
DATA X(32),Y(32)/2.93,2.80/
DATA X(33),Y(33)/2.95,3.10/
DATA X(34),Y(34)/2.96,2.70/
DATA X(35),Y(35)/2.98,2.20/
DATA X(36),Y(36)/3.00,1.15/
DATA X(37),Y(37)/3.03,1.10/
DATA X(38),Y(38)/3.10,1.50/
DATA X(39),Y(39)/3.20,1.80/
DATA X(40),Y(40)/3.40,2.20/
DATA X(41),Y(41)/3.60,1.15/
DATA X(42),Y(42)/3.80,1.10/
DATA X(43),Y(43)/4.00,1.90/
```



```
DATA X(44),Y(44)/4.10,1.85/
DATA X(45),Y(45)/4.20,1.80/
DATA X(46),Y(46)/4.25,1.90/
DATA X(47),Y(47)/4.30,2.05/
DATA X(48),Y(48)/4.40,1.80/
DATA X(49),Y(49)/4.80,1.30/
DATA X(50),Y(50)/4.90,1.20/
DATA X(51),Y(51)/4.95,1.50/
DATA X(52),Y(52)/5.00,1.25/
DATA X(53),Y(53)/5.20,1.10/
DATA X(54),Y(54)/5.30,1.05/
DATA X(55),Y(55)/5.35,1.05/
DATA X(56),Y(56)/5.40,1.70/
DATA X(57),Y(57)/5.45,1.10/
DATA X(58),Y(58)/5.60,1.00/
DATA X(59),Y(59)/6.00,1.00/
DATA X(60),Y(60)/6.20,1.10/
DATA X(61),Y(61)/6.25,1.80/
DATA X(62),Y(62)/6.30,2.60/
DATA X(63),Y(63)/6.35,1.50/
DATA X(64),Y(64)/6.40,1.10/
DATA X(65),Y(65)/6.60,0.50/
DATA X(66),Y(66)/6.80,0.80/
DATA X(67),Y(67)/7.20,0.80/
DATA X(68),Y(68)/7.30,0.85/
DATA X(69),Y(69)/7.35,1.40/
DATA X(70),Y(70)/7.40,1.70/
DATA X(71),Y(71)/7.50,1.80/
DATA X(72),Y(72)/7.60,1.40/
DATA X(73),Y(73)/7.61,1.10/
DATA X(74),Y(74)/7.70,1.50/
DATA X(75),Y(75)/7.80,2.10/
DATA X(76),Y(76)/7.90,1.85/
DATA X(77),Y(77)/8.00,1.80/
DATA X(78),Y(78)/8.20,1.80/
DATA X(79),Y(79)/8.30,1.15/
DATA X(80),Y(80)/8.40,1.10/
DATA X(81),Y(81)/8.60,1.13/
DATA X(82),Y(82)/9.00,1.14/
DATA X(83),Y(83)/10.0,1.15/
DATA X(84),Y(84)/11.0,1.20/
DATA X(85),Y(85)/12.0,1.25/
DATA X(86),Y(86)/13.0,1.31/
DATA X(87),Y(87)/14.0,1.36/
DATA X(88),Y(88)/15.0,1.40/
CALL INT(PAR,E,X,Y,88)
CSG=PAR*1.0E-24
RETURN
END
```



```

SUBROUTINE INT (EFF,EN,X,Y,M)
DIMENSION X(99),Y(99)
IF(EN-X(1)) 20,42,7
7 IF(EN-X(M)) 5,45,50
5 IF(EN-X(M-1)) 8,43,70
8 I=1
6 IF(EN-X(I)) 15,40,10
10 I=I+1
GO TO 6
15 IF(I-2) 20,25,30
20 WRITE (6,16) EN,X(1)
16 FORMAT (5X,3HX =,F12.8,25HBELOW RANGE OF LIMIT XL =,F12.8)
EFF=0.0
RETURN
25 D3D5=(X(2)-X(1))/(X(3)-X(2))
D3=X(2)-X(1)
D4=X(3)-X(1)
SP2=((Y(3)-Y(2))*D3D5+(Y(2)-Y(1))/D3D5)/D4
B=SP2/D3-(Y(2)-Y(1))/(D3**2)
C=2.*(Y(2)-Y(1))/D3-SP2
DX=EN-X(1)
EFF=(B*DX+C)*DX+Y(1)
RETURN
30 D1D3=(X(I-1)-X(I-2))/(X(I)-X(I-1))
D2=X(I)-X(I-2)
D3D5=(X(I)-X(I-1))/(X(I+1)-X(I))
D4=X(I+1)-X(I-1)
D3=X(I)-X(I-1)
SP1=((Y(I)-Y(I-1))*D1D3+(Y(I-1)-Y(I-2))/D1D3)/D2
SP2=((Y(I+1)-Y(I))*D3D5+(Y(I)-Y(I-1))/D3D5)/D4
A1=(SP1+SP2+2.*(Y(I-1)-Y(I))/D3)/(D3**2)
B=(3.*(Y(I)-Y(I-1))/D3-2.*SP1-SP2)/D3
DX=EN-X(I-1)
EFF=((A1*DX+B)*DX+SP1)*DX+Y(I-1)
RETURN
70 D3D5=(X(M-1)-X(M-2))/(X(M)-X(M-1))
D3=X(M-1)-X(M-2)
D4=X(M)-X(M-2)
SP2=((Y(M)-Y(M-1))*D3D5+(Y(M-1)-Y(M-2))/D3D5)/D4
B=SP2/D3-(Y(M-1)-Y(M-2))/D3**2
C=2.0*(Y(M-1)-Y(M-2))/D3-SP2
DX=EN-X(M-1)
EFF=(B*DX+C)*DX+Y(M-2)
RETURN
40 EFF=Y(1)
RETURN
42 EFF=Y(1)
RETURN
43 EFF=Y(M-1)
RETURN
45 EFF=Y(M)
RETURN
50 WRITE (6,17) EN,X(M)
17 FORMAT (5X,3HX =,F12.8,25HABOVE RANGE OF LIMIT XU =,F12.8)
EFF=0.0
RETURN
END

```


APPENDIX II

NUMERICAL VALUES FOR THE MEASURED CROSS SECTIONS

This appendix contains numerical values for the absolute differential cross sections discussed in the main text. Cross sections are presented for the reaction $^{40}\text{Ca}(\text{d},\text{n})^{41}\text{Sc}$ at deuteron bombarding energies of 5.0, 6.0 and 6.5 MeV, and for the reactions $^{42}\text{Ca}(\text{d},\text{n})^{43}\text{Sc}$ and $^{48}\text{Ca}(\text{d},\text{n})^{49}\text{Sc}$ at bombarding energies of 5.15 and 5.5 MeV, respectively. Relative differential cross sections are presented for neutrons leading to the ground state and 0.500 MeV of ^{17}F from the reaction $^{16}\text{O}(\text{d},\text{n})^{17}\text{F}$ reaction at bombarding energies of 6.0 and 6.5 MeV. These cross sections were extracted from the ^{17}F contaminant peaks occurring in the $^{40}\text{Ca}(\text{d},\text{n})^{41}\text{Sc}$ spectra. Relative differential cross sections are also presented for neutrons leading to the ground state and 2.365 MeV state of ^{13}N from the reaction $^{12}\text{C}(\text{d},\text{n})^{13}\text{N}$ at a deuteron bombarding energy of 6.5 MeV. These cross sections are the results of an experiment performed with a natural carbon target and were used to extract a ^{13}N contaminant from the ^{41}Sc 1.718 MeV peak.

ANGULAR DISTRIBUTION FOR THE GROUND STATE
OF ^{41}Sc FROM $^{40}\text{Ca}(\text{d},\text{n})^{41}\text{Sc}$. $E_{\text{d}} = 5.0 \text{ MEV}$.

<u>Angle (Lab.)</u>	<u>Angle (C.M.)</u>	<u>Cross Section (mb/sr)</u>	<u>Error (mb/sr)</u>
0.0	0.0	4.22	0.12
5.0	5.2	4.15	0.11
10.0	10.4	4.02	0.26
15.0	15.6	3.64	0.17
20.0	20.8	3.11	0.13
25.0	26.0	2.58	0.10
30.0	31.2	2.72	0.10
35.0	36.3	2.73	0.10
40.0	41.5	3.03	0.11
45.0	46.6	3.35	0.14
50.0	51.8	3.42	0.19
60.0	62.0	3.34	0.10
75.0	77.3	3.41	0.12
85.0	87.3	3.10	0.11
95.0	97.3	2.44	0.10
120.0	122.0	1.93	0.09
135.0	136.6	1.16	0.07
146.0	147.3	0.83	0.05

ANGULAR DISTRIBUTION FOR THE 1.718 MEV STATE
 OF ^{41}Sc FROM $^{40}\text{Ca}(\text{d},\text{n})^{41}\text{Sc}$. $E_{\text{d}} = 5.0 \text{ MEV}$.

<u>Angle (Lab.)</u>	<u>Angle (C.M.)</u>	<u>Cross Section (mb/sr)</u>	<u>Error (mb/sr)</u>
0.0	0.0	43.2	1.0
5.0	5.3	43.7	1.1
10.0	10.6	42.9	1.4
15.0	15.8	43.9	1.5
20.0	21.1	42.1	1.2
25.0	26.4	38.4	1.3
30.0	31.6	33.7	1.1
35.0	36.8	27.9	0.9
40.0	42.1	22.7	0.6
45.0	47.3	17.7	0.5
50.0	52.5	14.9	0.5
60.0	62.8	11.3	0.3
75.0	78.1	9.7	0.3
85.0	88.2	8.0	0.2
95.0	98.2	5.3	0.2
105.0	108.1	5.6	0.2
120.0	122.8	4.7	0.1
135.0	137.3	5.7	0.2
146.0	147.8	6.4	0.2

ANGULAR DISTRIBUTION FOR THE 2.096 MEV STATE
OF ^{41}Sc FROM $^{40}\text{Ca}(\text{d},\text{n})^{41}\text{Sc}$. $E_{\text{d}} = 5.0$ MEV.

<u>Angle (Lab.)</u>	<u>Angle (C.M.)</u>	<u>Cross Section (mb/sr)</u>	<u>Error (mb/sr)</u>
0.0	0.0	0.46	0.07
2.5	2.7	0.50	0.05
5.0	5.3	0.56	0.05
7.5	8.0	0.58	0.06
10.0	10.6	0.65	0.05
15.0	15.9	0.63	0.05
20.0	21.2	0.72	0.05
25.0	26.5	0.79	0.05
30.0	31.8	0.78	0.05
35.0	37.1	0.64	0.04
40.0	42.3	0.66	0.04
45.0	47.5	0.50	0.04
50.0	52.7	0.53	0.04
60.0	63.1	0.47	0.04
75.0	78.5	0.23	0.09
85.0	88.6	0.38	0.04
95.0	98.6	0.32	0.06
105.0	108.5	0.32	0.04
120.0	123.1	0.30	0.06
135.0	137.5	0.20	0.04
146.0	148.0	0.21	0.04

ANGULAR DISTRIBUTION FOR THE 2.415 MEV STATE
 OF ^{41}Sc FROM $^{40}\text{Ca}(\text{d},\text{n})^{41}\text{Sc}$. $E_{\text{d}} = 5.0 \text{ MEV}$.

<u>Angle (Lab.)</u>	<u>Angle (C.M.)</u>	<u>Cross Section (mb/sr)</u>	<u>Error (mb/sr)</u>
0.0	0.0	3.70	0.10
5.0	5.4	3.69	0.10
10.0	10.7	3.48	0.10
15.0	16.0	3.52	0.10
20.0	21.4	3.25	0.10
25.0	26.7	2.98	0.12
30.0	32.0	2.65	0.08
35.0	37.3	2.21	0.08
40.0	42.6	1.99	0.07
45.0	47.9	1.77	0.08
50.0	53.1	1.54	0.07
60.0	63.5	1.13	0.05
75.0	78.9	1.10	0.04
85.0	89.0	0.92	0.06
95.0	99.0	0.79	0.05
105.0	108.9	0.91	0.05
120.0	123.5	0.71	0.03
135.0	137.8	0.71	0.04
146.0	148.3	0.53	0.04

ANGULAR DISTRIBUTION FOR THE GROUND STATE
 OF ^{41}Sc FROM $^{40}\text{Ca}(\text{d},\text{n})^{41}\text{Sc}$. $E_{\text{d}} = 6.0 \text{ MEV.}$

<u>Angle (Lab.)</u>	<u>Angle (C.M.)</u>	<u>Cross Section (mb/sr)</u>	<u>Error (mb/sr)</u>
0.0	0.0	4.49	0.10
5.0	5.2	4.29	0.11
10.0	10.4	3.63	0.12
15.0	15.6	3.09	0.10
20.0	20.8	3.05	0.13
25.0	26.0	2.92	0.11
30.0	31.1	3.32	0.12
35.0	36.3	3.75	0.10
40.0	41.5	4.11	0.13
45.0	46.6	4.30	0.11
50.0	51.7	4.45	0.12
60.0	62.0	4.24	0.13
65.0	67.1	3.96	0.13
75.0	77.2	3.46	0.11
85.0	87.3	3.19	0.10
95.0	97.3	2.52	0.10
112.5	114.6	1.88	0.07
120.0	122.0	1.61	0.05
135.0	136.6	1.28	0.06
145.0	146.3	1.26	0.05

ANGULAR DISTRIBUTION FOR THE 1.718 MEV STATE
 OF ^{41}Sc FROM $^{40}\text{Ca}(\text{d},\text{n})^{41}\text{Sc}$. $E_{\text{d}} = 6.0 \text{ MEV}$.

<u>Angle (Lab.)</u>	<u>Angle (C.M.)</u>	<u>Cross Section (mb/sr)</u>	<u>Error (mb/sr)</u>
0.0	0.0	53.5	1.2
5.0	5.3	53.3	1.3
10.0	10.5	55.6	1.5
15.0	15.7	52.6	1.3
20.0	21.0	48.6	1.2
25.0	26.2	42.0	0.9
30.0	31.4	31.9	0.7
35.0	36.6	24.3	0.6
40.0	41.8	18.5	0.5
45.0	47.0	13.6	0.4
50.0	52.2	12.2	0.3
60.0	62.5	11.1	0.2
65.0	67.6	10.4	0.3
75.0	77.8	8.5	0.2
85.0	87.9	6.1	0.2
95.0	97.9	3.7	0.1
105.0	107.8	3.3	0.1
112.5	115.2	3.3	0.1
120.0	122.5	3.7	0.6
135.0	137.0	4.6	0.2
145.0	146.6	4.9	0.2

ANGULAR DISTRIBUTION FOR THE 2.415 MEV STATE
 OF ^{41}Sc FROM $^{40}\text{Ca}(\text{d},\text{n})^{41}\text{Sc}$. $E_{\text{d}} = 6.0$ MEV.

<u>Angle (Lab.)</u>	<u>Angle (C.M.)</u>	<u>Cross Section (mb/sr)</u>	<u>Error (mb/sr)</u>
0.0	0.0	5.21	0.12
5.0	5.3	5.14	0.12
10.0	10.6	4.78	0.15
15.0	15.9	4.35	0.13
20.0	21.1	4.00	0.12
25.0	26.4	3.15	0.08
30.0	31.7	2.54	0.07
35.0	36.9	2.04	0.06
40.0	42.1	1.57	0.07
45.0	47.3	1.28	0.04
50.0	52.5	1.25	0.06
60.0	62.9	1.11	0.05
65.0	68.0	1.18	0.05
75.0	78.2	1.13	0.06
85.0	88.3	0.88	0.06
95.0	98.3	0.50	0.03
105.0	108.2	0.50	0.03
112.5	115.5	0.45	0.06
120.0	122.9	0.47	0.03
135.0	137.3	0.54	0.04
145.0	146.9	0.61	0.03

ANGULAR DISTRIBUTION FOR THE 2.719 MEV STATE
 OF ^{41}Sc FROM $^{40}\text{Ca}(\text{d},\text{n})^{41}\text{Sc}$. $E_{\text{d}} = 6.0 \text{ MEV}$.

<u>Angle (Lab.)</u>	<u>Angle (C.M.)</u>	<u>Cross Section (mb/sr)</u>	<u>Error (mb/sr)</u>
0.0	0.0	1.34	0.06
5.0	5.3	1.16	0.05
10.0	10.6	1.03	0.07
15.0	15.9	0.90	0.08
20.0	21.2	0.52	0.07
25.0	26.5	0.39	0.07
45.0	47.5	0.27	0.06
60.0	63.1	0.28	0.05
65.0	68.2	0.30	0.07
75.0	78.4	0.23	0.04

ANGULAR DISTRIBUTION FOR THE 3.463 MEV STATE
 OF ^{41}Sc FROM $^{40}\text{Ca}(\text{d},\text{n})^{41}\text{Sc}$. $E_{\text{d}} = 6.0$ MEV.

<u>Angle (Lab.)</u>	<u>Angle (C.M.)</u>	<u>Cross Section (mb/sr)</u>	<u>Error (mb/sr)</u>
0.0	0.0	13.4	0.3
5.0	5.4	12.2	0.4
10.0	10.8	11.7	0.4
15.0	16.2	10.7	0.3
17.5	18.9	8.5	0.2
25.0	27.0	7.1	0.2
30.0	32.3	5.4	0.2
35.0	37.7	4.7	0.2
45.0	48.3	4.0	0.2
50.0	53.5	3.5	0.1
60.0	64.0	4.1	0.2
65.0	69.2	3.8	0.1
75.0	79.5	3.7	0.2
85.0	89.6	3.2	0.1
95.0	99.6	2.8	0.1
105.0	109.5	2.4	0.2
112.5	116.8	2.4	0.2

ANGULAR DISTRIBUTION FOR THE GROUND STATE
 OF ^{41}Sc FROM $^{40}\text{Ca}(\text{d},\text{n})^{41}\text{Sc}$. $E_{\text{d}} = 6.5 \text{ MEV}$.

<u>Angle (Lab.)</u>	<u>Angle (C.M.)</u>	<u>Cross Section (mb/sr)</u>	<u>Error (mb/sr)</u>
0.0	0.0	4.00	0.11
5.0	5.2	3.71	0.22
10.0	10.4	3.50	0.15
15.0	15.6	3.36	0.20
20.0	20.8	2.97	0.15
25.0	26.0	2.96	0.11
30.0	31.1	3.42	0.12
35.0	36.3	3.85	0.18
37.5	38.9	3.97	0.18
41.5	43.0	3.79	0.13
45.0	46.6	4.17	0.17
52.5	54.3	3.83	0.12
60.0	62.0	3.62	0.13
65.0	67.0	3.28	0.13
75.0	77.2	3.01	0.18
85.0	87.2	3.02	0.11
95.0	97.2	2.28	0.06
105.0	107.2	2.01	0.12
120.0	122.0	1.12	0.09
130.0	131.7	0.78	0.07
145.0	146.3	0.82	0.05

ANGULAR DISTRIBUTION FOR THE 1.718 MEV STATE
 OF ^{41}Sc FROM $^{40}\text{Ca}(\text{d},\text{n})^{41}\text{Sc}$. $E_{\text{d}} = 6.5 \text{ MEV}$.

<u>Angle (Lab.)</u>	<u>Angle (C.M.)</u>	<u>Cross Section (mb/sr)</u>	<u>Error (mb/sr)</u>
0.0	0.0	53.0	1.7
5.0	5.2	54.4	1.4
7.5	7.9	54.5	1.1
12.5	13.1	54.3	1.1
15.0	15.7	51.8	1.0
20.0	21.0	46.2	1.1
25.0	26.2	37.1	0.8
30.0	31.4	28.1	1.2
35.0	36.6	19.1	0.5
45.0	47.0	12.1	0.4
52.5	54.7	11.7	0.4
60.0	62.4	11.3	0.3
65.0	67.5	9.3	0.2
75.0	77.7	7.5	0.3
85.0	87.8	4.3	0.2
95.0	97.8	2.5	0.1
100.0	102.7	2.3	0.1
105.0	107.7	1.9	0.1
120.0	122.4	1.9	0.2
130.0	132.1	2.5	0.1
145.0	146.6	3.3	0.1

ANGULAR DISTRIBUTION FOR THE 2.415 MEV STATE
 OF ^{41}Sc FROM $^{48}\text{Ca}(\text{d},\text{n})^{41}\text{Sc}$. $E_{\text{d}} = 6.5 \text{ MEV}$.

<u>Angle (Lab.)</u>	<u>Angle (C.M.)</u>	<u>Cross Section (mb/sr)</u>	<u>Error (mb/sr)</u>
0.0	0.0	4.14	0.12
5.0	5.3	4.00	0.15
10.0	10.5	3.82	0.17
12.5	13.2	3.82	0.13
15.0	15.8	3.89	0.14
20.0	21.1	3.22	0.15
25.0	26.3	2.85	0.16
30.0	31.6	2.55	0.15
35.0	36.8	2.11	0.07
37.5	39.4	1.83	0.09
45.0	47.2	1.27	0.10
52.5	55.0	1.23	0.09
60.0	62.7	1.22	0.13
75.0	78.0	0.99	0.08
120.0	122.7	0.78	0.43
145.0	146.8	0.66	0.30

ANGULAR DISTRIBUTION FOR THE 3.463 MEV STATE
 OF ^{41}Sc FROM $^{40}\text{Ca}(\text{d},\text{n})^{41}\text{Sc}$. $E_{\text{d}} = 6.5 \text{ MEV}$.

<u>Angle (Lab.)</u>	<u>Angle (C.M.)</u>	<u>Cross Section (mb/sr)</u>	<u>Error (mb/sr)</u>
0.0	0.0	14.4	0.4
5.0	5.4	13.7	0.3
7.5	8.0	12.2	0.4
10.0	10.7	11.8	0.3
12.5	13.4	11.7	0.3
15.0	16.0	11.2	0.3
20.0	21.4	7.4	0.3
25.0	26.7	5.9	0.2
30.0	32.0	5.0	0.2
35.0	37.3	4.0	0.2
37.5	39.9	3.7	0.2
41.5	44.2	3.3	0.2
45.0	47.8	3.8	0.3
52.5	55.7	2.7	0.2
60.0	63.5	3.5	0.2
65.0	68.6	3.2	0.2
145.0	147.3	1.1	0.3

ANGULAR DISTRIBUTION FOR THE GROUND STATE
 OF ${}^4_3\text{Sc}$ FROM ${}^4_2\text{Ca}(\text{d},\text{n}){}^4_3\text{Sc}$. $E_{\text{d}} = 5.15 \text{ MEV}$.

<u>Angle (Lab.)</u>	<u>Angle (C.M.)</u>	<u>Cross Section (mb/sr)</u>	<u>Error (mb/sr)</u>
0.0	0.0	0.410	0.030
5.0	5.1	0.321	0.022
10.0	10.3	0.273	0.041
15.0	15.4	0.334	0.030
20.0	20.5	0.360	0.029
25.0	25.7	0.415	0.042
30.0	30.8	0.419	0.045
35.0	35.9	0.371	0.036
40.0	41.0	0.418	0.044
45.0	46.1	0.394	0.034
55.0	56.3	0.249	0.030
60.0	61.3	0.239	0.021
80.0	81.5	0.087	0.014
90.0	91.6	0.195	0.023

ANGULAR DISTRIBUTION FOR THE 0.475 MEV STATE
OF ^{43}Sc FROM $^{42}\text{Ca}(\text{d},\text{n})^{43}\text{Sc}$. $E_{\text{d}} = 5.15 \text{ MEV}$.

<u>Angle (Lab.)</u>	<u>Angle (C.M.)</u>	<u>Cross Section (mb/sr)</u>	<u>Error (mb/sr)</u>
0.0	0.0	0.068	0.011
5.0	5.1	0.113	0.014
10.0	10.3	0.190	0.030
15.0	15.4	0.306	0.021
20.0	20.5	0.418	0.030
25.0	25.7	0.351	0.025
30.0	30.8	0.265	0.026
35.0	35.9	0.188	0.022
40.0	41.0	0.162	0.021
45.0	46.1	0.138	0.021
50.0	51.2	0.113	0.046
55.0	56.3	0.107	0.022
60.0	61.4	0.087	0.014
65.0	66.5	0.054	0.014
70.0	71.5	0.080	0.025
80.0	81.6	0.029	0.012
90.0	91.6	0.037	0.009

ANGULAR DISTRIBUTION FOR THE 0.860 MEV STATE
OF ^{43}Sc FROM $^{42}\text{Ca}(\text{d},\text{n})^{43}\text{Sc}$. $E_{\text{d}} = 5.15 \text{ MEV}$.

<u>Angle (Lab.)</u>	<u>Angle (C.M.)</u>	<u>Cross Section (mb/sr)</u>	<u>Error (mb/sr)</u>
0.0	0.0	0.460	0.030
5.0	5.1	0.436	0.039
10.0	10.3	0.358	0.039
15.0	15.4	0.221	0.026
20.0	20.6	0.205	0.020
25.0	25.7	0.095	0.030
30.0	30.8	0.060	0.015
35.0	35.9	0.040	0.012
45.0	46.2	0.096	0.015
50.0	51.3	0.084	0.023
55.0	56.4	0.069	0.034
60.0	61.4	0.121	0.030
65.0	66.5	0.052	0.013
70.0	71.5	0.099	0.015
80.0	81.6	0.067	0.012
90.0	91.6	0.075	0.015

ANGULAR DISTRIBUTION FOR THE 1.177 MEV STATE
OF ^{43}Sc FROM $^{42}\text{Ca}(\text{d},\text{n})^{43}\text{Sc}$. $E_{\text{d}} = 5.15 \text{ MEV}$.

<u>Angle (Lab.)</u>	<u>Angle (C.M.)</u>	<u>Cross Section (mb/sr)</u>	<u>Error (mb/sr)</u>
0.0	0.0	0.262	0.022
5.0	5.1	0.343	0.027
10.0	10.3	0.493	0.047
15.0	15.4	0.753	0.041
20.0	20.6	0.993	0.062
30.0	30.8	0.537	0.037
35.0	36.0	0.336	0.024
40.0	41.1	0.281	0.035
45.0	46.2	0.196	0.034
50.0	51.3	0.229	0.072
55.0	56.4	0.324	0.023
60.0	61.5	0.310	0.024
65.0	66.5	0.300	0.025
70.0	71.6	0.292	0.023
80.0	81.7	0.080	0.018
90.0	91.7	0.103	0.014

ANGULAR DISTRIBUTION FOR THE 1.817 MEV STATE
 OF ^{43}Sc FROM $^{42}\text{Ca}(\text{d},\text{n})^{43}\text{Sc}$. $E_{\text{d}} = 5.15 \text{ MEV}$.

<u>Angle (Lab.)</u>	<u>Angle (C.M.)</u>	<u>Cross Section (mb/sr)</u>	<u>Error (mb/sr)</u>
0.0	0.0	0.202	0.035
5.0	5.2	0.244	0.035
15.0	15.5	0.513	0.029
20.0	20.6	0.622	0.037
25.0	25.8	0.462	0.029
30.0	30.9	0.378	0.027
35.0	36.0	0.279	0.027
40.0	41.1	0.178	0.021
45.0	46.3	0.160	0.028
50.0	51.4	0.235	0.020
55.0	56.5	0.201	0.019
60.0	61.5	0.228	0.021
65.0	66.6	0.190	0.022
70.0	71.7	0.201	0.021
80.0	81.8	0.092	0.023
90.0	91.8	0.061	0.012

ANGULAR DISTRIBUTION FOR THE 1.947 MEV STATE
 OF ${}^{43}\text{Sc}$ FROM ${}^{42}\text{Ca}(\text{d},\text{n}){}^{43}\text{Sc}$. $E_{\text{d}} = 5.15 \text{ MEV}$.

<u>Angle (Lab.)</u>	<u>Angle (C.M.)</u>	<u>Cross Section (mb/sr)</u>	<u>Error (mb/sr)</u>
0.0	0.0	0.137	0.030
5.0	5.2	0.093	0.024
15.0	15.5	0.062	0.014
20.0	20.6	0.037	0.016
30.0	30.9	0.022	0.013
40.0	41.2	0.042	0.013
55.0	56.5	0.043	0.014
60.0	61.6	0.035	0.013
65.0	66.6	0.029	0.013
70.0	71.7	0.047	0.014
90.0	91.8	0.026	0.009

ANGULAR DISTRIBUTION FOR THE 5.026 MEV STATE
 OF ^{43}Sc FROM $^{42}\text{Ca}(\text{d},\text{n})^{43}\text{Sc}$. $E_{\text{d}} = 5.15 \text{ MEV}$.

<u>Angle (Lab.)</u>	<u>Angle (C.M.)</u>	<u>Cross Section (mb/sr)</u>	<u>Error (mb/sr)</u>
0.0	0.0	1.21	0.11
5.0	5.2	1.10	0.10
15.0	15.7	1.01	0.11
20.0	20.9	1.30	0.07
25.0	26.1	1.09	0.06
30.0	31.3	0.99	0.06
35.0	36.5	0.74	0.10
50.0	52.0	0.38	0.04
55.0	57.2	0.39	0.04
65.0	67.4	0.36	0.03
70.0	72.5	0.32	0.07

ANGULAR DISTRIBUTION FOR THE 5.647 MEV STATE
 OF ^{43}Sc FROM $^{42}\text{Ca}(\text{d},\text{n})^{43}\text{Sc}$. $E_{\text{d}} = 5.15 \text{ MEV}$.

<u>Angle (Lab.)</u>	<u>Angle (C.M.)</u>	<u>Cross Section (mb/sr)</u>	<u>Error (mb/sr)</u>
0.0	0.0	0.483	0.084
5.0	5.3	0.454	0.062
15.0	15.8	0.336	0.050
20.0	21.0	0.375	0.050
25.0	26.3	0.403	0.033
30.0	31.5	0.391	0.043
35.0	36.7	0.281	0.035
40.0	42.0	0.326	0.043
45.0	47.1	0.223	0.057
60.0	62.6	0.214	0.036
70.0	72.9	0.160	0.029
90.0	93.0	0.071	0.018

ANGULAR DISTRIBUTION FOR THE 6.155 MEV STATE
OF ^{43}Sc FROM $^{42}\text{Ca}(\text{d},\text{n})^{43}\text{Sc}$. $E_{\text{d}} = 5.15 \text{ MEV}$.

<u>Angle (Lab.)</u>	<u>Angle (C.M.)</u>	<u>Cross Section (mb/sr)</u>	<u>Error (mb/sr)</u>
0.0	0.0	5.09	0.21
5.0	5.3	4.99	0.19
10.0	10.6	4.90	0.22
15.0	15.9	4.40	0.16
20.0	21.2	4.46	0.20
25.0	26.5	3.24	0.13
30.0	31.8	3.21	0.13
35.0	37.0	2.45	0.11
40.0	42.3	2.07	0.09
45.0	47.5	1.65	0.08
50.0	52.7	1.40	0.07
55.0	57.9	1.33	0.06
60.0	63.1	1.32	0.06
65.0	68.2	1.20	0.06
70.0	73.3	1.19	0.05
80.0	83.5	0.86	0.06
90.0	93.5	0.88	0.06

ANGULAR DISTRIBUTION FOR THE GROUND STATE
 OF ^{49}Sc FROM $^{48}\text{Ca}(\text{d},\text{n})^{49}\text{Sc}$. $E_{\text{d}} = 5.5 \text{ MEV.}$

<u>Angle (Lab.)</u>	<u>Angle (C.M.)</u>	<u>Cross Section (mb/sr)</u>	<u>Error (mb/sr)</u>
0.0	0.0	0.232	0.016
5.0	5.1	0.230	0.019
10.0	10.2	0.252	0.015
15.0	15.3	0.256	0.016
20.0	20.4	0.311	0.019
25.0	25.5	0.299	0.019
30.0	30.6	0.319	0.020
35.0	35.6	0.326	0.019
40.0	40.7	0.311	0.023
45.0	45.8	0.267	0.018
55.0	55.9	0.194	0.014
65.0	66.0	0.147	0.012
75.0	76.1	0.146	0.011
95.0	96.1	0.147	0.013
110.0	111.0	0.126	0.011
120.0	121.0	0.112	0.011

ANGULAR DISTRIBUTION FOR THE 3.071 MEV STATE
OF ^{49}Sc FROM $^{48}\text{Ca}(\text{d},\text{n})^{49}\text{Sc}$. $E_{\text{d}} = 5.5 \text{ MEV}$.

<u>Angle (Lab.)</u>	<u>Angle (C.M.)</u>	<u>Cross Section (mb/sr)</u>	<u>Error (mb/sr)</u>
0.0	0.0	0.419	0.033
5.0	5.1	0.485	0.042
10.0	10.2	0.636	0.038
15.0	15.3	0.702	0.053
20.0	20.4	0.729	0.044
25.0	25.5	0.567	0.044
30.0	30.6	0.368	0.023
35.0	35.7	0.247	0.020
40.0	40.8	0.200	0.017
45.0	45.9	0.194	0.014
55.0	56.0	0.240	0.015
65.0	66.1	0.211	0.014
75.0	76.2	0.114	0.011
95.0	96.3	0.075	0.012
110.0	111.2	0.081	0.010
120.0	121.1	0.066	0.013

ANGULAR DISTRIBUTION FOR THE 4.472 MEV STATE
 OF ^{49}Sc FROM $^{48}\text{Ca}(\text{d},\text{n})^{49}\text{Sc}$. $E_{\text{d}} = 5.5 \text{ MEV}$.

<u>Angle (Lab.)</u>	<u>Angle (C.M.)</u>	<u>Cross Section (mb/sr)</u>	<u>Error (mb/sr)</u>
0.0	0.0	0.245	0.018
5.0	5.1	0.298	0.025
10.0	10.2	0.393	0.027
15.0	15.4	0.453	0.031
20.0	20.5	0.529	0.030
25.0	25.6	0.406	0.027
30.0	30.7	0.275	0.021
35.0	35.8	0.125	0.016
40.0	40.9	0.075	0.013
45.0	46.0	0.089	0.009
55.0	56.1	0.138	0.012
65.0	66.2	0.122	0.012
75.0	76.3	0.073	0.012
95.0	96.4	0.036	0.008
110.0	111.3	0.046	0.007
120.0	121.2	0.049	0.008

ANGULAR DISTRIBUTION FOR THE 5.008 MEV STATE
 OF ^{49}Sc FROM $^{48}\text{Ca}(\text{d},\text{n})^{49}\text{Sc}$. $E_{\text{d}} = 5.5 \text{ MEV}$.

<u>Angle (Lab.)</u>	<u>Angle (C.M.)</u>	<u>Cross Section (mb/sr)</u>	<u>Error (mb/sr)</u>
0.0	0.0	0.079	0.015
10.0	10.2	0.101	0.017
15.0	15.4	0.110	0.013
20.0	20.5	0.100	0.015
25.0	25.6	0.081	0.014
30.0	30.7	0.080	0.012
35.0	35.8	0.044	0.012
40.0	40.9	0.040	0.010
45.0	46.0	0.046	0.012
55.0	56.2	0.013	0.009
65.0	66.3	0.049	0.007
75.0	76.4	0.047	0.010
95.0	96.4	0.027	0.009
110.0	111.3	0.026	0.009
120.0	121.2	0.008	0.003

ANGULAR DISTRIBUTION FOR THE 5.080 MEV STATE
 OF ^{49}Sc FROM $^{48}\text{Ca}(\text{d},\text{n})^{49}\text{Sc}$. $E_{\text{d}} = 5.5 \text{ MEV}$.

<u>Angle (Lab.)</u>	<u>Angle (C.M.)</u>	<u>Cross Section (mb/sr)</u>	<u>Error (mb/sr)</u>
0.0	0.0	0.058	0.014
10.0	10.2	0.081	0.016
15.0	15.4	0.088	0.012
20.0	20.5	0.093	0.015
25.0	25.6	0.095	0.014
30.0	30.7	0.108	0.013
35.0	35.8	0.105	0.012
40.0	40.9	0.076	0.011
45.0	46.0	0.064	0.010
55.0	56.2	0.066	0.008
65.0	66.3	0.044	0.026
75.0	76.4	0.012	0.009
95.0	96.4	0.027	0.008

ANGULAR DISTRIBUTION FOR THE 5.655 MEV STATE
 OF ^{49}Sc FROM $^{48}\text{Ca}(\text{d},\text{n})^{49}\text{Sc}$. $E_{\text{d}} = 5.5 \text{ MEV}$.

<u>Angle (Lab.)</u>	<u>Angle (C.M.)</u>	<u>Cross Section (mb/sr)</u>	<u>Error (mb/sr)</u>
0.0	0.0	0.044	0.015
5.0	5.1	0.087	0.011
10.0	10.3	0.158	0.012
15.0	15.4	0.231	0.015
20.0	20.5	0.266	0.017
25.0	25.6	0.217	0.017
30.0	30.7	0.164	0.016
35.0	35.8	0.099	0.010
40.0	40.9	0.074	0.012
45.0	46.0	0.055	0.016
55.0	56.2	0.077	0.009
65.0	66.3	0.080	0.010
75.0	76.4	0.079	0.023
95.0	96.5	0.017	0.004
120.0	121.3	0.015	0.004

ANGULAR DISTRIBUTION FOR THE 6.873 MEV STATE
 OF ^{49}Sc FROM $^{48}\text{Ca}(\text{d},\text{n})^{49}\text{Sc}$. $E_{\text{d}} = 5.5 \text{ MEV}$.

<u>Angle (Lab.)</u>	<u>Angle (C.M.)</u>	<u>Cross Section (mb/sr)</u>	<u>Error (mb/sr)</u>
0.0	0.0	0.570	0.037
5.0	5.1	0.279	0.027
10.0	10.3	0.181	0.015
20.0	20.6	0.138	0.013
25.0	25.7	0.097	0.011
30.0	30.8	0.101	0.013
35.0	35.9	0.069	0.008
40.0	41.0	0.064	0.011
45.0	46.1	0.056	0.009
65.0	66.5	0.037	0.011

ANGULAR DISTRIBUTION FOR THE 7.050 MEV STATE
 OF ^{49}Sc FROM $^{48}\text{Ca}(\text{d},\text{n})^{49}\text{Sc}$. $E_{\text{d}} = 5.5 \text{ MEV}$.

<u>Angle (Lab.)</u>	<u>Angle (C.M.)</u>	<u>Cross Section (mb/sr)</u>	<u>Error (mb/sr)</u>
0.0	0.0	0.049	0.018
5.0	5.1	0.066	0.016
10.0	10.3	0.091	0.010
20.0	20.6	0.133	0.012
25.0	25.7	0.115	0.015
30.0	30.8	0.045	0.010
35.0	35.9	0.043	0.009
40.0	41.1	0.020	0.008
45.0	46.2	0.022	0.066

RELATIVE ANGULAR DISTRIBUTION FOR THE GROUND STATE
OF ^{17}F FROM $^{16}\text{O}(\text{d},\text{n})^{17}\text{F}$. $E_{\text{d}} = 6.0 \text{ MEV.}$

<u>Angle (Lab.)</u>	<u>Angle (C.M.)</u>	<u>Cross Section (arb. units)</u>	<u>Relative Error</u>
0.0	0.0	0.128	0.006
5.0	5.5	0.125	0.007
7.5	8.3	0.134	0.008
10.0	11.0	0.164	0.009
12.5	13.8	0.194	0.009
15.0	16.5	0.217	0.008
17.5	19.3	0.240	0.007
20.0	22.0	0.245	0.008
25.0	27.5	0.290	0.009
30.0	33.0	0.298	0.009
35.0	38.4	0.275	0.009
40.0	43.8	0.252	0.008
45.0	49.2	0.189	0.007
50.0	56.6	0.151	0.006
60.0	65.2	0.089	0.004
65.0	70.4	0.069	0.004
75.0	80.8	0.057	0.003
85.0	91.0	0.070	0.005
95.0	101.0	0.071	0.004
105.0	110.8	0.086	0.003
112.5	118.0	0.084	0.004
120.0	125.2	0.079	0.003
135.0	139.2	0.064	0.003
145.0	148.4	0.047	0.004

RELATIVE ANGULAR DISTRIBUTION FOR THE 0.500 MEV STATE
 OF ^{17}F FROM $^{16}\text{O}(\text{d},\text{n})^{17}\text{F}$. $E_{\text{d}} = 6.0$ MEV.

<u>Angle (Lab.)</u>	<u>Angle (C.M.)</u>	<u>Cross Section (arb. units)</u>	<u>Relative Error</u>
0.0	0.0	1.64	0.03
2.5	2.8	1.49	0.03
5.0	5.6	1.40	0.03
7.5	8.3	1.24	0.03
10.0	11.1	1.14	0.03
12.5	13.9	0.90	0.02
15.0	16.7	0.72	0.02
17.5	19.4	0.53	0.01
20.0	22.2	0.38	0.01
25.0	27.7	0.177	0.005
30.0	33.2	0.096	0.005
35.0	38.7	0.073	0.004
40.0	44.1	0.097	0.009
45.0	49.5	0.092	0.005
50.0	54.9	0.113	0.005
60.0	65.6	0.085	0.005
65.0	70.8	0.077	0.004
75.0	81.2	0.062	0.004
85.0	91.4	0.065	0.005
95.0	101.4	0.049	0.001
105.0	111.2	0.073	0.004
112.5	118.4	0.063	0.004
120.0	125.6	0.031	0.004
135.0	139.5	0.029	0.009
145.0	148.7	0.042	0.006

RELATIVE ANGULAR DISTRIBUTION FOR THE GROUND STATE
 OF ^{17}F FROM $^{16}\text{O}(\text{d},\text{n})^{17}\text{F}$. $E_{\text{d}} = 6.5 \text{ MEV}$.

<u>Angle (Lab.)</u>	<u>Angle (C.M.)</u>	<u>Cross Section (arb. units)</u>	<u>Relative Error</u>
0.0	0.0	6.7	0.2
5.0	5.5	7.1	0.3
7.5	8.3	7.9	0.3
10.0	11.0	8.4	0.3
12.5	13.8	9.8	0.3
15.0	16.5	10.7	0.3
20.0	22.0	11.0	0.4
25.0	27.5	11.6	0.3
30.0	32.9	12.2	0.3
35.0	38.4	9.4	0.3
37.5	41.1	9.9	0.3
41.5	45.4	7.6	0.2
45.0	49.2	6.3	0.2
52.5	57.2	3.5	0.2
60.0	65.1	1.9	0.1
65.0	70.3	1.1	0.1
75.0	80.7	1.0	0.1
85.0	90.9	1.4	0.1
95.0	100.9	2.0	0.1
100.0	105.8	2.2	0.1
105.0	110.7	2.6	0.1
120.0	125.1	3.2	0.1
130.0	134.5	2.7	0.1
145.0	148.4	2.3	0.1

RELATIVE ANGULAR DISTRIBUTION FOR THE 0.500 MEV STATE
OF ^{17}F FROM $^{16}\text{O}(\text{d},\text{n})^{17}\text{F}$. $E_{\text{d}} = 6.5 \text{ MEV}$.

<u>Angle (Lab.)</u>	<u>Angle (C.M.)</u>	<u>Cross Section (arb. units)</u>	<u>Relative Error</u>
2.5	2.8	59.3	1.4
5.0	5.6	58.5	1.3
7.5	8.3	52.9	1.2
10.0	11.1	44.4	1.1
12.5	13.9	38.1	1.1
20.0	22.1	14.5	0.3
25.0	27.6	6.5	0.2
30.0	33.1	4.0	0.2
35.0	38.6	2.1	0.2
37.5	41.3	2.8	0.3
41.5	45.6	2.7	0.2
45.0	49.4	3.3	0.1
52.5	57.5	3.5	0.2
60.0	65.4	3.4	0.1
65.0	70.7	2.8	0.2
75.0	81.1	2.4	0.2
85.0	91.2	1.9	0.1
95.0	101.2	1.9	0.1
100.0	106.2	1.7	0.1
105.0	111.1	1.7	0.2
120.0	125.4	1.8	0.2
130.0	134.8	1.1	0.1
145.0	148.6	1.0	0.1

RELATIVE ANGULAR DISTRIBUTION FOR THE GROUND STATE
 OF ^{13}N FROM $^{12}\text{C}(\text{d},\text{n})^{13}\text{N}$. $E_{\text{d}} = 6.5 \text{ MEV}$.

<u>Angle (Lab.)</u>	<u>Angle (C.M.)</u>	<u>Cross Section (arb. units)</u>	<u>Relative Error</u>
0.0	0.0	10.38	0.29
5.0	5.6	11.06	0.35
10.0	11.2	11.77	0.50
15.0	16.8	10.10	0.33
20.0	22.3	8.47	0.26
25.0	27.9	7.46	0.25
30.0	33.4	5.46	0.20
40.0	44.3	2.82	0.11
50.0	55.2	2.27	0.08
60.0	65.9	2.17	0.08
75.0	81.5	1.25	0.06
85.0	91.7	1.31	0.06
95.0	101.7	1.29	0.06
105.0	111.5	1.22	0.07
115.0	121.1	1.24	0.06
120.0	125.8	1.11	0.07
130.0	135.2	0.82	0.05
135.0	139.8	0.80	0.05
145.0	148.9	0.54	0.04

RELATIVE ANGULAR DISTRIBUTION FOR THE 2.365 MEV STATE
 OF ^{13}N FROM $^{12}\text{C}(\text{d},\text{n})^{13}\text{N}$. $E_{\text{d}} = 6.5 \text{ MEV}$.

<u>Angle (Lab.)</u>	<u>Angle (C.M.)</u>	<u>Cross Section (arb. units)</u>	<u>Relative Error</u>
0.0	0.0	25.94	0.54
5.0	5.8	22.56	0.52
10.0	11.6	18.51	0.43
15.0	17.4	10.13	0.25
20.0	23.1	5.25	0.14
25.0	28.8	3.16	0.12
30.0	34.5	1.64	0.06
40.0	45.8	1.49	0.06
50.0	57.0	1.76	0.11
60.0	67.9	1.77	0.08
75.0	83.8	1.03	0.05
85.0	94.1	0.79	0.07
95.0	104.1	0.76	0.07
105.0	113.8	0.48	0.10
115.0	123.2	0.72	0.09
120.0	127.9	0.35	0.08
130.0	137.0	0.61	0.06
135.0	141.4	0.66	0.07
145.0	150.2	0.84	0.06

REFERENCES

- Aj 59 F. Ajzenberg-Selove and T. Lauretsen, Nucl. Phys. 11 (1959) 1
- Al 67 J.L. Alty, L.L. Green, R. Huby, G.D. Jones, J.R. Mines and J.F. Sharpey-Schafer, Nucl. Phys. A97 (1967) 541
- Al 67a J.L. Alty, L.L. Green, G.D. Jones and J.F. Sharpey-Schafer, Nucl. Phys. A100 (1967) 191
- Ar 64 D.D. Armstrong and A.G. Blair, Phys. Letters 10 (1964) 204
- Ar 65 D.D. Armstrong and A.G. Blair, Phys. Rev. 140B (1965) 1226
- Au 63 N. Austern, Selected Topics in Nuclear Theory, edited by F. Janouch (International Atomic Energy Agency, 1963) p. 17
- Au 64 N. Austern, R.M. Drisko, E.C. Harbert and G.R. Satchler, Phys. Rev. 133B (1964) 3
- Ba 57 S.J. Bame, E. Haddad, J.E. Perey and K.K. Smith, Rev. Sci. Instr. 28 (1957) 997
- Ba 61 R. Batchelor, W.B. Gilboy, J.B. Parker and J.H. Towle, Nucl. Instr. and Meth. 13 (1961) 70
- Ba 62 R.H. Bassel, R.M. Drisko and G.R. Satchler, Oak Ridge National Laboratory Report ORNL-3240 (UC - 34 - PHYSICS), 1962 (unpublished)
- Ba 64 R.H. Bassel, R.M. Drisko, G.R. Satchler, L.L. Lee, Jr., J.P. Schiffer and B. Zeidman, Phys. Rev. 136B (1964) 960
- Be 62 L.E. Beghean and M.K. Salomaa, Nucl. Instr. and Meth. 17 (1962) 181
- Be 65 T.A. Belote, A. Sperduto and W.W. Buechner, Phys. Rev. 139B (1965) 80
- Bo 65 R. Bock, H.H. Duhm and R. Stock, Phys. Letters 18 (1965) 61
- Br 60 J.E. Brolley, Jr. and J.L. Fowler, Fast Neutron Physics, Volume 1, ed. by J.B. Marion and J.L. Fowler (Interscience Publishers, Inc., New York, 1960) p. 73

- Br 65 L. Broman and J. Dubois, Nucl. Phys. 72 (1965) 529
- Br 67 L. Broman, University of Pennsylvania, preprint, 1967
- Bu 51 S.T. Butler, Proc. Phys. Soc. (London) A208 (1951) 559
- Bu 64 P.J.A. Buttle and L.J.B. Goldfarb, Proc. Phys. Soc. (London) 83 (1964) 701
- Bu 67 M.B. Burbank, M.Sc. Thesis, University of Alberta (1967)
- Ch 65 G. Chilosi, G.D. O'Kelley and E. Eichler, Bull. Am. Phys. Soc. 10 (1965) 92
- Ch 67 C. Chasman, K.W. Jones, R.A. Ristinen and J.T. Sample, Phys. Rev. Letters 18 (1967) 219
- Co 66 R.G. Cornwell, W. Happer, Jr. and J.D. McCullen, Phys. Rev. 141 (1966) 1106
- Cr 61 L. Cranberg, R.A. Fernald, F.S. Haln and E.F. Schrader, Nucl. Instr. and Meth. 12 (1961) 335
- Cu 66 B. Cujec, Nucl. Phys. 81 (1966) 523
- Da 65 W.K. Dawson, Program for the calculation of Plane Wave fits to (d,n) or (d,p) Angular Distributions, Nuclear Research Center, University of Alberta (1965)
- Da 66 W.G. Davies, Ph.D. Thesis, University of Alberta (1966)
- Di 65 J.K. Dickens, R.M. Drisko, F.G. Perey and G.R. Satchler, Phys. Letters 15 (1965) 337
- Do 66 W.E. Dorenbusch, T.A. Belote and O. Hansen, Phys. Rev. 146 (1966) 734
- Du 66 J. Dubois, S. Maripuu and O. Almén, Arkiv för Fysik 31 (1966) 65
- En 62 P.M. Endt and C. Van der Leun, Nucl. Phys. 34 (1962) 1
- Er 66 J.R. Erskine, A. Marinov and J.P. Schiffer, Phys. Rev. 142 (1966) 633
- Fl 67 B.H. Flowers and I.P. Johnstone Proc. Phys. Soc. 91 (1967) 310

Fo 60 T.K. Fowler and W.M. Good, Nucl. Instr. and Meth. 7 (1960) 245
 Fr 64 J.B. French, Argonne National Laboratory Report ANL-6878, ed.
 by F.E. Throw (1964) p. 181
 Ga 52 G.F.J. Garlick and G.T. Wright, Proc. Phys. Soc. (London) 65B
 (1966) 93
 Ge 67 D.A. Gedcke and W.J. McDonald, Bull. Am. Phys. Soc. 12 (1967)
 636
 Ge 67a D.A. Gedcke, A fast zero-crossing discriminator for time pick-
 off with pulsed beams, Nuclear Research Center Internal Report,
 University of Alberta (1967)
 Ge 67b D.A. Gedcke, Ph.D. Thesis, University of Alberta (1967)
 Ge 67c D.A. Gedcke and W.J. McDonald, private communication (1967)
 Ge 67d D.A. Gedcke and W.J. McDonald, Design of the Constant Fraction
 of Pulse Height Trigger for Optimum Time Resolution, Nuclear
 Research Center Internal Report, University of Alberta (1967)
 Ge 67e W.J. Gerace and A.M. Green, Nucl. Phys. 93 (1967) 110
 Go 60 M.D. Goldberg and J.M. LeBlanc, Phys. Rev. 119 (1960) 1992
 Go 61 M.D. Goldberg, J.D. Anderson, J.P. Stoering and C. Wong, Phys.
 Rev. 122 (1961) 1510
 Gr 66 A. Graue, Physica Norvegica 2 (1966) 7
 Ha 58 J.E. Hardy, Rev. Sci. Instr. 29 (1958) 705
 Hu 58 D.J. Hughes and R.B. Schwartz, Brookhaven National Laboratory
 Report BNL 325 (1958)
 Hu 65 R. Huby and J.R. Mines, Rev. Mod. Phys. 37 (1965) 406
 Jo 66 K.W. Jones, J.P. Schiffer, L.L. Lee, Jr., A. Marinov and J.L.
 Lerner, Phys. Rev. 145 (1966) 894
 Jo 67 R.C. Johnson and F.D. Santos, Phys. Rev. Letters, 19 (1967) 364
 La 63 N.O. Lassen and Clive Larsen, Nucl. Phys. 42 (1963) 183
 Le 58 C. Van der Leun and P.M. Endt, Physica 24 (1958) 1095

- Le 64 L.L. Lee, Jr., J.P. Schiffer, B. Zeidman, G.R. Satchler,
R.M. Drisko and R.H. Bassel, Phys. Rev. 136B (1964) 971
- Le 64a L.L. Lee, Jr. and J.P. Schiffer, Phys. Rev. 136B (1964) 405
- Le 67 H.G. Leighton, Ph.D. Thesis, University of Alberta (1967)
- Le 67a H.G. Leighton, G. Roy, D.P. Gurd and T.B. Grandy, Bull. Am.
Phys. Soc. 12 (1967) 682
- Li 54 T. Lindquist and A.C.G. Mitchell, Phys. Rev. 95 (1954) 1535
- Lu 57 C.R. Lubitz, Numerical Table of Butler-Born Approximation
Stripping Cross Sections, University of Michigan (1957)
unpublished
- Ma 56 D.W. Martin, J.M. Cork and S.D. Burson, Phys. Rev. 102 (1956)
457
- Ma 60 M.H. MacFarlane and J.B. French, Rev. Mod. Phys. 32 (1960) 567
- Ma 60a B.E.F. Macefield and J.H. Towle, Proc. Phys. Soc. 76 (1960) 56
- Ma 61 B.E.F. Macefield, J.H. Towle and W.B. Gilboy, Proc. Phys. Soc.
(London) 77 (1961) 1050
- Ma 65 J.H.E. Mattauch, W. Thiele and A.H. Wapstra, Nucl. Phys. 67
(1965) 1
- Ma 66 A. Marinov, L.L. Lee, Jr. and J.P. Schiffer, Phys. Rev. 145
(1966) 852
- Ma 66a J.B. Marion, Phys. Letters 21 (1966) 61
- Mc 60 G.J. McCullen, A.T.G. Ferguson and G.S. Mani, Nucl. Phys. 17
(1960) 116
- Mc 64 J.D. McCullen, B.F. Bayman and L. Zamick, Phys. Rev. 134B
(1964) 515
- Mc 67 W.R. McMurray, M. Peisach, R. Pretorius, P. van der Merwe and
I.J. Van Heerden, Nucl. Phys. A99 (1967) 6
- Mi 53 R. Middleton, F.A. El-Bedewi and C.T. Tai, Proc. Phys. Soc.
A66 (1953) 95
- Mo 67 C.E. Moss, Bull. Am. Phys. Soc. 12 (1967) 914

Ne 59 G.C. Neilson, W.K. Dawson and F.A. Johnson, Rev. Sci. Instr.
30 (1959) 963

Ob 66 A.W. Obst, M.Sc. Thesis, University of Alberta (1966)

Ok 56 G.D. O'Kelley, N.H. Lazer and E. Eichler, Phys. Rev. 101 (1956)
1059

Pe 62 F. Perey and B. Buck, Nucl. Phys. 32 (1962) 353

Pe 66 C.M. Perey and F.G. Perey, Phys. Rev. 152 (1966) 923

Pe 67 F.G. Perey, private communication (1967)

Ph 66 W.R. Phillips, R. De La Pena and T.A. Critchley, Bull. Am. Phys.
Soc. 11 (1966) 406, *ibid.*, preprint, University of Manchester
(1966)

Pl 65 H.S. Plendl, L.J. Defelice and R.K. Sheline, Nucl. Phys. 73
(1965) 131

Re 66 W.B. Reid and R.H. Hummel, Can. Nucl. Tech. (Jan. - Feb., 1966)
36

Ro 66 L. Rosen, Proc. 2nd Inter. Sym. on Polarization Phenomena of
Nucleons, ed. by P. Huber and H. Schopper (Birkhäuser Verlag
Basel, Bern, 1966) p. 253

Sa 64 G.R. Satchler, Nucl. Phys. 55 (1964) 1

Sc 66 J.J. Schwartz and W.P. Alford, Phys. Rev. 149 (1966) 820

Sc 66a S. Schwarz and H.O. Zetterström, Nucl. Instr. and Meth. 41 (1966)
93

Sc 67 J.J. Schwartz and W.P. Alford, Phys. Rev. 155 (1967) 1191

Sh 64 D.M. Sheppard, Ph.D. Thesis, Massachusetts Institute of Techno-
logy (1964)

Sm 65 W.R. Smith, Oak Ridge National Laboratory Report ORNL-TM-1151
(1965)

St 66 G.L. Strobel, Nucl. Phys. 86 (1966) 535

Te 66 J.W. Tepel, Nucl. Instr. and Meth. 40 (1966) 100

- To 61 W. Tobocman, Theory of Direct Nuclear Reactions (Oxford University Press, 1961)
- Ts 66 K. Tsukada, S. Tamaka, M. Maruyama and Y. Tomita, Nucl. Instr. and Meth. 39 (1966) 249
- Wi 63 D.L. Wieber, Nucl. Instr. and Meth. 24 (1963) 269
- Wi 64 D. Wilmore and P.E. Hodgson, Nucl. Phys. 55 (1964) 673
- Ya 61 B. Yaramis, Phys. Rev. 124 (1961) 836
- Yo 65 D.H. Youngblood, Ph.D. Thesis, Rice University (1965)

B29878